Ca' Foscari
University
of Venice

Master's Degree Programme in
Sustainable Chemistry and Technologies

Final Thesis

Synthesis and characterization of new phosphoramide ligands for the preparation of luminescent manganese and f-block metal complexes

Supervisor
Ch. Prof. Marco Bortoluzzi

Graduand
Alberto Gobbo
Matriculation Number 849283

Academic Year
2018 / 2019

INDEX

Abstract

New luminescent Ln(III) and Mn(II) complexes were prepared and their optical properties were investigated. The experimental work first concerned the synthesis of new neutral phosphoramide ligands, designed and studied in order to improve the efficiency of light absorption and ligand-to-metal energy transfer. Red emitting Eu(III) and green emitting Tb(III) nitrate complexes with phosphoramide ligands were synthesized, together with analogous Gd(III) derivatives in order to obtain information about the excited states of the ligands. The formal replacement of nitrate ions with beta-diketonate ligands such as dbm (dibenzoylmethanate) and tta (tenoyltrifluoroacetonate) afforded strong red-emitting species with general formulae $[Eu(\beta\text{-dike})_3L]$ and $[Eu(\beta\text{-dike})_3L_2]$. The same phosphoramide ligands allowed the isolation of Mn(II) halide complexes, showing green or red emissions depending upon the coordination number. The complexes and the ligands were characterized by UV-vis spectroscopy, IR, NMR and magnetism measurements, while the optical properties were investigated by PL, PLE, and lifetime measurements. The stability of the obtained complexes in polymer matrices was finally investigated.

INTRODUCTION

1.1 d-block luminescence

Many luminescent d-block metal complexes are well known and studied for their optical properties. Absorption and emission are due to transitions between molecular orbitals of the complexes, arising from the interaction of metal and ligands orbitals. The ligands usually present aromatic fragments, with good chelating and coordination properties and with an extended π-resonance. The presence of heavy atoms favours the *intersystem crossing* and the triplet state excitation, making the phenomenon of phosphorescence more probable. Luminescence arises from internal charge transfers of different types: MLCT (metal to ligand charge transfer), LMCT (ligand to metal charge transfer) and LLCT (ligand to ligand charge transfer). [1]

The MLCT is usually found in d^6, d^8 e d^{10} metals such as Re(I), Ru(II), Os(II), Ir(III), Pt(II), Au(I) and Au(III). In these cases, an electron is usually excited from a high-energy metal-centred occupied orbital to an unoccupied ligand-centred orbital having π* character, and the return to the ground state is accompanied by photon emission. The luminescent properties can be tuned by varying the extension of the π systems of the organic ligands. The presence of heavy metal centres favours the intersystem crossing, therefore for singlet molecules the transition commonly involves an excited triplet state ($S_0 \leftarrow T_1$) of the ligand levels. [2]

Rhenium(I) complexes have usually octahedral geometry and the most common ligands are chelating N-donors, aromatic and heterocyclic molecules, but also halides and carbonyl groups can be found. [3] In ruthenium(II) and osmium(II) luminescent complexes, polypyridine-based structures such as 2,2'-bipyridine (bpy) are used. The complex having formula $[Ru(bpy)_3]^{2+}$ is well known for its long lifetime and shows intense absorption and emission bands in the visible region of the spectra. [4] In iridium complexes ligands are generally N,C-donors forming cyclometalated structures, as occurs for the conjugate base of 2-phenylpyridine. [5] In luminescent platinum(II) and gold(III) derivatives having square planar geometry the metal centres are coordinated by aromatic heterocyclic polydentate ligands commonly used in combination with strong σ-C-donors, while gold(I) complexes with d^{10} configuration have linear geometry, stabilized by bidentate sulphur and phosphorus-donor ligands. [6]

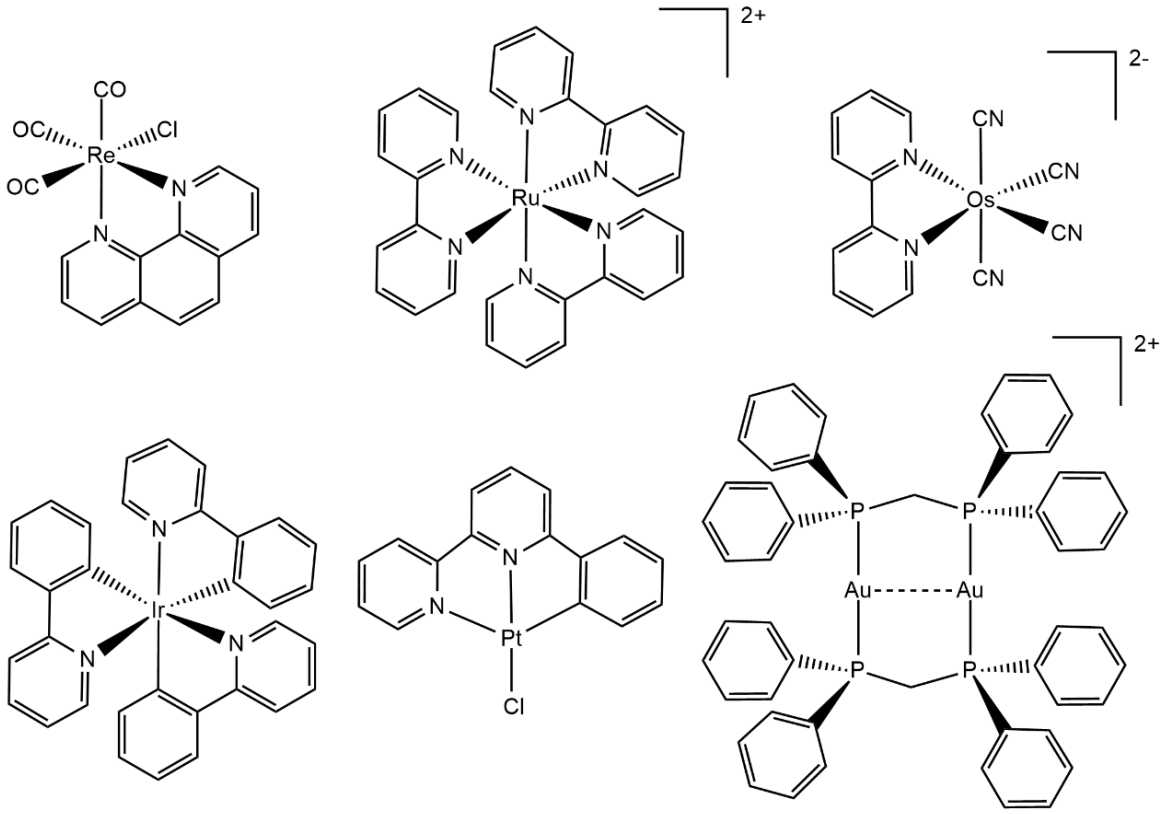

Figure 1. Some examples of d-block luminescent complexes.

The main drawbacks of the use of second and third row transition metals are their expensiveness and toxicity, forcing the research towards more bio- and economically compatible metals. When the MLCT mechanism is considered, the most interesting alternative is the most abundant and less expensive copper. Copper(I) has d^{10} electronic configuration, which does not allow d-d transition and favours the MLCT transitions instead. Tetrahedral mononuclear copper(I) luminescent complexes are known since the seventies, with P-, C-, S- and N-donors bulky bidentate ligands. Some examples of ligands are 2,9 bis-substituted derivatives of phenanthroline, giving complexes of general formula $[Cu(phen^{R2})_2]^+$, or bidentate P-donors ligands such as bis(2-(diphenylphosphino)phenyl)phenyl]ether. The presence of bulky ligands is necessary to avoid geometry distortion in the excited state, and to limit the probability of non-radiative decay as a consequence. Examples of polynuclear neutral complexes have formulae such as $[Cu_2X_2L_4]$ or $[Cu_4X_4L_4]$, where X are halide ions with bridging coordination modes among two or three metals centres and L is an aromatic fragment. The nature of the halide and the extension of π-conjugation influence the lifetimes and the position of the emission band, allowing the emission tuning. [7] Complexes of general

formula $[Cu(N^N)(PPh_3)_2]BF_4$, where N^N represents aromatic N-donor heterocycles, were the first Cu(I) luminescent complexes to be used in Organic Light Emitting Diodes (OLEDs), thanks to their thermal stability and the noteworthy luminescent properties. [8]

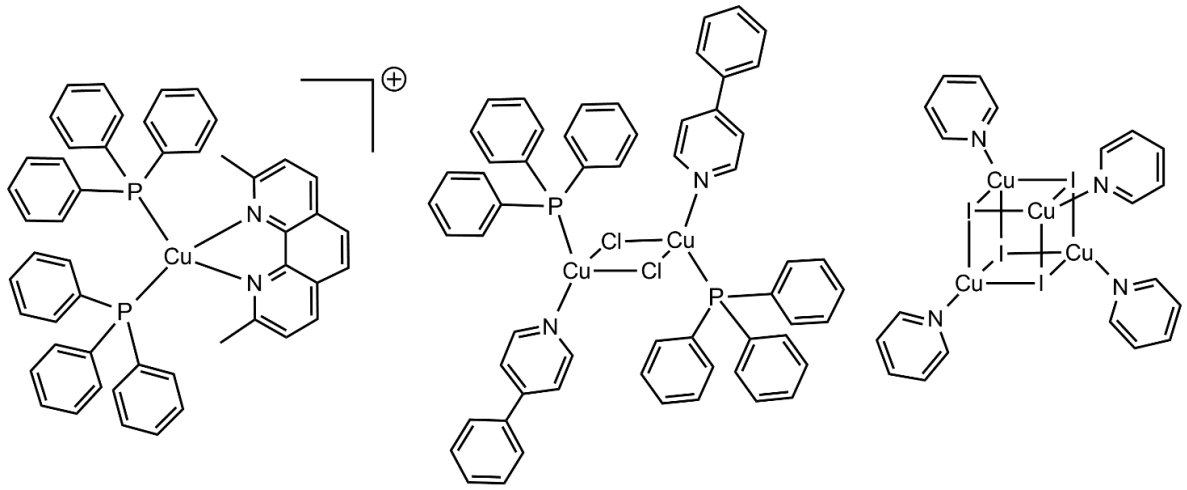

Figure 2. Some examples of Cu(I) luminescent complexes.

Metal-centred emissions can be seen for example in manganese(II) and chromium(III) derivatives. The ligands absorb the incident light thanks to their high absorption coefficient and after an *intersystem crossing*, the energy can be transferred to the metal, which behaves as emitting centre. The ligand field influences both the energy of the levels and the broadening of the bands. [1] The most common example of luminescent chromium device is ruby laser, where Cr(III) acts as dopant in synthetic Al_2O_3 crystal. In this system, absorption and emission are both due to chromium ions, with the latter associated to $^4A_2(^4F) \leftarrow {}^2E(^2G)$ red transition of the metal. [9] Several chromium coordination compounds also showed luminescent properties, and one of the most intriguing examples is the complex of formula $[CrL_2]^{3+}$, where L is a tridentate polypyridine ligand. On changing the oxidation state, different luminescence can be exhibited by chromium complexes. For instance, chelating diisocyanide molecules with bulky substituents turned out to be perfect ligands to obtain emitting Cr(0) complexes with a long-lived MLCT excited state. [10]

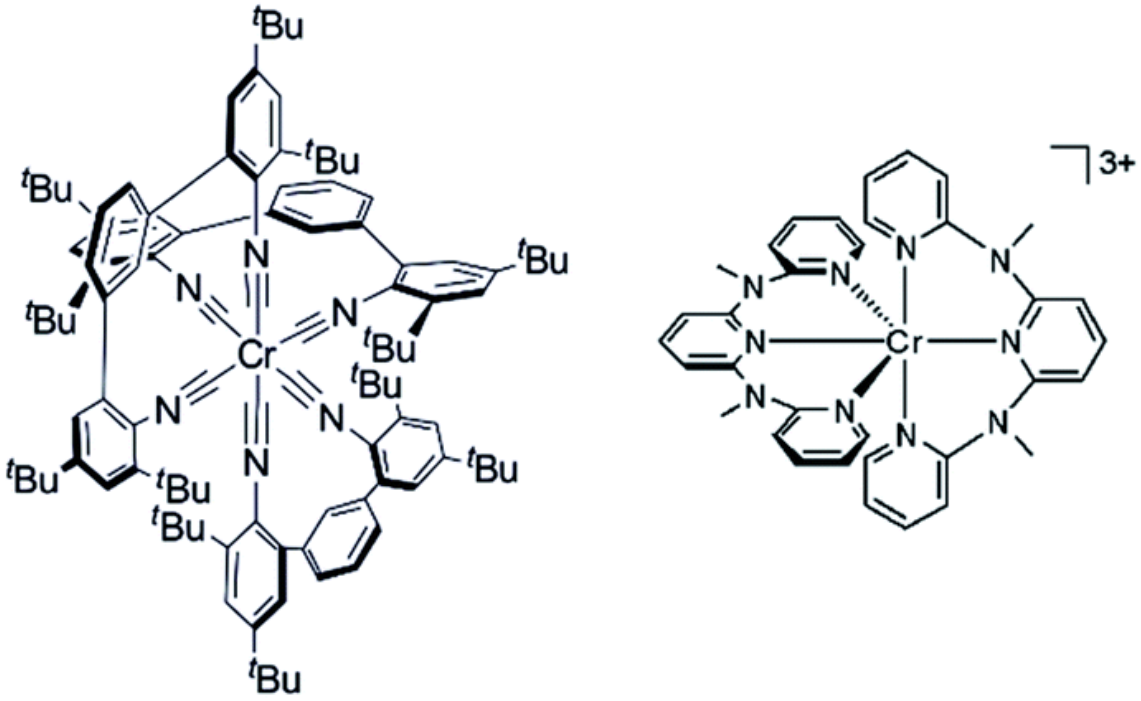

Figure 3. Some examples of isocyanide Cr(0) and polypyridine Cr(III) luminescent complex.

Among the applications of luminescent metal complexes, the most remarkable are the production of OLEDs, LEECs (light emitting electro-chemical cells), low energy consumption lamps and sensors in the biomedical field. However, second and third row transition metals and lanthanides show problems regarding toxicity, availability and expensiveness. These facts forced the research of luminescent materials towards alternative first row metals such as chromium and manganese. Compared to the others, manganese has been scarcely considered for its luminescent properties, although it is the fifth most abundant metal on earth and its minerals are widely distributed and well known for their luminescent properties. [11]

1.2 Manganese luminescence

Manganese ions are responsible for luminescence of most of the classes of minerals in nature, where it is usually present as impurity, substituting other cations in lattice and acting as luminescence emitting centre. [12] Manganese ions have an incomplete d-shell in most of the oxidation states, with generic d^n electronic configuration. Since d-electrons are not shielded by outer electrons, unlike in f-block elements, crystal field has a strong influence on the electronic and luminescence properties of the complexes. Among all its oxidation states, the most common and studied for their luminescence are +2 (d^5), +3 (d^4), +4 (d^3) and +5 (d^2).

Manganese(IV) is used as emitting centre in artificial phosphors, with red-orange emissions between 620 nm and 715 nm. [13] The use of Mn^{4+} aims to the production of warm-white led, in combination with blue-emitting chip and $Y_3Al_5O_{12}:Ce^{3+}$ yellow phosphor. The main drawback concerning the use of Mn^{4+} is the low efficiency and the only commercially available phosphor is $K_2SiF_6:Mn^{4+}$. [14] Manganese(V) has been found in magmatic apatite, where it replaces P atoms in sites with a tetrahedral environment. [15] Luminescence due to Mn^{3+} was not found in nature, but Mn^{3+} has been used in artificial garnet phosphors, with emission in the visible and the near infrared part of the spectrum. [16]

Manganese(II) has a $3d^5$ configuration with a sextet (^6S) ground state. It can be found in many minerals and it is responsible for red, orange, yellow and green emission, according to the different coordination geometries and the crystal field strength. When talking about spectroscopic transition the *term symbols* need to be considered. For d^5 high spin ion such as Mn^{2+}, the *term symbol* of the ground state is ^6S (L= 0). The electronic configuration of the ground state indicates a spherical distribution of the electron cloud around the metal centre, without sublevels separation due the crystal field strength and absence of d-d absorptions between levels with the same multiplicity. The excited state is only obtained by changing multiplicity from sextet to quartet, coupling two electrons in a single orbital. Transitions which imply changing in the system multiplicity are forbidden by the selection rules and show small absorption coefficients as a consequence. The first excited state due to two electron coupling is ^4G, composed by 9 sublevels which lose their degeneracy because of the crystal field. In the case of cubic-related symmetries (tetrahedron, octahedron), the sublevels are separated in four groups, $^4T_1$, $^4T_2$, $^4A_1$ and ^4E.

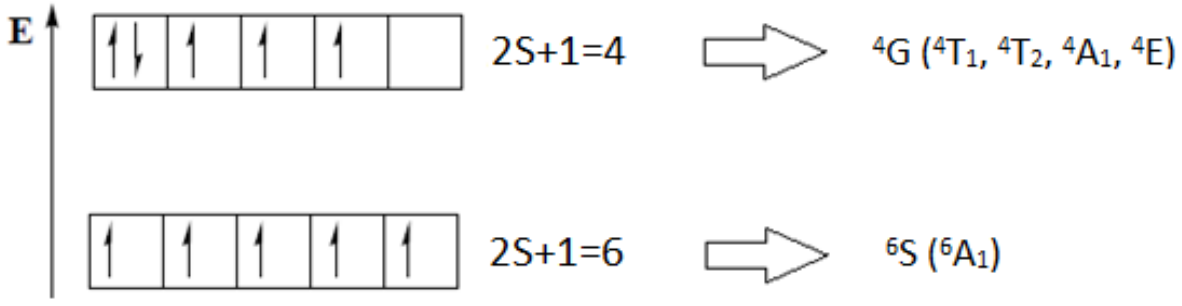

Figure 4. Electronic configuration of the ground and the first excited state in Mn^{2+} complexes.

Therefore, absorption spectra of Mn^{2+} complexes usually show several peaks, while emission are usually all due to the $^6A_1 \leftarrow {}^4T_1$ transition, i.e. from the excited state at lower energy. The emission is a phosphorescence, since it corresponds to a forbidden transition because of the change in multiplicity. Therefore, the lifetime is much longer than a common fluorescence. From the Tanabe-Sugano diagram for a d^5 ion, the presence of two distinct regions, due to low spin or high spin configuration, can be noticed. For low crystal field strength, the high spin configuration prevails because of the exchange interaction among parallel electrons. The nature and wavelength of the emission depends upon the geometry, because of the difference response of the excited state to the crystal field strength with respect to the ground state. Tanabe-Sugano diagram shows that an increase in the value of Dq produces a shift of $^6A_1 \leftarrow {}^4T_1$ and $^6A_1 \leftarrow {}^4T_2$ transitions towards longer wavelength. [17]

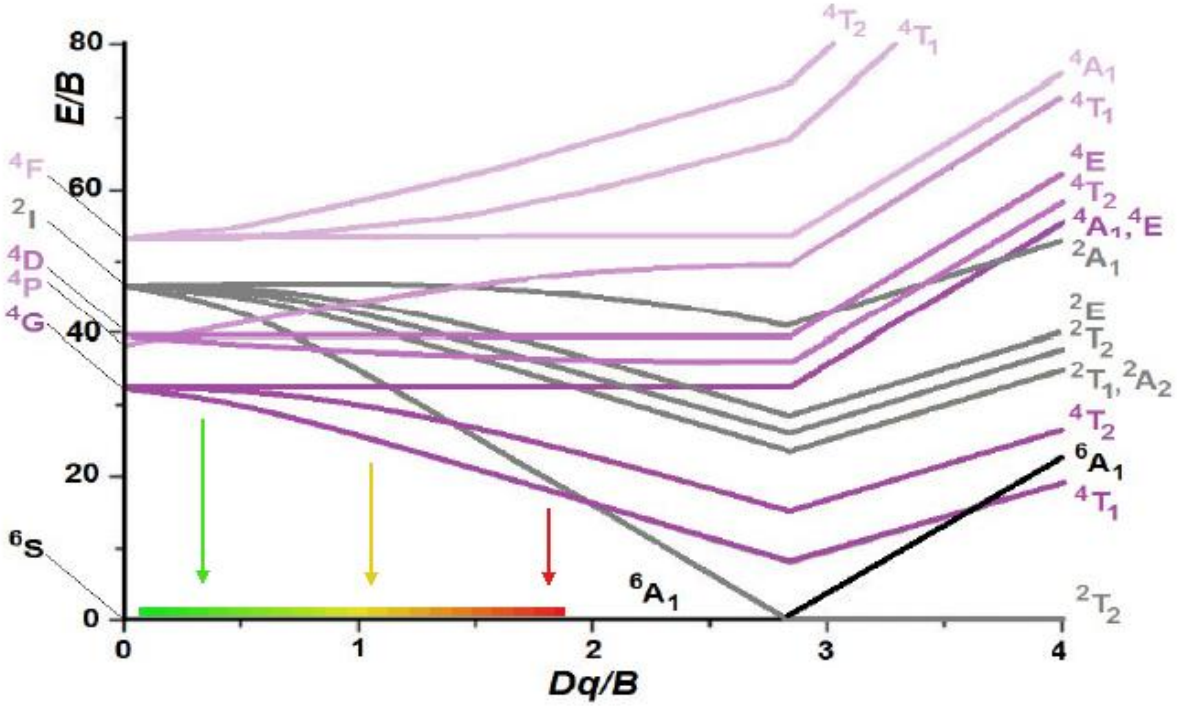

Figure 5. Tanabe-Sugano diagram for d^5 elements.

In octahedral complexes emissions are both spin and parity forbidden. On the other hand, in tetrahedral complexes the partial p-nature of the molecular orbitals involved in the transition makes the emission only spin forbidden, consequently shorter lifetimes are measured. The colour of the $^6A_1 \leftarrow {}^4T_1$ transition be can be modulated by varying the crystal field geometry, covering almost all the spectra from 480 to 700 nm. In the case of octahedral complexes, the

energy gap between the $^4T_1$ (^4G) and $^6A_1$ (^6S) levels generates emission in the yellow-red part of the spectra, while in the presence of a tetrahedral geometry the energy gap is higher because of the smaller crystal field strength and consequently green emission is observed.

Octahedral manganese (II) can be found in calcite ($CaCO_3$), where Mn^{2+} occupies some Ca^{2+} sites and generates a red-orange emission from the $^4T_1$ state centred at 620 nm, while Mn^{2+} impurities in willemite (Zn_2SiO_4) led to yellow-green emission at 525 nm. Different transitions can be involved in the luminescence: for instance, green emission at 500 nm and 505 nm can be observed for fluorite and anhydrite respectively, due to the $^6A_1 \leftarrow {}^4T_2$ transition [17].

1.2.1 Manganese(II) luminescent complexes

The d^5 electronic configuration of manganese(II) generates an isotropic electron distribution around the metal. The coordination geometry is primarily influenced by the properties of the ligands, such as the steric bulk, the electrostatic repulsions and the bite-angle. Manganese(II) is a hard Lewis acid, and its coordination chemistry is governed by σ interaction, mostly from O- and N-donor ligands and halide ions. Manganese(II) halides are versatile platforms for many reactions involving the coordination of additional organic ligands and usually some halide ions remain part of the final complex.

Tetrahedral manganese(II) complexes emitting in the green region are well known since decades. Most of these species are tetrahalomanganate complexes, ammonium salts of $[MnX_4]^{2-}$ (X = Cl, Br, I), or $MnBr_2(O{=}PPh_3)_2$, exhibiting both photo- and tribo-luminescence. [18] These species were first studied and isolated by Cotton and collaborators in the '60s. [19] More recently, tetrahalomanganate complexes as salts of methyl-triphenylphosphonium have been synthesized for their triboluminescence. [20] The emission is strongly influenced by the environment: for example, a correlation exists between the lifetime of the $^6A_1 \leftarrow {}^4T_1$ emission and the halide nature, with the heavier halides showing a decreased lifetime mainly due to higher spin-orbit coupling. [21] In addition to the green emission, ferroelectric $(diisopropylammonium)_2MnBr_4$ organic-inorganic hybrid also showed interesting properties as gas sensing platform, as well as the $[(N,N,N\text{-trimethyl(phenyl)methanaminium})_2][MnBr_4]$ hybrid, having high emissive quantum yield and exceptional thermal stability. [22] [23] More recently, oxygen-donor ligands received a particular attention: tetrahedral manganese(II) di-halide complexes such as $[MnX_2(dpepo)]$ (dpepo = bis[2-(diphenylphosphino)phenyl]ether

oxide; X = Cl, Br and I) showed strong green photoluminescence and air-stability. [24] Phosphoramide and phenylphosphonic diamide ligands have been also used to prepare neutral green-emitting manganese(II) complexes having formulae $[MnX_2\{O=PR(NMe_2)_2\}_2]$ (X=Br, I; R=NMe_2, Ph). [25]

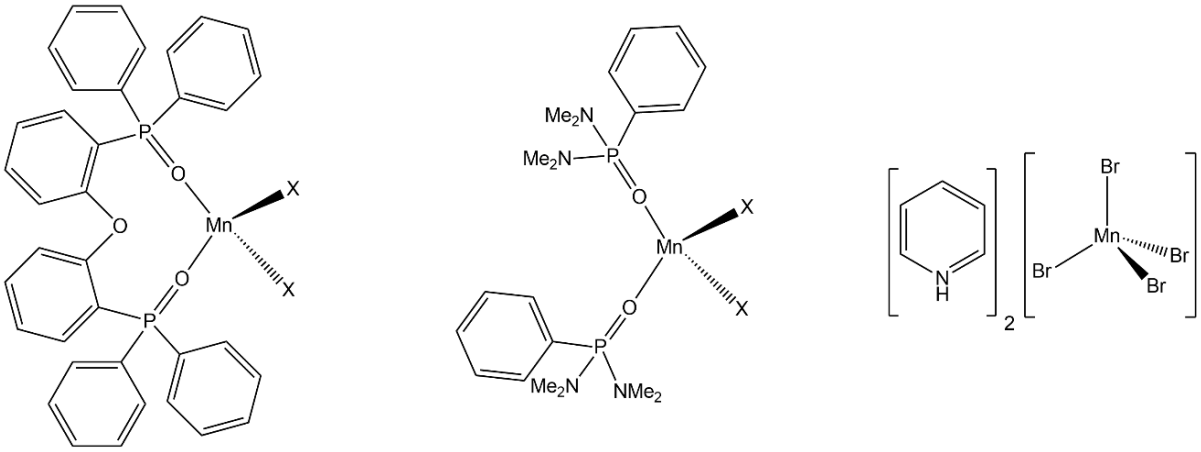

Figure 6. Some examples of green emitting manganese complexes.

Halide ions often act as bridging ligands among metal centres. For instance, species such as $[Mn(THF)_2X_2]$ (THF = tetrahydrofuran; X = Cl, Br, I) are halide-bridged pseudoctahedral polymers. The structures of polymeric species such as $[Mn_4Cl_8(THF)_6][Mn(THF)_2Cl_2]$ and $[MnCl_2(C_3H_4N_2)_2]$, where the metal centre experiences an octahedral environment, have been reported. [26] Mn(II) polymeric complexes with pentagonal bipyramidal geometry are also possible, like in $[Mn(H_2dapd)Cl_2]$, where H_2dapd = 2,6-diacetylpyridine dioxime. [27]

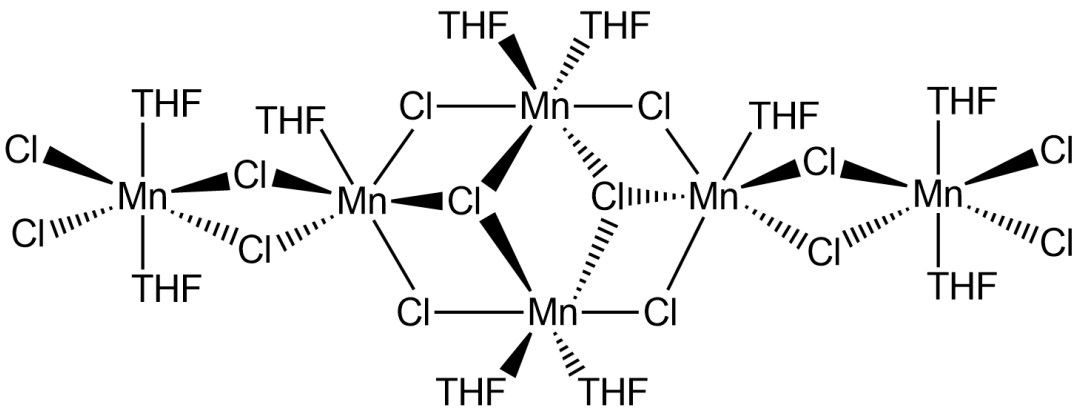

Figure 7. An example of manganese(II) coordination polymer.

Red-emitting manganese(II) with octahedral environment has been mostly used in inorganic emitting phosphors like $(Mn_xZn_{1-x})_2(HPO_3)F_2$, as dopant in zinc sulfide quantum rods, in CdS/ZnS Core/Shell nanocrystals, or in Cd–In–S nanocluster-based semiconductor. Ultralong lasting emission at longer wavelength, from red to infrared, was studied in Mn(II)-doped $Na(Al,Ga)Ge_3O_8$ glasses and (Al,Ga)-albite glass-ceramics. [28] Red emissions have been also observed in organic-inorganic hybrids, where Mn^{2+} is coordinated by six halides, such as trimethylchloromethyl ammonium trichloromanganese(II) ($[Me_3NCH_2Cl][MnCl_3]$), 3-pyrrolinium trichloromanganese(II) ($[C_4H_8N][MnCl_3]$) and pyrrolidinium trichloromanganese(II) ($[NH_2C_4H_8][MnCl_3]$). [29] Two coordination geometries of Mn^{2+} ions in one single molecule have been observed in the inorganic–organic hybrid complex $[(C_6H_{22}N_4)_2(H_3O)(MnCl_6)(MnCl_5)(Cl)_2]\cdot 3H_2O$, characterized by pink luminescence. [30] Crown ether 18-crown-6 can act as chelating ligand in reaction with manganese(II) bromide, forming $[MnBr_2$(18-crown-6)], $[Mn_3Br_6$(18-crown-6)$_2]$ and $[Mn_3Br_6$(18-crown-6)], all showing strong luminescence between yellow and red regions. [31] Another interesting chelating ligand, with nitrogen as donor atom, is the 4-(3,5-diphenyl-1H-pyrazol-1-yl)-6-(piperidin-1-yl)pyrimidine ligand (L), used to prepare $[MnL_2Cl_2]\cdot H_2O$, showing both ligand- and metal-centred transitions, and being the first manganese(II) complex with emission dependent upon the excitation wavelength. [32] Deep-red luminescence was also observed in organic–inorganic hybrid Mn(II) complexes with formulae $[MnL_3]MnX_4$ (X=Cl, Br), where L= 2-(diphenylphosphoryl)-N,N-diethylacetamide ($[Ph_2P(O)CH_2C(O)NEt_2]$), showing tetrahedral geometry in the anion and octahedral in the cation. [33] Orange emission was found recently in cationic manganese(II) complexes with chelating phosphine oxides such as $[Mn(dppmO_2)_3]^{2+}$ and $[Mn(dppeO_2)_3]^{2+}$, where $dppmO_2$ and $dppeO_2$ are bis(diphenylphosphino)methane dioxide and 1,2-bis (diphenylphosphino)ethane dioxide respectively. [34] Vapochromism due to a change of the ligand field has been also observed for a manganese(II) coordination polymer with $dppeO_2$, where the emission varies from green to red thanks to the reversible addition of DMF molecules, changing the geometry from tetrahedral to trigonal bipyramidal and leading to different luminescence proprieties as a result. [35]

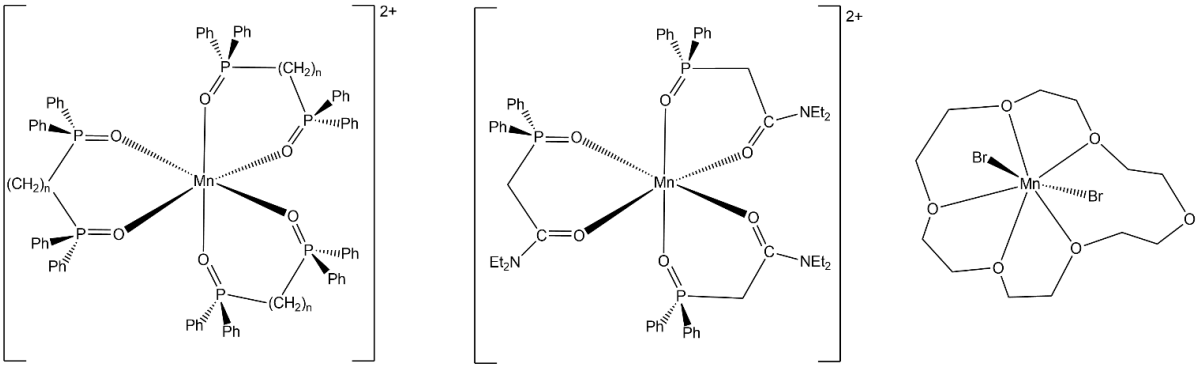

Figure 8. Some examples of red-emitting manganese(II) complexes.

1.3 Lanthanides

1.3.1 General features

Lanthanide series include 14 elements, from cerium (atomic number 58) to lutetium (atomic number 71). Some definitions also include lanthanum with atomic number 57 in the series, despite its configuration [Xe] $5d^1\,6s^2$ makes it formally part of the group 3 elements. Lanthanides, along with yttrium and scandium, are also defined as *rare earths*, due to their chemical similarities and because they are usually found in the same mineral deposits. Johann Gadolin in 1794 was the first to obtain yttrium oxide from a black mineral, now known as gadolinite. Over the next years, many scientists succeeded in the isolation of other lanthanide oxides. Promethium is the only radioactive element of the series, it is extremely rare and was first produced in 1945 as by-product of uranium fission. Because of the pronounced similarity of lanthanides, which complicates their separation and purification, it took many years for their complete identification; only through to the contribution of Henry Moseley, thanks to the x-ray spectra of the elements and to the chemical concept of atomic number, lanthanides found their correct position in the periodic table. [36]

Their abundance decreases with the increase of the atomic number, and those with an even atomic number are usually more abundant that those with an odd one because of a stronger nuclear force. The abundance also depends upon their early formations in supernovae: the heavier elements required more energy, in terms of temperature and pressure, and were then hardly produced.

	La	Ce	Pr	Nd	Pm	Sm	Eu	Gd	Tb	Dy	Ho	Er	Tm	Yb	Lu	Y
Crust (ppm)	35	66	9.1	40	0.0	7	2.1	6.1	1.2	4.5	1.3	3.5	0.5	3.1	0.8	31
Solar System (with respect to 10^7 atoms Si)	4.5	1.2	1.7	8.5	0.0	2.5	1.0	3.3	0.6	3.9	0.9	2.5	0.4	2.4	0.4	40.0

Table 1. Lanthanide abundance on earth and in the Solar System. [36].

The less abundant are thulium and lutetium, but they are even more abundant than some d-block metals such as bismuth, silver, mercury and arsenic. In nature, lanthanides are often mixed with yttrium and lanthanum in fluoro-carbonate minerals like bastnasite ($LnFCO_3$) or phosphate such as monazite and xenotime ($LnPO_4$), usually also containing a relevant amount of thorium. Despite the fact that lanthanides were originally discovered in Scandinavia, nowadays China is the leading producer, owning 70% of the world's total amount, where lanthanides are present as adsorbed in aluminum silicates. [37]

1.3.2 Extraction and purification

The difficulties of the extraction procedures are due to the nature of the 4f orbitals in Ln^{3+} ions; these orbitals do not directly influence the ions reactivity, being well shielded by the filled $5s^2$ and $5p^6$ shells, resulting in similar chemical behaviour. There are various extraction methods, which differ in costs, time and product purity. The highest purity, which is necessary for optical and electronic applications, can be achieved with ion-exchange chromatography, where lanthanides ions are treated with a chelating agent such as EDTA as eluent: the heaviest and smaller ions are more strongly coordinated by the anionic ligand, because of their higher charge density, and are then eluted first. Chemical separation works on Eu^{2+} only, the only lanthanide with stable divalent state that can be obtained by reduction with zinc amalgam and can be precipitated as $EuSO_4$. The longest method is the fractional crystallization and rely on the slightly different solubility of lanthanide salts such as bromates [$Ln(BrO_3)_3 \cdot 9H_2O$]. Alternatively, after a treatment with concentrated NaOH which produces a mixture of different oxides, CeO_2 and ThO_2 can be first easily separated from the acidified solution of the other lanthanides when the pH is maintained at 3.5. The same solution is then treated with an organic solvent like kerosene and a hydrophobic ligand such as tributyl phosphate [$(BuO)_3PO$]; lighter complexes are more soluble in the organic solution. The extraction procedure is repeated many times to separate all the lanthanides. [36]

1.3.3. Electronic configuration and coordination chemistry

Electrons in 4f orbitals suffer of high interelectronic repulsion, but unlike 5d orbitals they do not have radial nodes. In case on lanthanum, 5d orbitals are still at lower energy than 4f, but with the increase of the atomic number 4f orbitals gain more and more stability. So that, the electronic configuration becomes [Xe] $4f^1$ $5d^1$ $6s^2$ for cerium and [Xe] $4f^3$ $6s^2$ for praseodymium. Gadolinium differs from this behaviour because of the extra stabilization of the half-filled f-subshell. The most common oxidation state is Ln^{3+}, in which 4f orbitals lie at low energy because of the increment of the effective nuclear charge. The electronic configuration for Ln^{3+} ions is then [Xe] $4f^n$, where n goes from 1 for cerium to 14 for lutetium.

	Atom	Ln^{3+}	Ln^{4+}	Ln^{2+}
La	[Xe] $5d^1$ $6s^2$	[Xe]		
Ce	[Xe] $4f^1$ $5d^1$ $6s^2$	[Xe] $4f^1$	[Xe]	
Pr	[Xe] $4f^3$ $6s^2$	[Xe] $4f^2$	[Xe] $4f^1$	
Nd	[Xe] $4f^4$ $6s^2$	[Xe] $4f^3$	[Xe] $4f^2$	[Xe] $4f^4$
Pm	[Xe] $4f^5$ $6s^2$	[Xe] $4f^4$		
Sm	[Xe] $4f^6$ $6s^2$	[Xe] $4f^5$		[Xe] $4f^6$
Eu	[Xe] $4f^7$ $6s^2$	[Xe] $4f^6$		[Xe] $4f^7$
Gd	[Xe] $4f^7$ $5d^1$ $6s^2$	[Xe] $4f^7$		
Tb	[Xe] $4f^9$ $6s^2$	[Xe] $4f^8$	[Xe] $4f^7$	
Dy	[Xe] $4f^{10}$ $6s^2$	[Xe] $4f^9$	[Xe] $4f^8$	[Xe] $4f^{10}$
Ho	[Xe] $4f^{11}$ $6s^2$	[Xe] $4f^{10}$		
Er	[Xe] $4f^{12}$ $6s^2$	[Xe] $4f^{11}$		
Tm	[Xe] $4f^{13}$ $6s^2$	[Xe] $4f^{12}$		[Xe] $4f^{13}$
Yb	[Xe] $4f^{14}$ $6s^2$	[Xe] $4f^{13}$		[Xe] $4f^{14}$
Lu	[Xe] $4f^{14}$ $5d^1$ $6s^2$	[Xe] $4f^{14}$		
Y	[Kr] $4d^1$ $5s^2$	[Kr]		

Table 2. Electronic configurations of lanthanides and their ions. [36]

Other oxidation states can be found for favourable electronic configurations, for example when the 4f sub-shell is half or full filled (Eu^{2+}: [Xe] $4f^7$ and Yb^{2+}: [Xe] $4f^{14}$). [38] The 4f orbitals can be described by either cubic or non-cubic set (general set), depending on the orbital combinations. The first set is valid for a cubic environment and comprises f_{xyz}, $f_{z(x2-y2)}$, $f_{z(y2-z2)}$ and $f_{y(z2-x2)}$, f_{z3}, f_{x3} and f_{y3} orbitals. The shape and the low energy of 4f orbitals make them core orbitals, which do not influence the coordination chemistry of the ions. Their poor screening also causes the lanthanide contraction, which determines a decrease in the radius of lanthanide on increasing the atomic number.

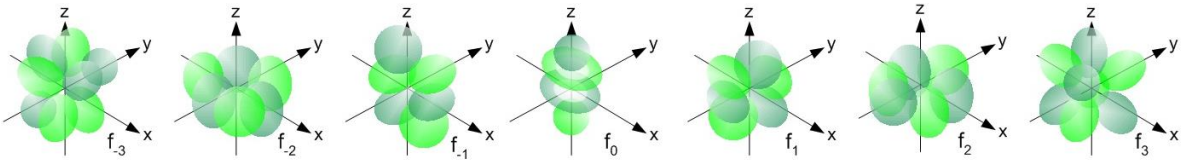

Figure 9. 4f orbitals (ungerade), general set solutions.

The decrease of the radius of Ln^{3+} ions along the series is the main reason of their different behaviour in coordination chemistry. The only orbitals participating in the formation of bonds are the empty 6s, 6p and 5d orbitals and for these reasons, coordination chemistry of lanthanides can be compared to that of a d^0 transition metal. Spectroscopic and magnetic properties are also poorly influenced by the environment. Ln^{3+} ions are hard acids, according the *Hard and Soft Acid and Bases* (HSAB) theory by Pearson: the coordination bonds are then highly promoted by electrostatic interactions with strong affinity for fluorine, oxygen and nitrogen donor atoms. Coordination geometries are mainly determined by electrostatic (first-order effect) and steric (second-order effect) repulsions among ligands, with the most common coordination numbers ranging from 6 to 9. Among the halide complexes, LnF_3 shows the stronger bonds, because of the hardness of fluorine ions, resulting in insoluble hydrated fluorine compound. Halide compounds with chloride, bromide and iodide are instead widely used in coordination chemistry as precursors for further reactions, as the halide-Ln bond can be easily hydrolyzed. [36]

Ba	La	Ce	Pr	Nd	Pm	Sm	Eu	Gd	Tb	Dy	Ho	Er	Tm	Yb	Lu	Hf
217.3	187.7	182.5	182.8	182.1	181.0	180.2	204.2	180.2	178.2	177.3	176.6	175.7	174.6	194.0	173.4	156.4
	La^{3+}	Ce^{3+}	Pr^{3+}	Nd^{3+}	Pm^{3+}	Sm^{3+}	Eu^{3+}	Gd^{3+}	Tb^{3+}	Dy^{3+}	Ho^{3+}	Er^{3+}	Tm^{3+}	Yb^{3+}	Lu^{3+}	Y^{3+}
	103.2	101.0	99.0	98.3	97.0	95.8	94.7	93.8	92.3	91.2	90.1	89.0	88.0	86.8	86.1	90.0

Table 3. Atomic and ionic radii of the lanthanides (pm). [36]

1.3.4 Spectroscopic and magnetic properties

Spectroscopic and magnetic properties of lanthanide ions are determined by electrons in 4f orbitals, which do not participate in the bond formation and are then not influenced by the presence and nature of the ligands. The extent of spin-orbit interaction is determined by the scalar product between L (total orbital angular momentum) and S (total spin) and depends on both the atomic number Z and the nucleus-electron distance r:

$$Vint \propto \frac{Z}{r^3} L \cdot S$$

In case of lanthanides this contribution cannot be ignored, because both the high atomic number and the small nucleus-electron distance in 4f orbitals. Therefore, in addition to S and L the term symbol for a lanthanide ion comprises the total angular momentum quantum number J, which arises from the combination of L and S and takes quantized values from |S+L| to |S-L| with unit steps variations. Term symbols describe the electronic states and are of the form $^{2S+1}L_J$ where 2S+1 is the multiplicity, L is the sum of m_l and corresponds to a letter (L = 0: S; L = 1: P; L = 2: D; L = 3: F; L = 4: G etc.), and J can vary from |S+L| to |S-L|. The ground states can be easily calculated using Hund's rules and correspond to states of maximum S and L. For f^n ions with n≤7 the lower state is given by the lower value of J, while for ions with n>7, the lower state is given by the higher value of J. The energy diagram containing both ground and excited states of all lanthanides is known as *Dieke diagram* and it is valid for both single ions and complexes. [39]

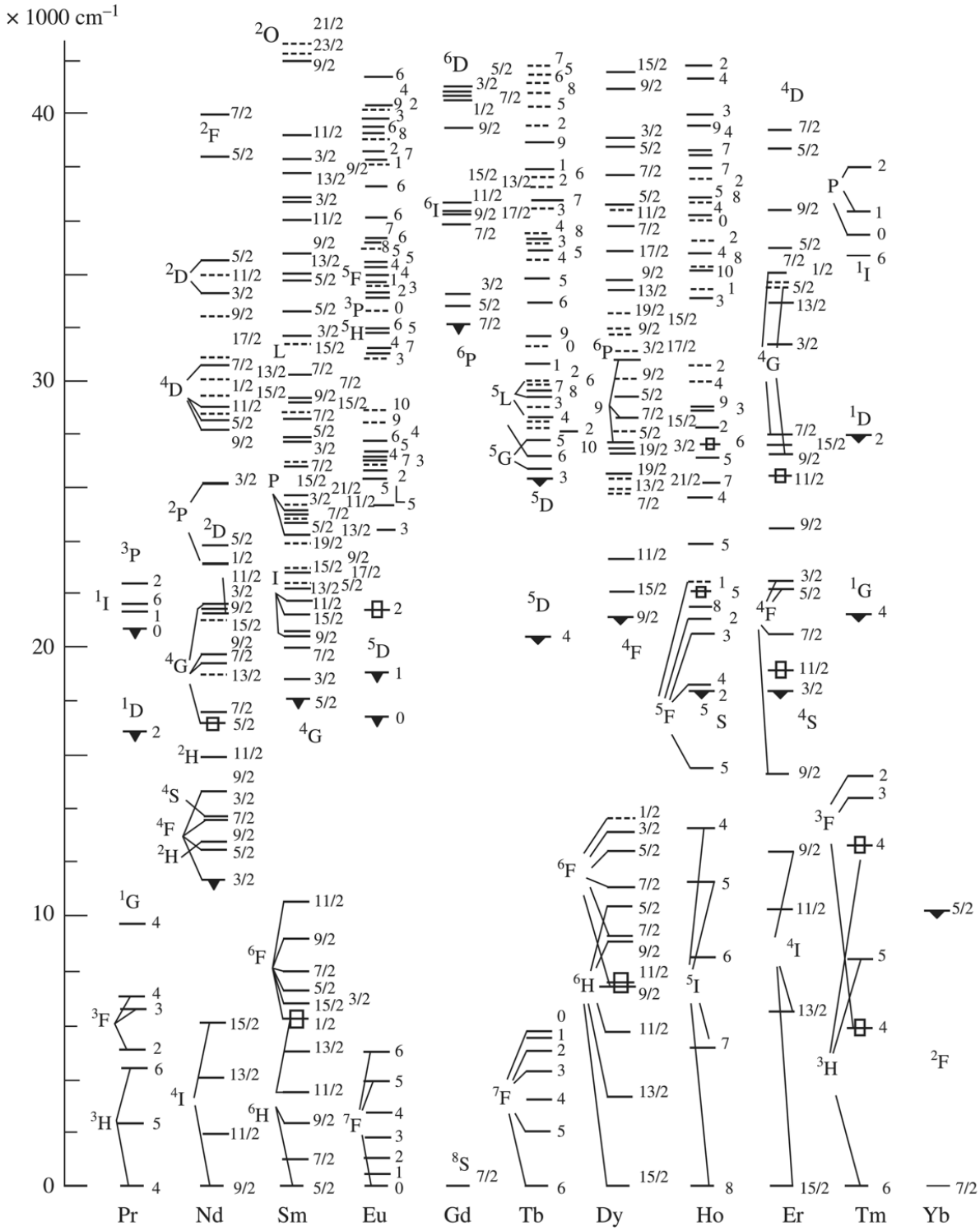

Figure 10. Dicke diagram for lanthanides. [39].

The main effect of the ligands is known as *Stark effect* and causes the splitting of a given spin-orbit level into Stark's sublevels with energy separation of the order of 100 cm^{-1}, which is really small compared to the slitting between J levels (1.000-10.000 cm^{-1}) or between L levels

(>10.000 cm^{-1}). Despite the small effect, Stark separation is sometimes useful to determine the coordination geometry of the complex. [40]

All Ln^{3+} ions also have unpaired electrons because Hund's rule and are thus paramagnetic centres. The magnetic moment is independent from the coordination geometry and for a given state it is calculated as follows:

$$\mu_j = g_j \sqrt{J(J+1)} \qquad\qquad g_j = \frac{3}{2} + \left[\frac{S(S+1) - L(L+1)}{2J(J+1)}\right]$$

where g_j is known as Landé factor. Experimental and theoretical magnetic moments show a good correspondence, except for ions like Sm^{3+} and Eu^{3+}: in these cases, at normal conditions, the excited J states can be partly populated and contribute to the value of μ_j. Experimental values of μ_j have been measured for complexes of general formula $[Ln(phen)_2(NO_3)_3]$ (for samarium $\mu_{j,theoric}$= 0.85 BM, $\mu_{j,exp}$= 1.64 BM; for europium $\mu_{j,theoric}$= 0.00 BM, $\mu_{j,exp}$= 3.36 BM).

1.3.5 Photoluminescence

Lanthanide luminescence relies on f-f transitions, and because 4f orbitals do not participate in the bond formation, absorbance and emission energy are not influenced by the crystal field and vibrational energy, resulting in sharp bands compared to d-d transition or organic chromophore bands.

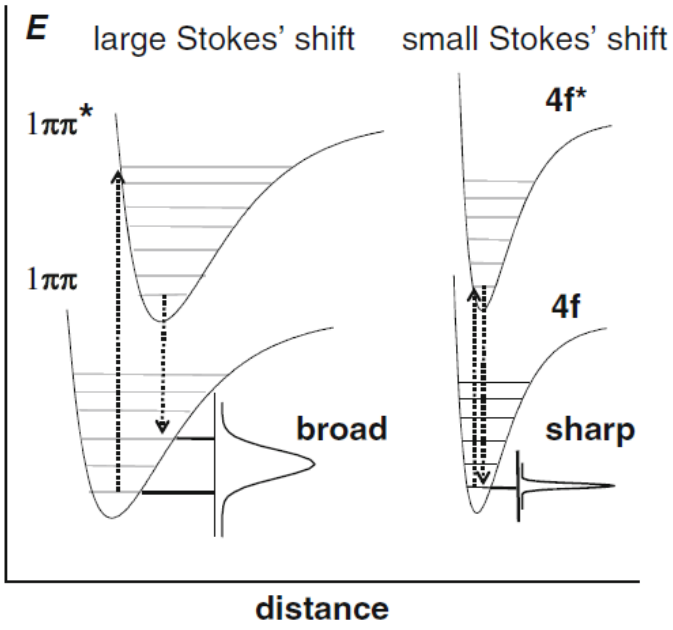

Figure 11. Configurational coordinate diagram for emission from an organic chromophore and a lanthanide ion. [39]

In organic molecules, the photon excitation usually leads to a lengthening of the chemical bonds, and the increase of internuclear distances affords broad emission and absorption bands. In lanthanides the internuclear distances remain almost constant in the 4f excited states, resulting in narrow bands and small Stokes' shift between absorption and emission. [39]

Absorption can be due to sharp intra-configurational 4f–4f transitions or broader 4f–5d transitions. Laporte's parity selection rule does not allow electric dipole transitions (ED) between orbitals with the same parity; however weak f-f transitions can still be observed thanks to mixing of higher electronic states of opposite parity, through permanent asymmetric ligand field or through asymmetric molecular vibrations. Magnetic dipole transitions (MD) are allowed instead even though naturally weaker. Quadrupolar f-f transitions are so weak that usually are not observed, while d←f transitions are highly energetic and occur at frequencies from Uv to higher. Sharp f-f emissions and long lifetimes (from micro to milliseconds), both due to Laporte's parity selection rule, are their most interesting features for optical and technological applications. Luminescent emissions cover the entire spectrum. Many Ln^{3+} emissions lie in the visible region of the spectra: orange emission for Sm^{3+} ($^4G_{5/2}\rightarrow{}^6H_J$, J=5/2-11/2), red for Eu^{3+} ($^5D_0\rightarrow{}^7F_J$, J=0-4), green for Tb^{3+} ($^5D_4\rightarrow{}^7F_J$, J=6-3) and yellow for Dy^{3+} ($^4F_{9/2}\rightarrow{}^6H_J$, J=15/2-13/2). Sm^{3+}, Dy^{3+} and some other ions such as Nd^{3+}, Ho^{3+}, Er^{3+}, Yb^{3+} and Pr^{3+} show also (or exclusively) emissions in the NIR region, while Gd^{3+} in the Uv. The intensity of the transitions depends upon selection rules based on the quantum number J of the excited and the ground state. In Eu^{3+} for example, all the transition $^5D_0\rightarrow{}^7F_J$ with J =0 – 6 can be seen, but $^5D_0\rightarrow{}^7F_2$ at 615 nm and $^5D_0\rightarrow{}^7F_4$ and 700 nm are usually the strongest. [36] Some bands, defined as hypersensitive, respond to changes in the symmetry and strength of the ligand field with strong intensity variations (the best-known hypersensitive transition is the $^5D_0\rightarrow{}^7F_2$ transition for Eu^{3+}). [41]

In photoluminescence applications, the low absorption coefficients of Ln(III) ions can be overtaken by means of organic ligands, usually with higher absorption efficiency in the Uv region. [42] The effect of the ligands in lanthanide complexes is called luminescence sensitization or antenna effect. The electron of an organic ligand gets promoted from the singlet ground state S_0 to the singlet excited state S_1 by means of a photon absorption, usually in the Uv region. The system can now relax radiatively back to the ground state of the ligand

with fluorescent ($S_0 \leftarrow S_1$) emission, typically in the order nanoseconds, or non-radiatively to a triplet excited state (T_1) at lower energy. Conversion to triplet state is called *intersystem crossing* (ISC), it is not allowed by spectroscopic rules, but it is energetically favoured and can occur if S_1 state has a long enough lifetime and in the presence of heavy atoms. The triplet state can also undergo radiative phosphorescence emission to the ligand ground state, another forbidden process, or promote the non-radiative energy transfer path called *antenna effect* to the lanthanide excited state. [43]

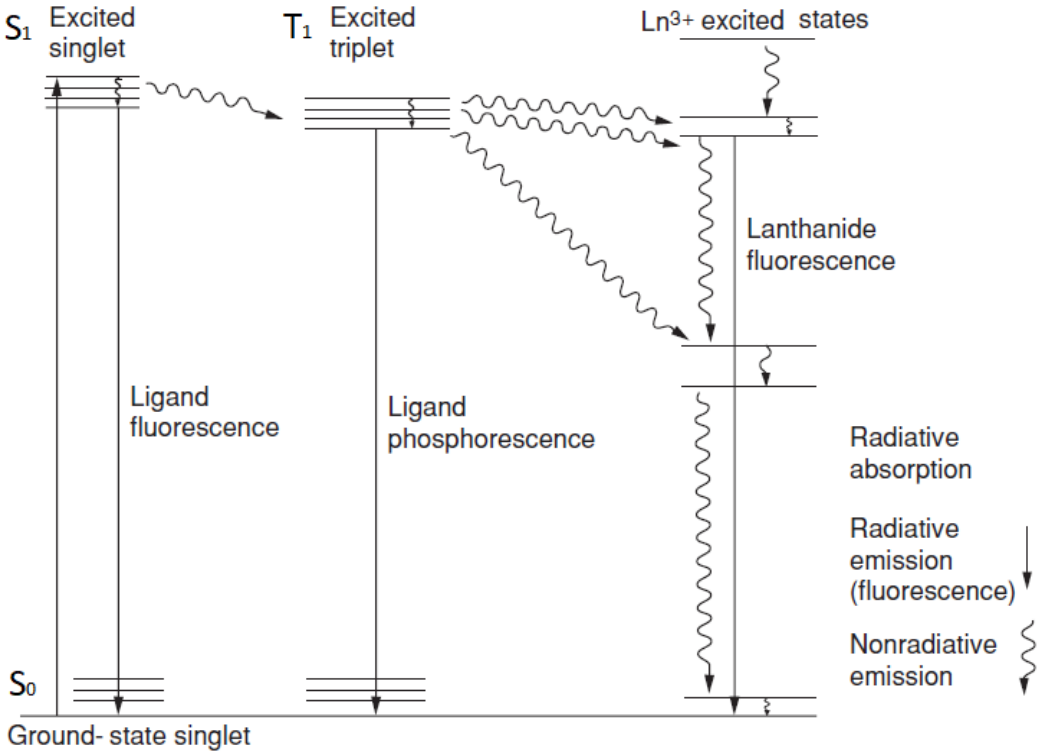

Figure 12. Antenna effect on Lanthanide complexes. [36]

In some cases, the lanthanide can also be directly excited by the singlet excited state of the ligand. [44] At this point, when the ion is excited, the system usually relaxes non-radiatively to the lowest excited spin-orbit level, which will be the emitting state, before to follow either a non-radiative path (usually thermal or vibrational dissipation) or a f-f radiative emission. The first case of antenna effect was observed by Weissman for β-diketonate complexes. [45] To act as an antenna, the energy of the ligand triplet level needs to be above the lanthanide resonant level (17200 cm^{-1} for Eu^{3+}, 20400 cm^{-1} for Tb^{3+} and 10100 cm^{-1} for Yb^{3+}), higher enough to avoid back energy transfer mechanism but sufficiently close to allow wave functions superposition (between 1800-2000 cm^{-1} for a typical europium complex).

The energy transfer depends on the distance between ligand and metal and can occur either with double-exchange Dexter of dipolar-dipolar Foster mechanism. Dexter mechanism implies two electrons exchange between ligand and metal and decades with e^{-d}, while in Förster mechanism only energy transfer is present and goes with d^{-6}. [46] When the divalent state is accessible, an additional mechanism is possible: the chromophore adsorbs the light and the lanthanide ion gets firstly reduced from Ln^{3+} to Ln^{2+} with an electron transfer from the ligand. Once the lanthanide spontaneously returns to the trivalent state, a finite fraction of Ln^{3+} excited state is formed, and emission associated to a f-f transition can occur. [47]

$$X + h\nu \rightarrow X^*$$

$$X^* + Yb^{3+} \rightarrow X^{\bullet+} + Yb^{2+}$$

$$X^{\bullet+} + Yb^{2+} \rightarrow X + Yb^{3+*}$$

There are many pathways through which the system relaxes without the photon emission. The triplet state of the ligand may interact with the oxygen in the air, interfering with the energy transfer to the lanthanide and its excitation. In coordination polymers, if many emitting centres are too close to each other, coordination quenching can occur. In aqueous solution or in the presence of atmospheric moisture, vibrational relaxation processes are mainly due to the interaction with water molecules, which somehow interact with the lanthanide ion. In addition to this, the energy gap law states that if the energy difference between the emitting and the higher J level of the ground state is small, non-radiative processes are favoured.

The efficiency of a radiative emission can be evaluated on the basis of the intrinsic quantum yield (Q_i) and lifetime. The intrinsic quantum yield considers the relation between radiative and non-radiative processes and has the following form:

$$Q_i = \frac{k_r}{k_r + k_{nr}} = \frac{\tau_{obs}}{\tau_{rad}}$$

where k_r and k_{nr} are the rate constants for the radiative and non-radiative process respectively. The observed lifetime is usually indicated as τ_{obs}. The quantum yield can also be written as the ratio of observed lifetime and radiative lifetime. When the overall efficiency is questioned, the overall quantum yield (Q_o) should be considered and it is the ratio between absorbed and

emitted photons. In this case additional aspects of the complex need to be considered, such as the efficiency of the energy transfer between ligand and metal ($Q_O = \eta_t Q_i$, where η_t represents the efficiency). Moreover, the molar extinction coefficient of the ligand and the position of the absorbance bands play a crucial role to determine the luminescence performances. For these reasons it is often difficult to compare the luminescence efficiency of different samples. [39]

1.3.6 Luminescent complexes

Sensitization of lanthanide luminescence can be achieved using π-conjugated organic chromophores as ligands, which are usually aromatic molecules with high molar absorption coefficient and an efficient intersystem crossing. [48]

The most common ligands for lanthanide luminescent complexes are β-diketonates, many of them commercially available with a wide range of substituents. β-diketonates are bidentate anionic ligands, the corresponding complexes present excellent optical properties and can be easily prepared by deprotonation of the α-hydrogen with a soft base. [49]

There are three main types of β-diketonate complexes: tris complexes ($[Ln(\beta\text{-dike})_3]$), Lewis adducts of the tris complexes and tetrakis complexes. Tris complexes are coordinatively unsaturated, the ligands usually have chelating-bridging coordination mode, and/or the metal centre can coordinate other Lewis base ligands, water or solvent molecules. Anhydrous tris complexes are hard to obtain, even though some examples are reported for lanthanum, neodymium, samarium, europium, gadolinium and terbium dinuclear trisacetylacetonates, where the metal centre is eight-coordinated. Octahedral mononuclear complexes are rare, one example being the Lu(III) derivative of the bulky 2,2,6,6-tetramethylheptane-3,5-dionate. [50] Tetrakis complexes are anions of general formula $Ln(\beta\text{-dike})_4]^-$ and the counterion can be an alkali ion, a quaternary ammonium ion or a protonated organic molecule. Eight-coordinated compounds with β-diketonates usually show square antiprismatic or dodecahedral geometries. Among the most efficient β-diketonates, complexes of general formula $[Ln(\beta\text{-dike})_3L]$ can be found, where L usually is a neutral bi-dentate ligand such as 1,10-phenantroline or a bis-phosphine oxide.

The simplest β-diketonate is acetylacetonate (acac), but many substituents such as aromatics, etero-aromatics and halides can be used instead of two methyl groups. [48] Antenna effect can be due both to β-diketonates and aromatic Lewis bases. The energy transfer depends upon the relative energy of the ligand triplet state and the lanthanide resonance level.

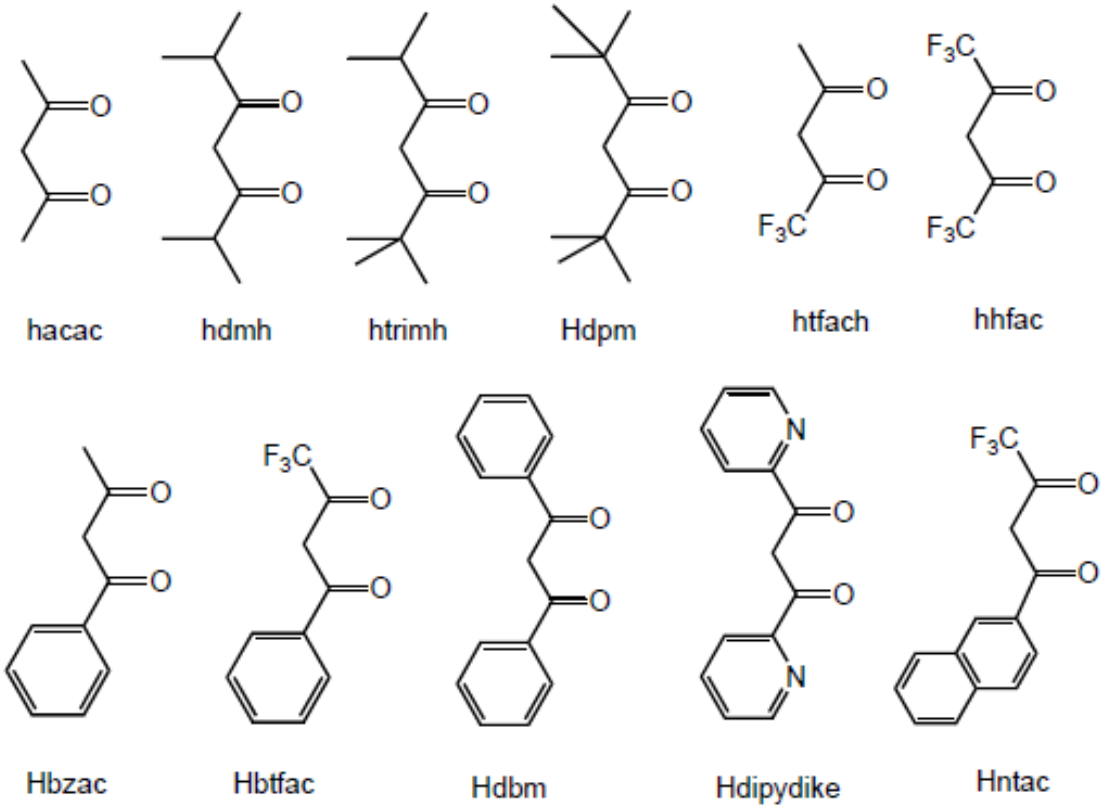

Figure 13. Some examples of β-diketonates.

Intersystem crossing between singlet to triplet state of the ligand is strongly influenced by the different substituents. In general, β-diketonates with combinations of aromatic and aliphatic substituents show higher efficiency in the energy transfer mechanisms and a higher luminescence of the relative complexes, probably due to a non-symmetric environment around the metal ion. [51] Organic fluorinated chains also improve luminescence, because of the formation of a hydrophobic shell around the complex, avoiding interaction with water. One of the most common Lewis bases is 1,10-phenantroline (phen), but many other N and O-donor ligands such as 2,2'-bipiridine, 2,2',6',2''-terpyridine, phosphine oxides, sulphoxides and poly-dentate ethers can be used.

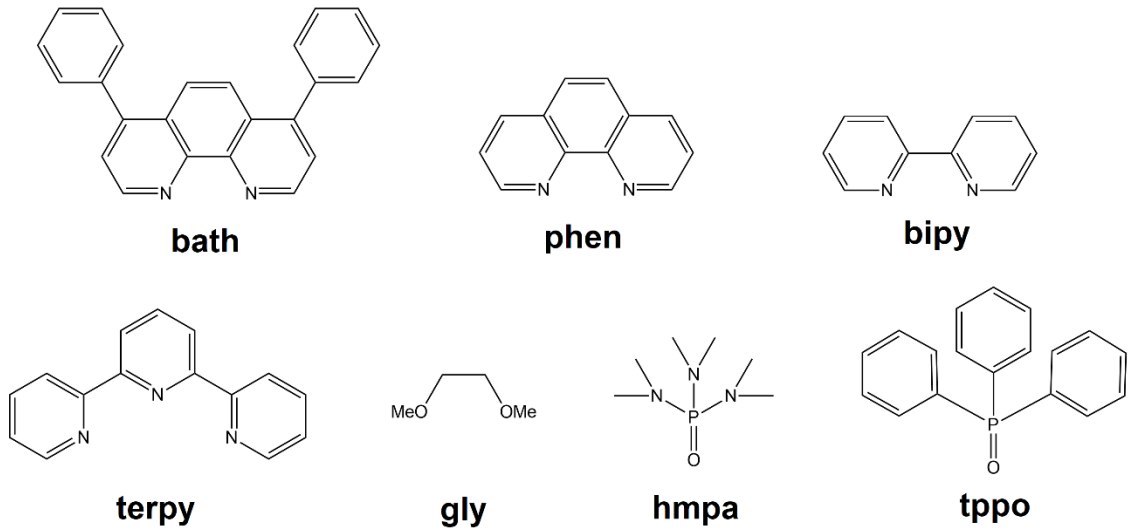

Figure 14. Examples of Lewis acids used as neutral ligands in lanthanide complexes.

The first synthesis for the preparation of β-diketonate complexes dates back in 1961 and it is known as "piperidine method": piperidine is added to a solution containing $LnCl_3$ and β-diketone in water, ethanol or methanol. The method has been later optimized by Crosby and Whan in 1962. [52] Alternatively, sodium salts of β-diketones can undergo metathesis with $LnCl_3$. Direct reaction between the Ln^0 and neutral β-diketones with hydrogen evolution has also been reported for the preparation of $Sm(acac)_3$. [53] When starting a synthesis from nitrate salts of formula $Ln(NO_3)_3{\cdot}3H_2O$, nitrate groups can remain part of the coordination sphere, and additional ligands can be used to replace water molecules. THF molecules usually coordinate Ln ions in solution and the lability of the bond makes THF adducts versatile reagents for subsequent substitutions. [N,O]-donor ligands are also often used. For example, the dipicolinate ligand (DPA, pyridine-2,6-dicarboxylate) can be obtained from dipicolinic acid (pyridine-2,6-dicarboxylate) and resulted to be an excellent ligand for Ln^{3+} ions. Salts of complexes like $M_3[Eu(DPA)_3]$ with different inorganic and organic cations (Li^+, Na^+, K^+, Rb^+, Cs^+, NH_4^+, and pyridinium) have been synthesized and showed interesting luminescence properties. [54] The ligand coordinates the metal thanks to the doublets on the nitrogen atom and the oxygen atoms; three ligands can therefore saturate the coordination sphere with a coordination number of nine, avoiding the addition of water molecules which might reduce the emission properties of the complex. Ligands of similar structure have been used to prepare water soluble complexes of Eu^{3+} and Tb^{3+}. Thanks to their water stability and long emission lifetime they are studied as potential luminescent probes for biological systems. [55] Many of

these ligands with different substituent on the aromatic ring have been also studied for luminescence sensitization and for potential grafting with biological materials. [56]

Cyclens and cryptand-like ligands are also able to coordinate Ln^{3+} thanks to their cavity-like geometry. The coordination chemistry of these ligands strongly depends upon the ionic radii of the lanthanides. The structure of these systems enables the protection of the metal centre from water molecules and from the formation of polynuclear species, improving in this sense the luminescence properties. Cyclens and tris-bipyridine cryptates have also been functionalized with amides, carboxylates, phosphates, and the respective complexes can be neutral, anionic or cationic depending on the ligand charge. [57]

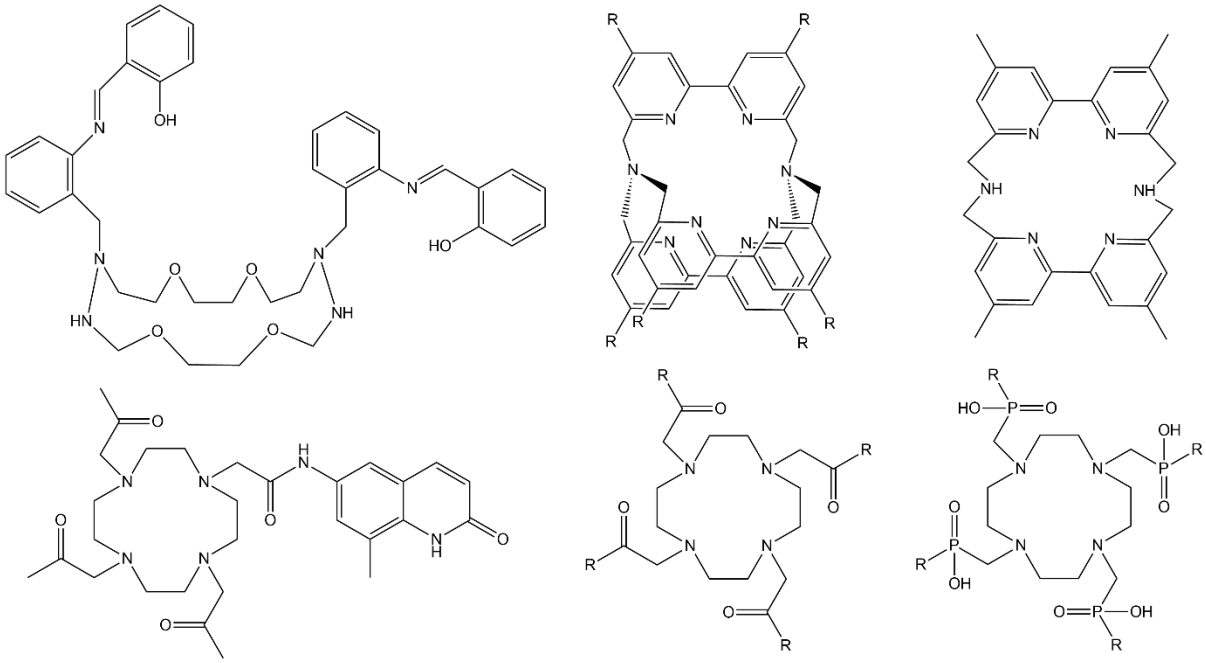

Figure 15. Examples of cyclens used as ligands.

Poly(pyrazolyl)borates, also known as *scorpionates*, can be also used. [58] The coordination is possible thanks to the doublets on the nitrogen atoms and the chelating effect. Possible substitutions on 3 and 5 positions of the aromatic rings make them versatile structures and enable modifications of the steric and electronic properties of the complexes. The first examples had the general formula $[Ln(HBPz_3)_3]$ (Pz = pyrazol-1-yl). [59]

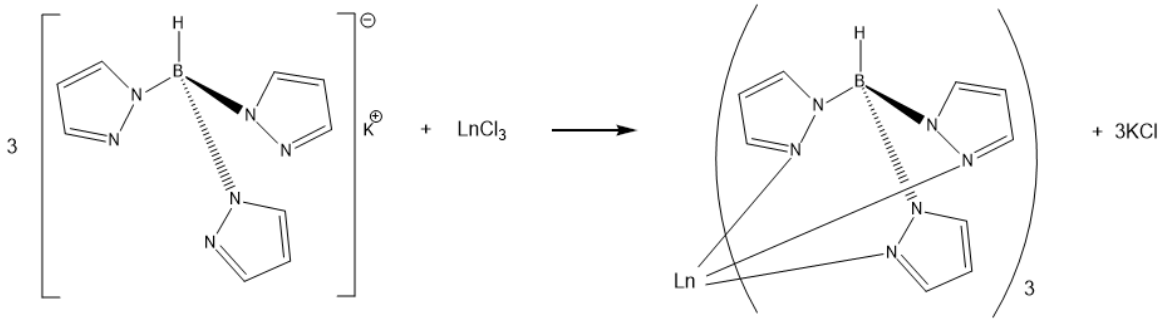

Figure 16. Synthesis of homoleptic tris(pyrazolyl)borate lanthanide complexes.

This family of ligands can act as antenna for some lanthanide ions showing strong luminescence in the visible and in the IR region. The coordination number of nine means the saturation on the coordination sphere, avoiding interaction with water molecules and increasing the luminescence efficiency. [60]

1.3.7 Materials and matrices

Powder samples are not directly used for most of the applications. Lanthanide luminescence complexes can be hosted in different matrices, increasing stability, avoiding concentration quenching and interaction with water molecules. Two different host matrices can be used: inorganic and polymeric. Among the most common inorganic matrices transparent alumina-silicate are found. Sol-gel processes allow to use low temperature, avoiding the decomposition of the complexes or the organic ligands. This route comprises a series of hydrolysis and condensations reactions, starting from a silicon alkoxide in the presence of water and an acid or a base as catalyst. The first example of doped silica gel dates back in 1993, when Matthews and co. prepared luminescence glasses using $[Eu(tta)_3(H_2O)_2]$ and $(pipH)[Eu(tta)_4]$ as complexes. [61] Many doped sol-gel glasses with europium β-diketonate complexes show higher luminescence than the analogues doped with $EuCl_3$, and they also exhibited longer lifetime than the free complexes. [62] The disadvantages of these materials are their fragility, the poor solubility of the complexes and the persistence of water molecules in the inorganic network. Organic/inorganic hybrid materials called *ormosils* (*organically modified silicates*) were then prepared. In these organo-silicates, the organic molecules can be either blended (Class I materials) or covalently bonded (Class II materials) to the inorganic matrices. [63] Alternatively, zeolites in which lanthanide complexes such as $[Ln(\beta\text{-dike})_2]^+$ and $[Ln(\beta\text{-dike})]^{2+}$ were introduced, replacing the inorganic cations in the network, were studied. [64] Polymeric

doped materials are usually more flexible, lighter, resistant, and can be produced with desired shapes. Polymers such as polymethylmethacrylate (PMMA), polyvinylalcohol (PVA), polyethylene (PE), polystyrene (PS), polyurethanes, polyesters, polycarbonates, polyimides and epoxy resins can be used. There are many different routes for the preparation of doped polymers, and they are usually cheaper and more affordable than sol-gel derivatives. Fluorinated or deuterated polymers such as poly(hexafluoro isopropyl methacrylate) (P-FiPMA) and poly(methylmethacrylate) (PMMA-d_8) are used for emission in the IR regions. The simplest procedure involves the dissolution of the complex and the polymer in a solvent, which is then eliminated by slow evaporation. Alternatively, the complex is dissolved directly in a monomer solution and the polymerization occurs with the addition of an initiator. In this case, the complex becomes part of the copolymer chains. Finally, the polymer chains can be functionalized with an antenna ligand, able to coordinate the lanthanide precursors. [49] Lanthanide complexes may be also dissolved in liquid matrices such as liquid-crystals. Photoluminescent liquid crystals were obtained with different neutral β-diketonate complexes such as $[Eu(tta)_3(phen)]$ in N-(4-methoxybenzylidene)-4-butylaniline (MBBA) and 4-n-pentyl-4-cyanobiphenyl (5CB) liquid crystals, or by stabilizing anionic complexes such as $[Eu(tta)_4]^-$ or $[LnCl_6]^{3-}$ with N-butyl-N'-methyl-imidazole. [65]

1.3.8 Applications

Over the past years, lanthanide(III) complexes have been widely used in advanced technologies. [49] [66] Their magnetic and optical properties have been exploited in the field of medicine [67], as sensors and biological probes [68], and for magnetic and optical imaging [69], luminescent electronic devices and lasers. [70] Their nature of Lewis acids also increased their use as catalyst in organic synthesis, bioorganic chemistry and homogeneous catalysis [71] [42].

Luminescent emissions are narrow, easy to recognize, and the emission colours cover the entire spectrum from UV to visible and near-infrared. Their use in medicine is due to the potentially high selectivity towards different tissues, to the presence of water or lipids, and thus to the ability of identify specific molecules and interactions. Thanks to the longer lifetime compared to autofluorescence of a biological sample or organic molecules, luminescence can be exploited for practical applications such as imaging microscopy and lifetime mapping in

biological environment. [72] Among the most studied ions Eu^{3+} and Tb^{3+} need to be cited, because of their long lifetime, narrow emissions in the red and green region of the spectra respectively, and the relatively small toxicity in human body. [73] Gadolinium(III) complexes are often used in clinical MRI to increase the contrast by highlighting differences among tissues with different proton density, relaxation times, rates of water diffusion, or chemical shifts. [74] Even NIR emitters, such as pyridine-based complexes of Nd^{3+} and Yb^{3+} received particular interest as diagnostic tools for bio-medical applications. [75]

In analytic chemistry, lanthanide photoluminescence is also useful in the identification of ions such as nitrates, chlorides, and acetates, thanks the sensibility of the emission of some Eu(III) complexes to the presence of such species. [76] Some Tb^{3+} complexes are instead sensible to pH variations, because of the luminescence quenching due to protonation. [77] Narrow emissions are also useful for the preparation of lasers, and the long lifetime favours the population inversion and the stimulated emission. The most known example is Nd:YAG laser, where Nd^{3+} is used and dopant, partially substituting Y^{3+} atoms, and generating a strong NIR emission at 1064 nm. Stimulated emission is also exploited in erbium-doped fiber amplifiers. [70] [78]

Lanthanide complexes also find applications in silicon based solar cells, aiming to improve the light conversion and to cover the whole solar spectrum. Some of the most studied phenomena to improve the conversion efficiency are down-shifting, down-conversion and up-conversion. For these purposes, lanthanide complexes with antenna ligands and large absorption in the UV-vis region of the spectra have great potentiality thanks to high quantum yields, great separation between the absorption and emission regions, and the presence of discrete energy levels. [79]

The production of luminescent devices, such as television screens, computer and smartphone monitors and low consumption lamps are one of the most intriguing applications. Most of these devices require the ability to give electroluminescence in different matrixes. Many lanthanide complexes showing electroluminescence phenomena are exploited for the production of Organic Light Emitting Diodes (OLEDs). OLEDs are gaining more and more attention over the years because of their flexibility, lightness, and the low supply voltage

required. Besides the excellent colours brilliance and contrast, some drawbacks such as high production costs and low durability need to be faced. [80]

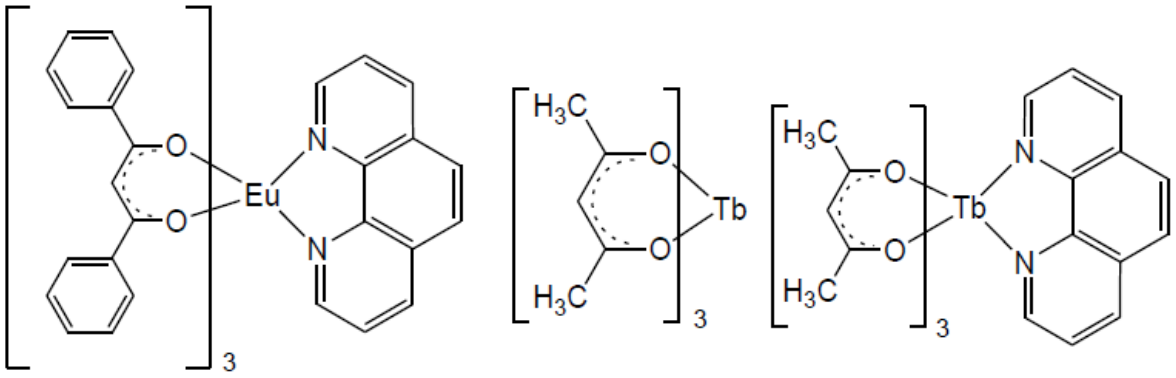

[Eu(dbm)$_3$(phen)] [Tb(acac)$_3$] [Tb(acac)$_3$(phen)]

Figure 17. Some lanthanide complexes used in OLEDs.

1.4 Phosphoramide O-donor ligands

1.4.1 Manganese

The first examples of phosphoramide ligands for d-block metals date back in the '70s where the proprieties of hexamethylphosphoric triamide (hmpa), nonamethylimidodiphosphoramide (nipa), and phenylbis(dimethylamino)phosphine oxide (papo) as ligands were studied. Further information about structures and configurations were obtained for [M(hmpa)$_4$](ClO$_4$)$_2$ complexes (M= Mn(II), Fe(II), Co(II), Ni(II), Cu(II), Zn(II)), and the manganese(II) derivative showed a tetrahedral geometry. [81] Recently, green-emitting manganese (II) complexes with phosphoramide and phenylphosphonic diamide ligands were prepared [82] and their tetrahedral geometry was confirmed by x-ray diffraction measurement on [MnX$_2$(hmpa)$_2$] (X = Cl, Br) and [MnBr$_2${O=PPh(NMe$_2$)$_2$}$_2$]. [83]

1.4.2 Lanthanides

Phosphoramide ligands fit perfectly with the lanthanide affinity for hard ligands and electronegative donor atoms. Hexamethylphosphoramide and its derivatives have been widely used as ligands in the chemistry of lanthanide elements. The first examples date back to the 60' where complexes of lanthanides of the type [LnCl$_3$(hmpa)$_3$] and [Ln(hmpa)$_3$](ClO$_4$)$_3$ have been prepared and studied because of the unusual coordination number and the few

studies on monodentate ligands. [84] Later studies also showed the formation of complexes such as $[LnCl_3L_3]$ where L is trimorpholinophosphine oxide, but the luminescence properties of the obtained complexes were not investigated. [85] Bidentate ligands such as nipa (nonamethylimidodiphosphoramide, $[(CH_3)_2N]_2P(O)N(CH_3)P(O)[N(CH_3)_2]_2$)) and ompa (octamethylpyrophosphoramide, $[(CH_3)_2N]_2P(O)OP(O)[N(CH_3)_2]$)) were also used to prepare complexes of general formula $[Ln(ClO_4)(nipa)_3]$, $[Ln(ompa)_2(NO_3)_3]$ and $[Ln_2(ompa)_3(NO_3)_6]$. [86] The phosphoramidate ligand TIP (O,O',N-triisopropyl phosphoramidate, $[(OC_3H_7)_2P(O)(NHCH_3)]$) was used to prepare $[Ln(TIP)_3(NO_3)_3]$ complexes. [87] Anionic ligands like picrate were also useful to prepare $[Ln(pic)_3(hmpa)_3]$ complexes, [88] while further studies on the $[LnCl_3(hmpa)_3]$ complexes showed reversible *fac–mer* isomerization by variable temperature ^1H NMR spectroscopy. [89] Lanthanide complexes with phosphoramide ligands to be used and studied as emitting molecules were considered later, and usually only as heteroleptic complexes; some examples are Tb(III)-dibenzoylmethanate complexes such as $[Tb(dbm)(NO_3)_2(hmpa)_2]$ [90], or $[Eu(NO_3)_3(hmpa)_3]$ and $[Eu(NO_3)_2(hmpa)_3]NO_3{\cdot}HQuin$ (HQuin=quinaldic acid), these last showing intense photoluminescence and triboluminescence. [91] Complexes of general formula $[Ln(depma)(NO_3)_3(hmpa)_2]$ (depma = 9-diethylphosphono-methylanthracene; Ln = Dy, Gd) are examples of magneto-optic materials. [92] Ligands such as 1,3-dimethyl-2-phenyl-1,3-diazaphospholidine-2-oxide and related species were proposed as efficient extraction agents for group 3 and lanthanide ions. However, the coordination chemistry of such phosphoramide and phosphine oxide ligands towards lanthanide ions was poorly explored. [93] The X-ray structure of the β-diketonate Eu(III) heptacoordinate compound $[Eu(dbm)_3(hmpa)]$ has been reported by Panin et al. [94], and comparable phenylphosphonic diamide derivatives were recently studied by the research group were this thesis was developed.

1.5 Aim of the thesis

Phosphoramide ligands turned out the be suitable ligands to prepare manganese (II) and lanthanide (III) complexes. Especially for manganese, little variations on the ligand structure can lead to heavy changes to the coordination ability, the absorption coefficient, the energy transfer efficiency, and finally to the geometry of the complex.

The use of phosphoramide ligands based on the hexamethylphosphoramide skeleton is well-known and studied, but there are only few examples of neutral manganese or lanthanide luminescent complexes with phosphoramide or arylphosphonic diamide ligands. Complexes such as $MnX_2[O=P(NMe_2)_2Ph]_2$ and $MnX_2[O=P(NMe_2)_3]_2$ revealed a quite good air-stability in the solid state, and the P=O fragment showed a strong affinity for lanthanides too, with a good luminescence of nitrate and dibenzoylmethanate phosphoramide complexes.

These promising optical properties triggered me to study new ligands with similar chemical proprieties and potentially higher suitability for preparation of luminescent complexes, in order to improve the energy transfer mechanism, to enhance and shift the absorption region to lower energy wavelengths, and to study the effects of the ligands to the coordination geometry.

Phosphoramide precursors show a high versatility and reactivity, making them a perfect platform for further modifications. Based on the coordination properties of the simple hexamethylphosphoramide, the first part of this work aimed to the synthesis of similar ligands, by replacing one $[NMe_2]$ fragment with light-harvesting groups and creating more rigid structures, trying to reduce the non-radiative decay. Secondly, the coordination ability of the newly prepared ligands (L) were tested, preparing β-diketonate Eu(III) heptacoordinate/ octacoordinate compounds $[Eu(\beta\text{-dike})_3L]$ and $[Eu(\beta\text{-dike})_3L_2]$ and both octahedral and tetrahedral Mn(II) complexes $[MnX_2L_2]$.

2. EXPERIMENTAL PART

2.1 Instruments and analytical techniques

Many of the syntheses requiring inert atmosphere (O_2< 5 ppm, H_2O< 1ppm) were performed in a glove-box *MBraun Labstar*, with an air purification system and automatic pressure control, using nitrogen as inert gas. IR spectra were obtained within 4000 and 400 cm^{-1} with a *Perkin-Elmer®SpectrumOne* spectrometer. Stable powder samples were dispersed in KBr. In the case of moisture-sensitive samples layers of the power were deposited between two KBr windows in glove-box and the system sealed to avoid any interaction with the atmosphere. UV-vis spectra were registered at room temperature with a *Perkin Elmer Lambda®35* spectrophotometer, between 220 and 700 nm. Most of the samples were prepared as dichloromethane solutions with known concentration.

Preliminary photoluminescence measurements (PL) were performed on solid state samples at room temperature with an *OceanOptics Flame T* spectrophotometer. For these measures, the excitation wavelength was either at 280 nm or 375 nm, the emission spectra registered between 400 and 1035 nm, and the reflected radiation cut at 395 nm with a longpass filter. More advanced photoluminescence *(PL),* photoluminescence excitation (PLE), and lifetime measurements were carried out at the University of Luleå in Sweden, with a *Edimbourgh Instruments FLS980* spectrophotofluorimeter using continuous and pulsed xenon lamps as light sources. Additional PL, PLE and lifetime measurements were carried out with a *Horiba Jobin Yvon Fluorolog-3* spectrophotofluorimeter. The instrument uses a xenon lamp as light source with continuous emission. The desired wavelength is tuned by a *Czerny-Turner* double-grating monochromator. A LED pulsed source centered at 377 nm was used to obtain the lifetime values. The detection system includes a single-grating monochromator *iHR320* coupled with a *Hamamatsu R928* photomultiplier. The Multi-Channel Scaling (MCS) techniques was used for the lifetime determinations.

NMR spectra were registered with the spectrometers *Bruker Avance 300* and *Bruker Ascend 400,* with a frequency of 300.13 MHz and 400.13 MHz for protons, respectively. The partially deuterated fraction of the solvent was quoted with respect to tetramethylsilane and used as internal reference for ^{1}H and $^{13}C\{^{1}H\}$ spectra. $^{31}P\{^{1}H\}$ chemical shifts are reported with respect

to 85% H_3PO_4, with downfield shifts considered positive. ^{19}F chemical shifts are referred to $CFCl_3$. $CDCl_3$, $(CD_3)_2CO$ and $(CD_3)_2SO$ were used as solvents, obtained by Sigma-Aldrich and Euriso-Top. Naphtyl fragments were numbered as the bromonaphtalene precursors.

Melting points were obtained with a BÜCHI B-535 apparatus. Magnetic susceptibilities were measured on solid samples at room temperature with a MK1 magnetic susceptibility balance (Sherwood Scientific Ltd) and corrected for diamagnetic contribution by means of tabulated Pascal's constants [95].

2.2 Synthesis of the ligands

2.2.1 Synthesis of *N,N,N',N'*-tetramethyl-*P*-phenylphosphonic diamide, $O=P(NMe_2)_2Ph$

The synthesis was performed with slight modifications with respect to a reported procedure. [96] In a 100 ml flask 20 g of $[NH_2Me_2]Cl$ (0.245 mol) and the stochiometric amount of NaOH (9.8 g) were poured. The two solid reagents were mixed with a magnetic stirrer under inert atmosphere of N_2. This first flask was connected to a second containing a solution of 2.8 mL of phenylphosphonic dichloride ($POCl_2Ph$, 10 mmol) in 50 mL of CH_2Cl_2 and kept at room temperature. The two flasks were separated by solid NaOH filter. The solid mixture was then heated at 200° C and gaseous dimethylamine was formed. The gas bubbled into the second flask containing the CH_2Cl_2 solution, reacting with $POCl_2Ph$. At the end of the reaction, the organic phase was washed twice with 20 ml of water to eliminate the by-product dimethylammonium hydrochloride. The solution was dried over anhydrous sodium sulphate and the solvent was evaporated under reduced pressure. The product is a white solid. Yield > 85%.

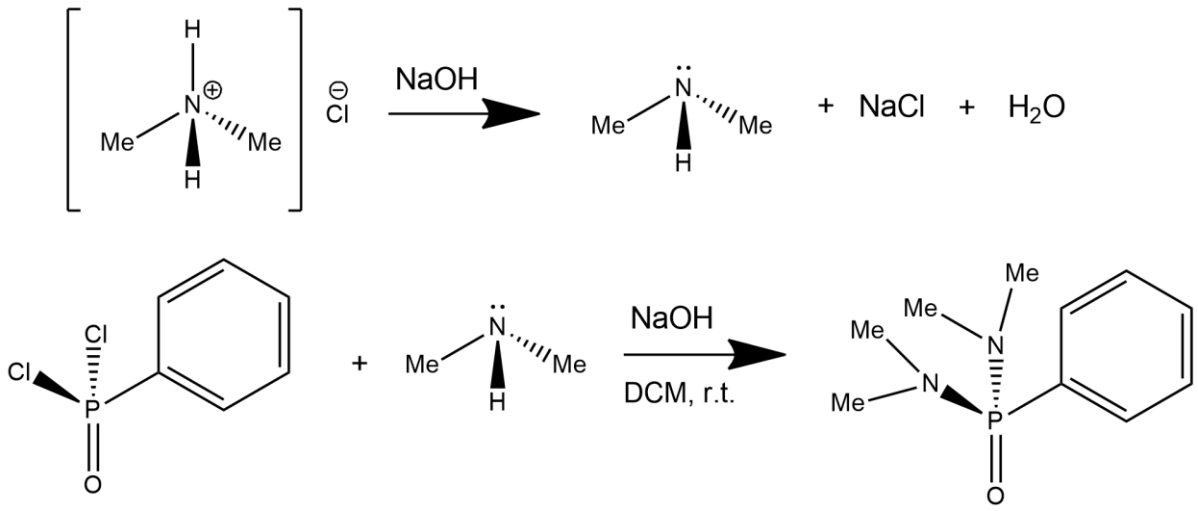

Figure 18. Synthesis of N,N,N',N'-tetramethyl-P-phenylphosphonic diamide, O=P(NMe$_2$)$_2$Ph.

Characterization of O=P(NMe$_2$)$_2$Ph

IR (KBr, cm^{-1}): 3055 m, 2991 m (aromatic $\nu_{C\text{-}H}$), 2928 m, 2894 m, 2872 m, 2839 m ($\nu_{C\text{-}H}$), 1640/1588 w, 1484 w (aromatic $\nu_{C\text{-}C}$), 1458 w, 1441 m ($\delta_{C\text{-}H}$), 1280-1287 m (in-plane aromatic $\delta_{C\text{-}H}$), 1203 s ($\nu_{P\text{-}O}$), 1114 sh, m ($\nu_{C\text{-}N}$), 969 s ($\nu_{P\text{-}N}$), 737 w (out-of-plane aromatic $\delta_{C\text{-}H}$).
NMR ^{1}H NMR ($CDCL_3$, 298 K), δ: 7.71 (m, 2H, Ph-H), 7.43 (m, 3H, Ph-H, Ph-H), 2.60 (d, 12H, J_{PH} = 10 Hz, N-Me). $^{31}P\{^1H\}$ NMR ($CDCL_3$, 298 K), δ: 29.68 (FWHM = 2 Hz).
UV-VIS (CH_2Cl_2, r.t., nm): 272 (ε = 976 M^{-1}cm^{-1}), 265 (ε = 809 M^{-1}cm^{-1}), 258 (ε = 551 M^{-1}cm^{-1}), <250.

2.2.2 Synthesis of *N,N,N',N'*-tetramethyl-*P*-naphtalen-1-ylphosphonic diamide, O=P(NMe$_2$)$_2$(1-Naph), and *N,N,N',N'*-tetramethyl-*P*-naphtalen-2-ylphosphonic diamide, O=P(NMe$_2$)$_2$(2-Naph)

These syntheses were performed with the same procedure in a glove-box under N_2 inert atmosphere. In the inner part of a double-wall reactor, 2.795 g (13.5 mmol) of the proper bromonaphthalene precursor were dissolved in 30 ml of THF. Cold gaseous N_2 was then continuously fluxed in the outer part of the reactor. Once the system reached the desired temperature of -40 °C, 8.5 mL of 1.6 M butyllithium solution (13.5 mmol) in hexanes were slowly added to the THF solution. The as-formed Li-1-naphthalene (or Li-2-naphthalene) suspension in THF was then slowly added into a second double-wall reactor, containing a stochiometric amount (2 ml) of *N,N,N',N'*-tetramethylphosphorodiamidic chloride

$P(O)Cl(NMe_2)_2$ in 20 of THF at -40 °C. The reaction mixture was allowed to warm to room temperature. After 12h, the reaction was quenched with cold water, most of the solvent evaporated under reduced pressure and the product extracted with diethyl ether (3 x 10 mL). The organic fraction was then dried over anhydrous sodium sulphate, filtered and washed with cyclohexane. Both products are a pale-yellow oils. Yield > 76% in both the cases.

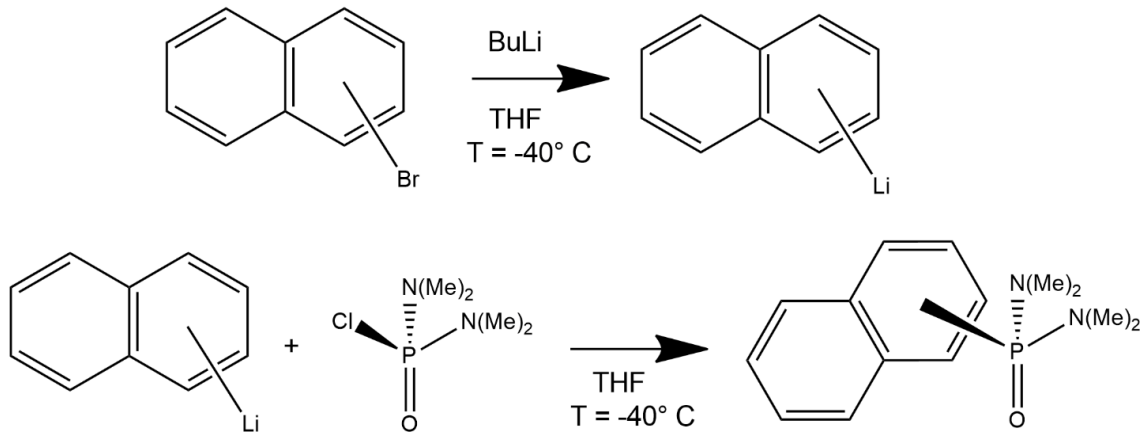

Figure 19. Synthesis of N,N,N',N'-tetramethyl-P-naphtalen-1-ylphosphonic diamide, $O=P(NMe_2)_2$(1-Naph), and N,N,N',N'-tetramethyl-P-naphtalen-2-ylphosphonic diamide, $O=P(NMe_2)_2$(2-Naph).

Characterization of $O=P(NMe_2)_2$(1-Naph)

IR (KBr, cm^{-1}): 3096 m, 3058 m, 3041 m, 3003 m, (aromatic ν_{C-H}), 2922 m, 2903 m, 2850 m, 2803 m (ν_{C-H}), 1622/1592 w, 1505 w, 1483 w, (aromatic ν_{C-C}) 1457 m (δ_{C-H}), 1301-1290 m (in-plane aromatic δ_{C-H}), 1188 s (ν_{P-O}), 1144 m (ν_{C-N}), 978 s (ν_{P-N}), 816 m, 783 m (out-of-plane aromatic δ_{C-H}), 692 s (out-of-plane aromatic δ_{C-C}).

NMR ^{1}H NMR ($CDCl_3$, 298 K), δ: 8.80 (d, 1H, J_{HH} = 8.5 Hz, Naph-H), 7.98 (d, 1H, J_{HH} = 8.3 Hz, Naph-$H_{(4)}$), 7.88 (dt, 1H, J_{HH} = 8.1 Hz, J_{HH} = 1.4 Hz, Naph-H), 7.70 (ddd, 1H, J_{PH} = 16.0 Hz, J_{HH} = 7.0 Hz, J_{HH} = 1.3 Hz, Naph-$H_{(2)}$), 7.60 (ddd, 1H, J_{HH} = 8.5 Hz, J_{HH} = 6.8 Hz, J_{HH} = 1.4 Hz, Naph-H), 7.53 (ddd, 1H, J_{HH} = 8.1 Hz, J_{HH} = 6.8 Hz, J_{HH} = 1.3 Hz, Naph-H), 7.49 (ddd, 1H, J_{HH} = 8.3 Hz, J_{HH} = 7.0 Hz, J_{PH} = 2.7 Hz, Naph-$H_{(3)}$), 2.75 (d, 12H, J_{PH} = 9.3 Hz, N-Me). $^{31}P\{^1H\}$ NMR ($CDCl_3$, 298 K), δ: 30.71 (FWHM = 2 Hz). $^{13}C\{^1H\}$ NMR ($CDCl_3$, 298 K), δ: 134.02 (Naph-C_{ipso}, J_{CP} = 9.9 Hz), 133.97 (Naph-C_{ipso}, J_{CP} = 10.8 Hz), 132.58 (Naph-$CH_{(4)}$, J_{CP} = 3.1 Hz), 131.75 (Naph-$CH_{(2)}$, J_{CP} = 9.4 Hz), 128.57 (Naph-CH, J_{CP} = 1.6 Hz), 128.05 (Naph-$C_{ipso(1)}$, J_{CP} = 152.2 Hz), 127.37 (Naph-CH, J_{CP} = 4.4 Hz), 127.33 (s, Naph-CH), 126.28 (s, Naph-CH), 124.47 (Naph-$CH_{(3)}$, J_{CP} = 15.2 Hz), 36.73 (N-Me, J_{CP} = 4.5 Hz).

UV-vis (CH_2Cl_2, r.t., nm): 355 (ε = 2400 $M^{-1}cm^{-1}$), 318 (ε = 4500 $M^{-1}cm^{-1}$), 287 (ε = 19900 $M^{-1}cm^{-1}$), <250.

Characterization of O=P(NMe$_2$)$_2$(2-Naph)

IR (KBr, cm^{-1}): 3054 m, 2995 m (aromatic ν_{C-H}), 2927 m, 2894 m, 2848 m, 2804 m (ν_{C-H}), 1627/1591 w, 1500 w, 1480 w, (aromatic ν_{C-C}) 1459 m (δ_{C-H}), 1291-1274 m (in-plane aromatic δ_{C-H}), 1191 s (ν_{P-O}), 1087 sh, m (ν_{C-N}), 974 s (ν_{P-N}), 859 m, 824 m, 741 m (out-of-plane aromatic δ_{C-H}), 696 s (out-of-plane aromatic δ_{C-C}).

NMR ^{1}H NMR (acetone-d_6, 298 K), δ: 8.41 (d, 1H, J_{PH} = 13.6 Hz, Naph-$H_{(1)}$), 8.06 (dd, 1H, J_{HH} = 7.8 Hz, 1.5 Hz, Naph-H), 8.01 (dd, 1H, J_{HH} = 8.4 Hz, J_{PH} = 3.1 Hz, Naph-$H_{(4)}$), 7.98 (d, 1H, J_{HH} = 7.8 Hz, Naph-H), 7.78 (ddd, 1H, J_{HH} = 8.4 Hz, 1.5 Hz, J_{PH} = 9.7 Hz, Naph-$H_{(3)}$), 7.64 (td, 1H, J_{HH} = 7.0, 1.5, Naph-H), 7.60 (td, 1H, J_{HH} = 7.0, 1.5, Naph-H), 2.64 (d, 12H, J_{PH} = 10.1 Hz, N-Me). $^{31}P\{^1H\}$ NMR (acetone-d_6, 298 K), δ: 28.49 (FWHM = 3 Hz). $^{13}C\{^1H\}$ NMR (acetone-d_6, 298 K), δ: 134.57 (Naph-C_{ipso}, J_{CP} = 2.4 Hz), 133.69 (Naph-$CH_{(1)}$, J_{CP} = 8.5 Hz), 132.87 (Naph-C_{ipso}, J_{CP} = 14.2 Hz), 128.78 (Naph-CH), 128.77 (Naph-$C_{ipso(2)}$, J_{CP} = 151.6 Hz), 127.83 (Naph-CH, J_{CP} = 12.3 Hz), 127.72 (Naph-CH), 127.66 (Naph-CH), 127.57 (Naph-CH, J_{CP} = 8.7 Hz), 126.59 (Naph-CH), 35.62 (N-Me, J_{CP} = 3.3 Hz).

UV-vis (CH_2Cl_2, r.t., nm): 324 (ε = 7900 $M^{-1}cm^{-1}$), 315 (ε = 6500 $M^{-1}cm^{-1}$), 309 (ε = 8000 $M^{-1}cm^{-1}$), 290 (ε = 39300 $M^{-1}cm^{-1}$), 279 (ε = 59100 $M^{-1}cm^{-1}$), < 266.

2.2.3 Synthesis of *N,N,N',N'*-tetramethyl-*P*-indol-1-ylphosphonic diamide, O=P(NMe$_2$)Ind

The synthesis was performed in glove-box under N_2 inert atmosphere, with slight modifications respect to a reported procedure. [97] In a 100 ml flask, 1.581 g of indole was dissolved in 20 ml of THF. A stochiometric amount of potassium *tert*-butoxide (1.514 g) was then slowly added to the solution under stirring. The as-obtained suspension was then slowly added to a second 100 ml flask, containing a stochiometric amount (2 ml) of *N,N,N',N'*-tetramethylphosphorodiamidic chloride in THF. After 12h the solvent was evaporated under reduced pressure. The obtained product was re-dissolved in a small amount of CH_2Cl_2 and the solution was cleared by centrifugation to eliminate KCl as by-product. The product precipitated by slow addition of cyclohexane and was then recovered by filtration on gooch. The product is a pale-yellow solid. Yield > 52%.

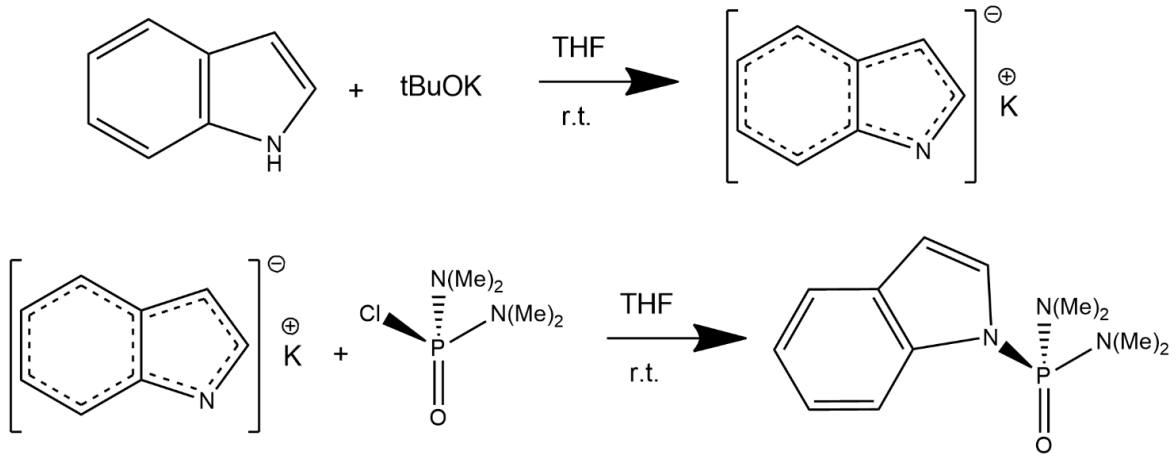

Figure 20. Synthesis of N,N,N',N'-tetramethyl-P-indol-1-ylphosphonic diamide, O=P(NMe$_2$)Ind.

Characterization of O=P(NMe$_2$)$_2$Ind

IR (KBr, cm^{-1}): 3126 m, 3102 m, 3072 w, 3000 m (aromatic $\nu_{C\text{-}H}$), 2933 m, 2856 m, 2819 m, 2810 m ($\nu_{C\text{-}H}$), 1655 w, 1579 w, 1517 w, 1488 w (aromatic $\nu_{C\text{-}C}$ and $\nu_{C\text{-}N}$), 1450 m, 1437 w ($\delta_{C\text{-}H}$), 1310-1269 m (in-plane aromatic $\delta_{C\text{-}H}$), 1227 s ($\nu_{P\text{-}O}$), 1160 sh, m ($\nu_{C\text{-}N}$), 997-987 s ($\nu_{P\text{-}N}$), 780-740 w (out-of-plane aromatic $\delta_{C\text{-}H}$), 678 s (out-of-plane aromatic $\delta_{C\text{-}C}$).

NMR ^{1}H NMR ($CDCL_3$, 298 K) δ: 7.94 (m, 1H, J_{HH} = 8.1 Hz, Ind-$H_{6\text{-ring}}$), 7.61 (m, 1H, J_{HH} = 7.7 Hz Ind-$H_{6\text{-ring}}$), 7.30-7.18 (m, 3H, Ind-H), 6.64 (m, 1H, Ind-$H_{5\text{-ring}}$), 2.73 (d, 12H, N-Me, J_{PH} = 10.2 Hz). $^{31}P\{^1H\}$ NMR ($CDCL_3$, 298 K) δ: 14.73 (FWHM = 5 Hz).

UV-VIS (CH_2Cl_2, r.t., nm): 287 (ε = 5140 M^{-1}cm^{-1}), 260 max (ε = 20550 M^{-1}cm^{-1}).

2.2.4 Synthesis of 1,3-dimethyl-2-phenyl-1,3-diazaphospholidine-2-oxide, O=P(MeNCH$_2$CH$_2$NMe)Ph

The synthesis was performed in glove-box under N_2 inert atmosphere, following a reported procedure. [98] In a 250 ml flask, 2 ml of phenylphosphonic dichloride ($POCl_2Ph$, 14.1 mmol) and 3.92 ml of triethylamine (NEt_3, 28.2 mmol) are dissolved in 20 ml of CH_2Cl_2. A solution containing 1.5 ml of *N,N'*-dimethylethylenediamine (14.1 mmol) in 10 ml of $CH_2Cl_2$was then slowly added to the first flask. After stirring overnight, the reaction was quenched with water to eliminate the by-product triethylammonium chloride, and the product was extracted with CH_2Cl_2. The organic solution was than dried over anhydrous sodium sulphate and filtered. The solvent was eliminated under reduced pressure and the same procedure was then repeated using EtOH as solvent. Evaporation of the solvent gave an oily product which was finally

dissolved in a small amount of CH_2Cl_2. The slow evaporation of the solvent gave pale-yellow crystals. Yield > 70%.

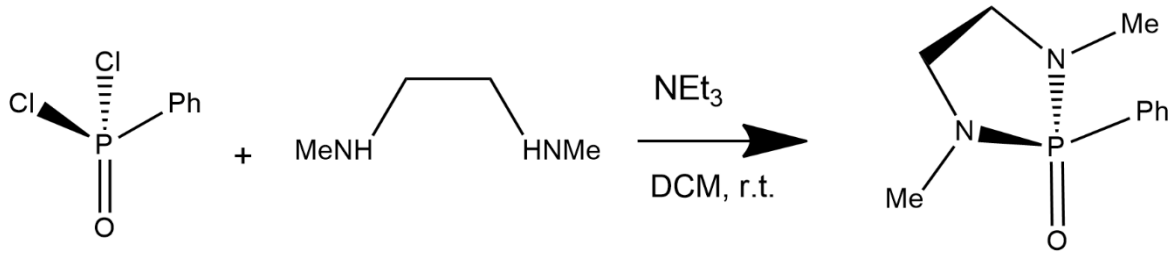

Figure 21. Synthesis of 1,3-dimethyl-2-phenyl-1,3-diazaphospholidine-2-oxide, O=P(NMeCH$_2$CH$_2$NMe)Ph.

Characterization of O=P(MeNCH$_2$CH$_2$NMe)Ph

IR (KBr, cm^{-1}): 3070 w, 3050 w (aromatic ν_{C-H}), 2990 w, 2957 w, 2887 w, 2855 w, 2810 w (ν_{C-H}), 1694 w, 1591 w, 1479 w (aromatic ν_{C-C}), 1456 m, 1437 w, 1432 w, 1380 w (δ_{C-H}), 1186 s (ν_{P-O}), 1127/1052 s (ν_{C-N}), 998 s (ν_{P-N}), 722 m (out-of-plane aromatic δ_{C-H}).
NMR ^{1}H NMR ($CDCL_3$, 298 K) δ: 7.55 (m, 2H, Ph-H_{meta}), 7.30 (m, 1H, Ph-H_{para}), 7.27 (m, 2H, Ph-H_{orto}), 3.22 (m, 2H, CH_2), 3.07 (m, 2H, CH_2), 2.35 (d, 6H, J_{HP}=10.0 Hz, N-Me). $^{31}P\{^1H\}$ NMR ($CDCL_3$, 298 K) δ: 29.29 (FWHM = 2 Hz). $^{13}C\{^1H\}$ NMR (acetone-d_6, 25°C), δ: 132.36 (d, J_{CP}=9.8 Hz, Ph-C_{meta}), 131.37 (d, J_{CP}=2.9 Hz, Ph-C_{para}), 130.10 (d, J_{CP}=156.3 Hz, Ph-C_{ipso}), 128.27 (d, J_{CP}=13.6 Hz, Ph-C_{orto}), 31.45 (d, J_{CP}=5.6 Hz, -CH_2CH_2-), 48.29 (d, J_{CP}=8.8 Hz, N-Me).
UV-VIS (CH_2Cl_2, r.t., nm): 273 (ε = 2730 $M^{-1}cm^{-1}$), 266 max (ε = 4600 $M^{-1}cm^{-1}$), < 260.

2.2.5 Synthesis of 1,3-diphenyl-2-phenyl-1,3-diazaphospholidine-2-oxide, O=P(PhNCH$_2$CH$_2$NPh)Ph

In a 250 ml flask, 2 ml of phenylphosphonic dichloride ($POCl_2Ph$, 14.1 mmol) and 3.9 ml of triethylammine (NEt_3, 28.2 mmol) are dissolved in 20 ml of CH_2Cl_2. A solution containing 2.99 g of *N,N'*-diphenylethylenediamine (14.1 mmol) in 10 ml of $CH_2Cl_2$was then slowly added to the first flask. After three days, the reaction mixture was washed with water to eliminate triethylammonium chloride. The organic solution was then dried over anhydrous sodium sulphate and filtered. The product precipitated from the CH_2Cl_2 solution by slow addition of Et_2O and it was then recovered by filtration on gooch. The product is a pale-yellow solid. Yield > 70%.

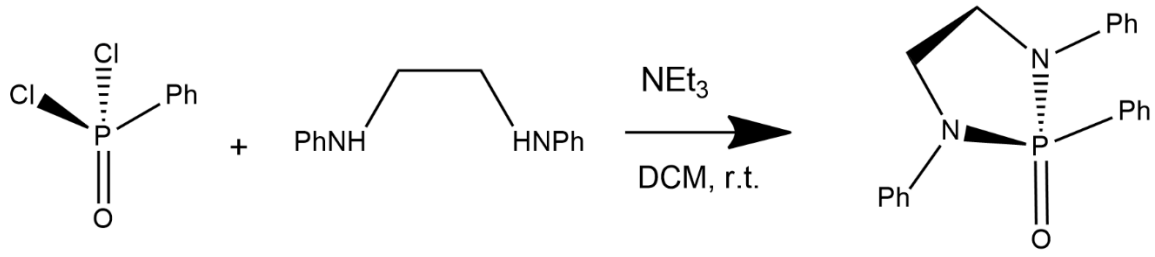

Figure 22. Synthesis of 1,3-diphenyl-2-phenyl-1,3-diazaphospholidine-2-oxide, O=P(NPhCH$_2$CH$_2$NPh)Ph.

Characterization of O=P(PhNCH$_2$CH$_2$NPh)Ph

IR (KBr, cm^{-1}): 3055 w, 3055 w (aromatic ν_{C-H}), 2963 w, 2919 w, 2887 w, 2849 w (ν_{C-H}), 1603 w, 1499 w (aromatic ν_{C-C}), 1437 w, 1432 w, 1380 w (δ_{C-H}), 1205/1191 s (ν_{P-O}), 1140/1048 s (ν_{C-N}), 933 s (ν_{P-N}), 692 s, 746 s (out-of-plane aromatic δ_{C-H}).

NMR ^{1}H NMR ($CDCL_3$, 298 K) δ: 7.84 (m, 2H, *P*-Ph-H$_{meta}$), 7.41 (m, 3H, *P*-Ph-H$_{para}$, *P*-Ph-H$_{orto}$), 4.02 (m, 4H, CH_2), 7.28-7.14 (m, 6H, *N*-Ph-H$_{meta}$, *N*-Ph-H$_{orto}$), 6.95 (m, 2H, *N*-Ph-H$_{para}$). ^{31}P{^{1}H} NMR ($CDCL_3$, 298 K) δ: 18.81 (FWHM = 2 Hz).

2.3 Synthesis of the complexes

All these syntheses were performed in glove-box under N_2 inert atmosphere at room temperature.

2.3.1 Synthesis of [MnX$_2${O=P(NMe$_2$)$_2$Ar}$_2$] where X=Cl, Br and Ar=1-Naph, 2-Naph

In a 100 ml flask, 1 mmol of the manganese salt, $MnCl_2$ or $MnBr_2$, were dissolved in 20 ml of EtOH. A small excess of the desired ligand (2.1 mmol), O=P(NMe$_2$)$_2$(1-Naph) or O=P(NMe$_2$)$_2$(2-Naph), was dissolved in 10 ml of EtOH and slowly added under stirring to the flask containing the manganese salt. After 12 hours under stirring the solvent was evaporated under reduced pressure, the obtained solid was dissolved in the minimum amount of CH_2Cl_2 and the solution was cleared by filtration. The product precipitated by addition of Et_2O and was then filtered and washed with fresh Et_2O. Yield > 80% in all the cases.

Characterization of [$MnCl_2${$O=P(NMe_2)_2$(1-Naph)}$_2$]

IR (KBr, cm^{-1}): 3057 m, 2999 m (aromatic ν_{C-H}), 2928 m, 2858 m, 2848 m, 2810 m (ν_{C-H}), 1622/1591 w, 1506 w, 1484 w, (aromatic ν_{C-C}) 1459 m (δ_{C-H}), 1302 m (in-plane aromatic δ_{C-H}), 1185 s (ν_{P-O}), 1140 m (ν_{C-N}), 1001-988 s (ν_{P-N}), 777 m, 749 m (out-of-plane aromatic δ_{C-H}).
Uv-vis (CH_2Cl_2, r.t., nm): 318 (ε = 2030 $M^{-1}cm^{-1}$), 314 (ε = 3030 $M^{-1}cm^{-1}$), 284 (ε = 20730 $M^{-1}cm^{-1}$), 279 (ε = 20400 $M^{-1}cm^{-1}$), <248.
PL (solid sample, r.t., $\lambda_{excitation}$ = 300 nm), nm: max 638 ($^4T_1(^4G) \rightarrow {}^6A_1(^6S)$, FWHM=2400 cm^{-1}).
PL (solid sample, r.t., $\lambda_{excitation}$ = 340 nm), nm: max 638, ($^4T_1(^4G) \rightarrow {}^6A_1(^6S)$).
PLE (solid sample, r.t., $\lambda_{emission}$ = 640 nm), nm: 475, 438, 423 (Mn^{2+} excitation), <360 (ligands excitation). τ (solid sample, r.t., $\lambda_{excitation}$ = 300 nm, $\lambda_{emission}$ = 640 nm), ms: τ_1= 1.676 (80%), τ_2= 0.325 (20%).
CIE coordinates: x = 0.637 y = 0.350. Colour purity: 96%

Characterization of [$MnBr_2${$O=P(NMe_2)_2$(1-Naph)}$_2$]

IR (KBr, cm^{-1}): 3057 m, 3000 m (aromatic ν_{C-H}), 2930 m, 2904 m, 2854 m, 2811 m (ν_{C-H}), 1625/1591 w, 1506 w, 1483 w, (aromatic ν_{C-C}) 1460 m (δ_{C-H}), 1303 m (in-plane aromatic δ_{C-H}), 1184 s (ν_{P-O}), 1144 m (ν_{C-N}), 1002-990 s (ν_{P-N}), 777 m, 749 m (out-of-plane aromatic δ_{C-H}).
Uv-vis (CH_2Cl_2, r.t., nm): 319 (ε = 1710 $M^{-1}cm^{-1}$), 314 (ε = 2400 $M^{-1}cm^{-1}$), 287 (ε = 12270 $M^{-1}cm^{-1}$), 279 (ε = 11160 $M^{-1}cm^{-1}$), <254.
PL (solid sample, r.t., $\lambda_{excitation}$ = 300 nm), nm: max 643 ($^4T_1(^4G) \rightarrow {}^6A_1(^6S)$, FWHM=2400 cm^{-1}).
PL (solid sample, r.t., $\lambda_{excitation}$ = 340 nm), nm: max 642, ($^4T_1(^4G) \rightarrow {}^6A_1(^6S)$, FWHM=2400 cm^{-1}).
PLE (solid sample, r.t., $\lambda_{emission}$ = 640 nm), nm: 441, 424, 463 (Mn^{2+} excitation), <387 (ligands excitation). τ (solid sample, r.t., $\lambda_{excitation}$ = 300 nm, $\lambda_{emission}$ = 640 nm), ms: τ_1= 1.581 (77%), τ_2= 0.237 (23%).
CIE coordinates: x = 0.631, y = 0.351. Colour purity: 96%

Characterization of [$MnCl_2${$O=P(NMe_2)_2$(2-Naph)}$_2$]

IR (KBr, cm^{-1}): 3054 m, 2997 m (aromatic ν_{C-H}), 2930 m, 2900 m, 2853 m, 2811 m (ν_{C-H}), 1626/1592 w, 1499 w, 1482 w, (aromatic ν_{C-C}) 1459 m (δ_{C-H}), 1291-1275 m (in-plane aromatic δ_{C-H}), 1168 s (ν_{P-O}), 1130 m/1090 sh,m (ν_{C-N}), 986 s (ν_{P-N}), 861 w, 824 w, 746 (out-of-plane aromatic δ_{C-H}), 757 m (ν^{as}_{NPN}), 703 m (out-of-plane aromatic δ_{C-H}).

Uv-vis (CH_2Cl_2, r.t., nm): 324 (ε = 2100 $M^{-1}cm^{-1}$), 316 (ε = 1570 $M^{-1}cm^{-1}$), 310 (ε = 1850 $M^{-1}cm^{-1}$), 279 (ε = 11790 $M^{-1}cm^{-1}$), 266 (ε = 11330 $M^{-1}cm^{-1}$), <264.

PL (solid sample, r.t., $\lambda_{excitation}$ = 280 nm), nm: max 631 ($^4T_1(^4G) \rightarrow {}^6A_1(^6S)$, FWHM=2300 cm^{-1}).

PL (solid sample, r.t., $\lambda_{excitation}$ = 300 nm): max 636 ($^4T_1(^4G) \rightarrow {}^6A_1(^6S)$, FWHM=2400 cm^{-1}).

PLE (solid sample, r.t., $\lambda_{emission}$ = 640 nm), nm: 438, 422 (Mn^{2+} excitation), <404 (ligands excitation). τ (solid sample, r.t., $\lambda_{excitation}$ = 300 nm, $\lambda_{emission}$ = 640 nm), ms: τ_1= 0.996 (54%), τ_2= 0.156 (46%).

CIE coordinates: x = 0.625, y = 0.361. Colour purity: 96%

Characterization of [$MnBr_2${$O=P(NMe_2)_2$(2-Naph)}$_2$]

IR (KBr, cm^{-1}): 3054 m, 2997 m (aromatic ν_{C-H}), 2927 m, 2899 m, 2851 m, 2809 m (ν_{C-H}), 1627/1592 w, 1499 w, 1482 w, (aromatic ν_{C-C}) 1460 m (δ_{C-H}), 1298-1274 m (in-plane aromatic δ_{C-H}),1168 s (ν_{P-O}), 1130/1090 sh,m (ν_{C-N}), 986 s (ν_{P-N}), 861 w, 824 w, 757 m (out-of-plane aromatic δ_{C-H}), 757 m (ν^{as}_{NPN}), 703 m (out-of-plane aromatic δ_{C-H}).

Uv-vis (CH_2Cl_2, r.t., nm): 325 (ε = 1940 $M^{-1}cm^{-1}$), 316 (ε = 1300 $M^{-1}cm^{-1}$), 310 (ε = 1580 $M^{-1}cm^{-1}$), 279 (ε = 10970 $M^{-1}cm^{-1}$), 269 (ε = 10680 $M^{-1}cm^{-1}$), <263.

PL (solid sample, r.t., $\lambda_{excitation}$ = 300 nm), nm: max 630 ($^4T_1(^4G) \rightarrow {}^6A_1(^6S)$, FWHM=2600 cm^{-1}).

PL (solid sample, r.t., $\lambda_{excitation}$ = 340 nm), nm: max 632 ($^4T_1(^4G) \rightarrow {}^6A_1(^6S)$, FWHM=2600 cm^{-1}).

PLE (solid sample, r.t., $\lambda_{emission}$ = 640 nm), nm: 441, 426 (Mn^{2+} excitation), <407 (ligands excitation). τ (solid sample, r.t., $\lambda_{excitation}$ = 300 nm, $\lambda_{emission}$ = 640 nm), ms: τ1= 0.688 (22%), τ2= 0.070 (78%).

CIE coordinates: x = 0.621, y = 0.366. Colour purity: 96%

2.3.2 Synthesis of [MnX_2{$O=P(NMe_2)_2$Ind}$_2$] where X=Cl, Br, I

In a 100 ml flask, 1 mmol of the manganese salt, $MnCl_2$, $MnBr_2$ or MnI_2, were dissolved in 20 ml of EtOH. A small excess of $O=P(NMe_2)_2$(Ind) (2.1 mmol) was dissolved in 10 ml of EtOH and slowly added under stirring to the flask containing the manganese salt. After 12 hours under stirring the solvent was evaporated under reduced pressure, the obtained solid was dissolved in the minimum amount of CH_2Cl_2 and the obtained solution was cleared by filtration. The product precipitated with addition of Et_2O and was then filtered and washed with fresh Et_2O. Yield > 80% in all the cases.

Characterization of [$MnCl_2${$O=P(NMe_2)_2(Ind)$}$_2$]

IR (KBr, cm^{-1}): 3130 m, 3103 m, 3072 w, 3057 m, 3000 w (aromatic ν_{C-H}), 2948 m, 2915 m, 2863 m, 2825 m (ν_{C-H}), 1602 w, 1526 w, 1479 w (aromatic ν_{C-C} and ν_{C-N}), 1450 m (δ_{C-H}), 1307-1272 m (in-plane aromatic δ_{C-H}), 1170 s (ν_{P-O}), 1160 m (ν_{C-N}), 1010-998 s (ν_{P-N}), 783-735 m (out-of-plane aromatic δ_{C-H}).

Uv-vis (CH_2Cl_2, r.t., nm): 287 (ε = 5200 $M^{-1}cm^{-1}$), 276 (ε = 9680 $M^{-1}cm^{-1}$), 260 (ε = 19230 M^{-1} cm^{-1}).

PL (solid sample, r.t., $\lambda_{excitation}$ = 300 nm), nm: max 527 ($^4T_1(^4G) \rightarrow {}^6A_1(^6S)$, FWHM 2800 cm^{-1}).

PLE (solid sample, r.t., $\lambda_{emission}$ = 528 nm), nm: < 315, 290 sh ($^4F \leftarrow {}^6S$, ligands), 334-391 ($^4P,^4D \leftarrow {}^6S$), 420/ 427-448 ($^4G \leftarrow {}^6S$). τ (solid sample, r.t., $\lambda_{excitation}$ = 377 nm, $\lambda_{emission}$ = 510 nm), μs: 1248.

CIE coordinates: x = 0.320, y = 0.589. Colour purity: 74%

Characterization of [$MnBr_2${$O=P(NMe_2)_2(Ind)$}$_2$]

IR (KBr, cm^{-1}): 3130 m, 3103 m, 3072 w, 3057 m, 3000 w (aromatic ν_{C-H}), 2946 m, 2913 m, 2862 m, 2825 m (ν_{C-H}), 1612 w, 1526 w, 1483 w (aromatic ν_{C-C} and ν_{C-N}), 1450 m (δ_{C-H}), 1309-1270 m (in-plane aromatic δ_{C-H}), 1166 s (ν_{P-O}), 1160 w (ν_{C-N}), 1011-997 s (ν_{P-N}), 780-733 m (out-of-plane aromatic δ_{C-H}).

Uv-vis (CH_2Cl_2, r.t., nm): 287 (ε = 3570 $M^{-1}cm^{-1}$), 276 (ε = 6220 $M^{-1}cm^{-1}$), 257 (ε = 18370 M^{-1} cm^{-1}).

PL (solid sample, r.t., $\lambda_{excitation}$ = 290 nm), nm: max 535 ($^4T_1(^4G) \rightarrow {}^6A_1(^6S)$, FWHM = 3500 cm^{-1}).

PLE (solid sample, r.t., $\lambda_{emission}$ = 530 nm): < 310, 290 sh ($^4F \leftarrow {}^6S$, ligands), 336-392 ($^4P,^4D \leftarrow {}^6S$), 420-476 ($^4G \leftarrow {}^6S$). τ (solid sample, r.t., $\lambda_{excitation}$ = 377 nm, $\lambda_{emission}$ = 528 nm), μs: 546.

CIE coordinates: x = 0.326, y = 0.579. Colour purity: 73%

Characterization of [MnI_2{$O=P(NMe_2)_2(Ind)$}$_2$]

IR (KBr, cm^{-1}): 3132 m, 3109 m, 3072 w, 3058 m, 3000 w (aromatic ν_{C-H}), 2934 m, 2905 m, 2856 m, 2819 m (ν_{C-H}), 1604 w, 1526 w, 1483 w (aromatic ν_{C-C} and ν_{C-N}), 1450 m (δ_{C-H}), 1309-1270 m (in-plane aromatic δ_{C-H}), 1160 s (ν_{P-O}), 1008-999 s (ν_{P-N}), 777-725 m (out-of-plane aromatic δ_{C-H}).

Uv-vis (CH_2Cl_2, r.t., nm): 287 (ε = 4380 $M^{-1}cm^{-1}$), 275 (ε = 6340 $M^{-1}cm^{-1}$), 257 (ε = 18370 M^{-1} cm^{-1}).

PL (solid sample, r.t., $\lambda_{excitation}$ = 300 nm): max 519 ($^4T_1(^4G) \rightarrow {}^6A_1(^6S)$, FWHM = 2100 cm^{-1}), 660 broad ($^4T_1(^4G) \rightarrow {}^6A_1(^6S)$).

PLE (solid sample, r.t., $\lambda_{emission}$ = 520 nm, nm): < 305, 288 sh ($^4F \leftarrow {}^6S$, ligands), 344-394 ($^4P,^4D \leftarrow {}^6S$), 423-480 ($^4G \leftarrow {}^6S$). τ (solid sample, r.t., $\lambda_{excitation}$ = 377 nm, $\lambda_{emission}$ = 510 nm), μs: τ1= 671, τ2= 43.

CIE coordinates: x = 0.394, y = 0.535 . Colour purity: 79%

2.3.3 Synthesis of $[MnX_2\{O=P(MeNCH_2CH_2NMe)Ph\}_2]$ where X=Cl, Br, I

These syntheses were carried out following the procedure above described for $[MnX_2\{O=P(NMe_2)_2Ind\}_2]$.

Characterization of $[MnCl_2\{O=P(MeNCH_2CH_2NMe)Ph\}_2]$

IR (KBr, cm^{-1}): 3056 w, 3017 w (aromatic ν_{C-H}), 2968 w, 2938 w, 2917 w, 2886 w, 2848 w, 2819 w (ν_{C-H}), 1632 w, 1590 w, 1481 w (aromatic ν_{C-C}), 1467 m, 1438 w, 1380 w (δ_{C-H}), 1168-1150 s (ν_{P-O}), 1043 m (ν_{C-N}), 981 s (ν_{P-N}), 734 m (out-of-plane aromatic δ_{C-H}).

Uv-vis (CH_2Cl_2, r.t., nm): 273 (ε = 2240 $M^{-1}cm^{-1}$), 266 (ε = 3300 $M^{-1}cm^{-1}$), <260.

PL (solid, r.t., $\lambda_{excitation}$ = 270 nm), nm: 508 ($^4T_1(^4G) \rightarrow {}^6A_1(^6S)$, FWHM = 2100 cm^{-1}).

PLE (solid sample, r.t., $\lambda_{emission}$ = 508 nm), nm: < 320 ($^4F \leftarrow {}^6S$, ligands), 338-384 ($^4P,^4D \leftarrow {}^6S$), 422 ($^4G \leftarrow {}^6S$). τ (solid sample, r.t., $\lambda_{excitation}$ = 377 nm, $\lambda_{emission}$ = 508 nm), μs: 916.

CIE coordinates: x = 0.199, y = 0.624 . Colour purity: 59%

Characterization of $[MnBr_2\{O=P(MeNCH_2CH_2NMe)Ph\}_2]$

IR (KBr, cm^{-1}): 3056 w, 3021 w (aromatic ν_{C-H}), 2973 w, 2938 w, 2918 w, 2886 w, 2846 w, 2820 w (ν_{C-H}), 1621 w, 1590 w, 1484 w (aromatic ν_{C-C}), 1468 m, 1438 w, 1378 w (δ_{C-H}), 1165-1150 s (ν_{P-O}), 1040 m (ν_{C-N}), 983 s (ν_{P-N}), 732 m (out-of-plane aromatic δ_{C-H}).

Uv-vis (CH_2Cl_2, r.t., nm): 277 (ε = 1980 $M^{-1}cm^{-1}$), 265 (ε = 3130 $M^{-1}cm^{-1}$), <260.

PL (solid, r.t., $\lambda_{excitation}$ = 280 nm), nm: 509 ($^4T_1(^4G) \rightarrow {}^6A_1(^6S)$, FWHM = 2500 cm^{-1}).

PLE (solid, r.t., $\lambda_{emission}$ = 530 nm), nm: < 320 ($^4F \leftarrow {}^6S$, ligands), 336-391 ($^4P,^4D \leftarrow {}^6S$), 424 ($^4G \leftarrow {}^6S$). τ (solid, r.t., $\lambda_{excitation}$ = 377 nm, $\lambda_{emission}$ = 508 nm), μs: 683.

CIE coordinates: x = 0.224, y = 0.627 . Colour purity: 58%

Characterization of [MnI_2{O=P(MeNCH$_2$CH$_2$NMe)Ph}$_2$]

IR (KBr, cm^{-1}): 3078 w, 3055 w (aromatic ν_{C-H}), 2972 w, 2937 w, 2919 w, 2884 w, 2848 w, 2818 w (ν_{C-H}), 1590 w, 1481 w (aromatic ν_{C-C}), 1468 m, 1438 w, 1377 w (δ_{C-H}), 1163 s (ν_{P-O}), 1120-1040 m (ν_{C-N}), 731 m (out-of-plane aromatic δ_{C-H}).

Uv-vis (CH_2Cl_2, r.t., nm): 365 broad (ε = 810 $M^{-1}cm^{-1}$), 275 (ε = 3420 $M^{-1}cm^{-1}$), 266 (ε = 4380 $M^{-1}cm^{-1}$), <260.

PL (solid, r.t., $\lambda_{excitation}$ = 290 nm), nm: 512 ($^4T_1(^4G)\rightarrow{}^6A_1(^6S)$, FWHM = 2400 cm^{-1}).

PLE (solid, r.t., $\lambda_{emission}$ = 510 nm), nm: < 325 ($^4F\leftarrow{}^6S$, ligands), 340-396 ($^4P,^4D\leftarrow{}^6S$), <420 ($^4G\leftarrow{}^6S$). τ (solid, r.t., $\lambda_{excitation}$ = 377 nm, $\lambda_{emission}$ = 510 nm), μs: 137.

CIE coordinates: x = 0.237, y = 0.620 . Colour purity: 64%

2.3.4 Synthesis of [Eu(tta)$_3$L] where L= O=P(NMe$_2$)$_2$1-Naph, O=P(NMe$_2$)$_2$2-Naph, O=P(NMe$_2$)$_2$Ind, O=P(NMe$_2$)$_2$Ph

In a 100 ml flask, 1 mmol of anhydrous $EuCl_3$ was dissolved in 15 ml of THF. In a 50 ml flask, thenoyltrifluoroacetone (tta, 3 mmol, 0.67 g) was dissolved in 15 ml of THF and potassium *tert*-butoxide (3 mmol, 0.34 g) was slowly added to this solution under stirring. After 2 hours the as formed potassium-thenoyltrifluoroacetonate was slowly added to the solution containing $EuCl_3$. After 4 more hours of stirring, the desired ligand dissolved in 10 mL of THF (1 mmol) was slowly added to the β-diketonate europium complex solution. After 12 hours under stirring the solvent was evaporated under reduced pressure and the obtained solid re-dissolved in the minimum amount of CH_2Cl_2. The solution was cleared by centrifugation and concentrated. The product precipitated by addition of Et_2O and was then filtered and washed with fresh Et_2O. Yield > 80% in all the cases.

Characterization of [Eu(tta)$_3${O=P(NMe$_2$)$_2$(1-Naph)}]

IR (KBr, cm^{-1}): 1605-1305 (ν_{tta}), 1141 ($\nu_{P=O}$).

NMR ^{1}H NMR (DMSO-*d$_6$*, 298 K) δ: 8.90-7.53 (m, 7H, Naph-H), 7.44 (s, 3H, β-dike-thioph), 6.51 (s, 3H, β-dike-thioph), 6.35 (s, 3H, β-dike-thioph), 3.80 (s, 3H, β-dike-CH), 2.63 (d, 12H,

J_{PH} = 9.2 Hz, N-Me). $^{31}P\{^{1}H\}$ NMR (DMSO-d_6, 298 K), δ: 28.7 (FWHM = 70 Hz). ^{19}F NMR (DMSO-d_6, 298 K), δ: -78.3.

UV-VIS (CH_2Cl_2, r.t.), nm: 342 (ε = 32.000 $M^{-1}cm^{-1}$), 292 (ε = 13000 $M^{-1}cm^{-1}$), 277 (ε = 14100 $M^{-1}cm^{-1}$).

PL (solid, $\lambda_{excitation}$ = 375 nm, r.t.), nm: 580 ($^5D_0 \rightarrow {}^7F_0$, 1.0%), 590, 594, 596 ($^5D_0 \rightarrow {}^7F_1$, 5.0%), 614 ($^5D_0 \rightarrow {}^7F_2$, 83.4%), 652, 655 ($^5D_0 \rightarrow {}^7F_3$, 4.6%), 691, 702 ($^5D_0 \rightarrow {}^7F_4$, 6.0%).

PLE (solid, $\lambda_{emission}$ = 613 nm, r.t.), nm: < 480 (350 max, ligands excitation), 464 ($^5D_2 \leftarrow {}^7F_0$).

τ (solid, $\lambda_{excitation}$ = 380 nm, $\lambda_{emission}$ = 613 nm), μs: 346. Q_{Eu}^{Eu} = 34%.

CIE coordinates: x = 0.612, y = 0.331. M.p. (°C) 70 (dec).

Characterization of [Eu(tta)$_3${O=P(NMe$_2$)$_2$(2-Naph)}]

IR (KBr, cm^{-1}): 1608-1305 (ν_{tta}), 1140 ($\nu_{P=O}$).

NMR: ^1H NMR (DMSO-d_6, 298 K), δ: 8.48 (s, br, 1H, Naph-H), 8.05 (d, 1H, J_{HH} = 8.1 Hz, Naph-H), 8.02 (dd, 1H, J_{HH} = 8.5 Hz, J_{PH} = 3.3 Hz, Naph-H), 7.98 (d, 1H, J_{HH} = 8.1 Hz, Naph-H), 7.81 (s, br, 1H, Naph-H), 7.63 (ddd, 1H, J_{HH} = 8.1 Hz, 7.0 Hz, 1.4 Hz, Naph-H), 7.58 (ddd, 1H, J_{HH} = 8.1 Hz, 7.0 Hz, 1.4 Hz, Naph-H), 7.43 (s, 3H, β-dike-thioph), 6.51 (s, 3H, β-dike-thioph), 6.34 (s, 3H, β-dike-thioph), 3.81 (s, 3H, β-dike-CH), 2.63 (d, 12H, J_{PH} = 10.1 Hz, N-Me). $^{31}P\{^{1}H\}$ NMR (DMSO-d_6, 298 K), δ: 28.2 (FWHM = 380 Hz). ^{19}F NMR (DMSO-d_6, 25°C), δ: -78.3.

UV-VIS (CH_2Cl_2, r.t.), nm: 343 (ε = 49500 $M^{-1}cm^{-1}$), 275 (ε = 39800 $M^{-1}cm^{-1}$).

PL (solid, $\lambda_{excitation}$ = 375 nm, r.t.), nm: 580 ($^5D_0 \rightarrow {}^7F_0$, 1.1%), 589-596 ($^5D_0 \rightarrow {}^7F_1$, 4.9%), 614 ($^5D_0 \rightarrow {}^7F_2$, 83.6%), 652, 655 ($^5D_0 \rightarrow {}^7F_3$, 4.1%), 692, 702 ($^5D_0 \rightarrow {}^7F_4$, 6.3%).

PLE (solid, $\lambda_{emission}$ = 613 nm, r.t.), nm: < 480 (381 max, ligands excitation), 464 ($^5D_2 \leftarrow {}^7F_0$).

τ (solid, $\lambda_{excitation}$ = 380 nm, $\lambda_{emission}$ = 612 nm), μs: 360. Q_{Eu}^{Eu} = 36%.

CIE coordinates: x = 0.652, y = 0.334. M.p. (°C) 65 (dec).

Characterization of [Eu(tta)$_3${O=P(NMe$_2$)$_2$Ind}]

IR (KBr, cm^{-1}): 1605-1289 (ν_{tta}), 1141 ($\nu_{P=O}$).

NMR ^1H NMR (DMSO-d_6, 25°C), δ: 7.87 (d, 1H, J_{HH} = 8.3 Hz, Ind-H), 7.59 (d, 1H, J_{HH} = 8.2 Hz, Ind-H), 7.44 (s, 3H, β-dike-thioph), 7.35 (dd, 1H, J_{HH} = 3.4 Hz, J_{PH} = 2.7 Hz, Ind-H), 7.20 (ddd, 1H, J_{HH} = 8.3 Hz, 7.2 Hz, 1.3 Hz, Ind-H), 7.14 (ddd, 1H, J_{HH} = 8.2 Hz, 7.2 Hz, 1.1 Hz, Ind-H), 6.68 (ddd, 1H, J_{HH} = 3.4 Hz, 0.9 Hz, J_{PH} = 2.5 Hz, Ind-H), 6.51 (s, 3H, β-dike-thioph), 6.35 (s, 3H, β-

dike-thioph), 3.79 (s, 3H, β-dike-CH), 2.61 (d, 12H, J_{PH} = 10.1 Hz, N-Me). $^{31}P\{^{1}H\}$ NMR (DMSO-d_6, 25°C), δ: 13.6 (FWHM = 90 Hz). ^{19}F NMR (DMSO-d_6, 25°C), δ: -78.3.

UV-VIS (CH_2Cl_2, r.t.), nm: 344 (ε = 53.000 $M^{-1}cm^{-1}$), 277 (ε = 25.000 $M^{-1}cm^{-1}$),

PL (solid, $\lambda_{excitation}$ = 375 nm, r.t.), nm: 580 ($^5D_0 \rightarrow {}^7F_0$, 1.2%), 589, 595, 597 ($^5D_0 \rightarrow {}^7F_1$, 5.6%), 614 ($^5D_0 \rightarrow {}^7F_2$, 84.3%), 652, 656 ($^5D_0 \rightarrow {}^7F_3$, 2.9%), 692, 702 ($^5D_0 \rightarrow {}^7F_4$, 6.0%).

PLE (solid, $\lambda_{emission}$ = 612 nm, r.t.), nm: < 480 (398 max, ligands excitation), 464 ($^5D_2 \leftarrow {}^7F_0$).

τ (solid, $\lambda_{excitation}$ = 377 nm, $\lambda_{emission}$ = 612 nm), μs: 376. Q_{Eu}^{Eu} = 33%.

CIE coordinates: x = 0.663, y = 0.335. M.p. (°C) 78 (dec).

Characterization of [Eu(tta)$_3${O=P(NMe$_2$)$_2$Ph)}]

IR (KBr, cm^{-1}): 1613-1302 (ν_{tta}), 1144 ($\nu_{P=O}$).

NMR ^1H NMR (DMSO-d_6, 298 K), δ: 7.73 (s, br, 1H, P-Ph), 7.60-7.47 (m, 3H, P-Ph), 7.44 (s, 3H, β-dike-thioph), 6.51 (s, 3H, β-dike-thioph), 6.35 (s, 3H, β-dike-thioph), 3.81 (s, 3H, β-dike-CH), 2.56 (d, 12H, J_{PH} = 8.9 Hz, N-Me). $^{31}P\{^{1}H\}$ NMR (DMSO-d_6, 298 K), δ: 28.3 (FWHM = 230 Hz). ^{19}F NMR (DMSO-d_6, 298 K), δ: -78.3.

UV-VIS (CH_2Cl_2, r.t.), nm: 343 (ε = 52000 $M^{-1}cm^{-1}$), 272 (ε = 19900 $M^{-1}cm^{-1}$).

PL (solid, $\lambda_{excitation}$ = 375 nm, r.t.), nm: 580 ($^5D_0 \rightarrow {}^7F_0$, 1.2%), 590, 594, 596 ($^5D_0 \rightarrow {}^7F_1$, 5.5%), 614 ($^5D_0 \rightarrow {}^7F_2$, 84.1%), 654 ($^5D_0 \rightarrow {}^7F_3$, 3.5%), 692, 702 ($^5D_0 \rightarrow {}^7F_4$, 5.7%).

PLE (solid, $\lambda_{emission}$ = 612 nm, r.t.), nm: < 480 (425, 376 max, ligands excitation), 464 ($^5D_2 \leftarrow {}^7F_0$). τ (solid, $\lambda_{excitation}$ = 377 nm, $\lambda_{emission}$ = 613 nm), μs: 380. Q_{Eu}^{Eu} = 30%.

CIE coordinates: x = 0.664, y = 0.335. M.p. (°C) 74 (dec).

2.3.5 Synthesis of [Eu(dbm)$_3$L] where L= O=P(NMe$_2$)$_2$1-Naph, O=P(NMe$_2$)$_2$2-Naph, O=P(NMe$_2$)$_2$Ind.

These syntheses were carried out following the procedure already described for [Eu(tta)$_3$L], using dibenzoylmethane (dbm 0.68 g) instead of thenoyltrifluoroacetone.

Characterization of [Eu(dbm)$_3${O=P(NMe$_2$)$_2$(1-Naph)}]

IR (KBr, cm^{-1}): 1595-1383 (ν_{dbm}), 1157 ($\nu_{P=O}$).

NMR ^1H NMR (DMSO-d_6, 298 K), δ: 8.80-7.54 (m, 7H, Naph-H), 7.21 (s, 2H, β-dike-CH), 7.20 (s, 1H, β-dike-CH), 6.82 (t, 6H, J_{HH} = 7.5 Hz, β-dike-Ph), 6.67 (dd, 12H, J_{HH} = 7.5 Hz, 7.0 Hz, β-dike-

Ph), 5.73 (d, 12H, J_{HH} = 7.0 Hz, β-dike-Ph), 2.62 (d, 12H, J_{PH} = 9.2 Hz, N-Me). $^{31}P\{^{1}H\}$ NMR (DMSO-d_6, 298 K), δ: 28.6 (FWHM = 60 Hz).

UV-VIS (CH_2Cl_2, r.t.), nm: 346 (ε = 49300 $M^{-1}cm^{-1}$), 294 (ε = 14300 $M^{-1}cm^{-1}$), 253 (ε = 20800 $M^{-1}\,cm^{-1}$).

PL (solid, $\lambda_{excitation}$ = 375 nm, r.t.), nm: 580 ($^5D_0\rightarrow{}^7F_0$, 1.4%), 589, 594, 597 ($^5D_0\rightarrow{}^7F_1$, 4.5%), 613, 626 ($^5D_0\rightarrow{}^7F_2$, 85.4%), 651, 655 ($^5D_0\rightarrow{}^7F_3$, 4.9%), 702, 706 ($^5D_0\rightarrow{}^7F_4$, 3.8%).

PLE (solid, $\lambda_{emission}$ = 613 nm, r.t.), nm: < 480 (396 max, ligands excitation), 464 ($^5D_2\leftarrow{}^7F_0$).

τ (solid, $\lambda_{excitation}$ = 380 nm, $\lambda_{emission}$ = 613 nm), μs: 215. Q_{Eu}^{Eu} = 24%.

CIE coordinates: x = 0.632, y = 0.326. M.p. (°C) 74 (dec).

Characterization of [Eu(dbm)$_3${O=P(NMe$_2$)$_2$(2-Naph)}]

IR (KBr, cm^{-1}): 1595-1386 (ν_{dbm}), 1158 ($\nu_{P=O}$).

NMR ^{1}H NMR (DMSO-d_6, 198 K), δ: 8.42 (d, br, 1H, J_{PH} = 14.1 Hz, Naph-$H_{(1)}$), 8.18 (d, 1H, J_{HH} = 8.1 Hz, Naph-H), 8.09-7.95 (m, 2H, Naph-H), 7.70-7.53 (m, 3H, Naph-H), 7.20 (s, 2H, β-dike-CH), 7.19 (s, 1H, β-dike-CH), 6.80 (t, 6H, J_{HH} = 7.4 Hz, β-dike-Ph), 6.65 (t, 12H, J_{HH} = 7.4 Hz, β-dike-Ph), 5.71 (d, 12H, J_{HH} = 7.4 Hz, β-dike-Ph), 2.62 (d, 12H, J_{PH} = 10.1 Hz, N-Me). $^{31}P\{^{1}H\}$ NMR (DMSO-d_6, 298 K), δ: 27.7 (FWHM = 280 Hz).

UV-VIS (CH_2Cl_2, r.t.), nm: 391 (ε = 8900 $M^{-1}cm^{-1}$), 346 (ε = 70300 $M^{-1}cm^{-1}$), 291 (ε = 24500 $M^{-1}cm^{-1}$), 251 (ε = 46000 $M^{-1}cm^{-1}$).

PL (solid, $\lambda_{excitation}$ = 375 nm, r.t.), nm: 580 ($^5D_0\rightarrow{}^7F_0$, 1.4%), 589, 594, 598 ($^5D_0\rightarrow{}^7F_1$, 4.4%), 613, 626 ($^5D_0\rightarrow{}^7F_2$, 85.7%), 651, 656 ($^5D_0\rightarrow{}^7F_3$, 5.0%), 702, 706 ($^5D_0\rightarrow{}^7F_4$, 3.5%).

PLE (solid, $\lambda_{emission}$ = 613 nm, r.t.), nm: < 480 (392 max, ligands excitation), 464 ($^5D_2\leftarrow{}^7F_0$).

τ (solid, $\lambda_{excitation}$ = 380 nm, $\lambda_{emission}$ = 612 nm), μs: 240. Q_{Eu}^{Eu} = 27%.

CIE coordinates: x = 0.654, y = 0.337. M.p. (°C) 70 (dec).

Characterization of [Eu(dbm)$_3${O=P(NMe$_2$)$_2$Ind}]

IR (KBr, cm^{-1}): 1595-1386 (ν_{dbm}), 1168 ($\nu_{P=O}$).

NMR ^{1}H NMR (DMSO-d_6, 298 K), δ: 8.22-7.10 (m, 6H, Ind-H), 7.20 (s, 2H, β-dike-CH), 7.19 (s, 1H, β-dike-CH), 6.82 (t, 6H, J_{HH} = 7.3 Hz, β-dike-Ph), 6.67 (t, 12H, J_{HH} = 7.3 Hz, β-dike-Ph), 5.73 (d, 12H, J_{HH} = 7.3 Hz, β-dike-Ph), 2.61 (d, 12H, J_{PH} = 10.1 Hz, N-Me). $^{31}P\{^{1}H\}$ NMR (DMSO-d_6, 298 K), δ: 13.5 (FWHM = 30 Hz).

UV-VIS (CH_2Cl_2, r.t.), nm: 393 (ε = 8100 $M^{-1}cm^{-1}$), 346 (ε = 64700 $M^{-1}cm^{-1}$), 252 (ε = 75400 $M^{-1}cm^{-1}$).

PL (solid, $\lambda_{excitation}$ = 400 nm, r.t.), nm: 580 ($^5D_0 \rightarrow {}^7F_0$, 1.5%), 589, 595, 597 ($^5D_0 \rightarrow {}^7F_1$, 4.6%), 614, 626 ($^5D_0 \rightarrow {}^7F_2$, 86%), 652, 656 ($^5D_0 \rightarrow {}^7F_3$, 4.1%), 692, 702, 706 ($^5D_0 \rightarrow {}^7F_4$, 3.8%).

PLE (solid, $\lambda_{emission}$ = 612 nm, r.t.), nm: < 480 (423 max, ligands excitation), 464 ($^5D_2 \leftarrow {}^7F_0$).

τ (solid, $\lambda_{excitation}$ = 377 nm, $\lambda_{emission}$ = 612 nm), μs: 274. Q_{Eu}^{Eu} = 29%.

CIE coordinates: x = 0.661, y = 0.336. M.p. (°C) 69 (dec).

2.3.6 Synthesis of [Eu(dbm)$_3${O=P(MeNCH$_2$CH$_2$NMe)Ph}$_2$] and [Eu(tta)$_3${O=P(MeNCH$_2$CH$_2$NMe)Ph}$_2$]

These syntheses were carried out following the same procedure already described for [Eu(tta)$_3$L] and [Eu(dbm)$_3$L], where L is O=P(MeNCH$_2$CH$_2$NMe)Ph and using a metal to ligand ratio of 1:2.

Characterization of [Eu(tta)$_3${O=P(MeNCH$_2$CH$_2$NMe)*Ph}$_2$]*

IR (KBr, cm^{-1}): 1616-1302 s (ν_{tta}), 1182 s, 1136 s ($\nu_{P=O}$).

NMR ^{1}H NMR (DMSO-d_6, 298 K), δ: 7.72-7.45 (m, 10H, P-Ph), 7.43 (s, 3H, β-dike-thioph), 6.51 (s, 3H, β-dike-thioph), 6.35 (s, 3H, β-dike-thioph), 3.79 (s, 3H, β-dike-CH), 3.29-3.22 (m, 4H, N-CH$_2$), 3.22-3.15 (m, 4H, N-CH$_2$), 2.37 (d, 12H, J_{PH} = 10.0 Hz, N-Me). $^{31}P\{^1H\}$ NMR (DMSO-d_6, 298 K), δ: 28.1 (FWHM = 170 Hz). ^{19}F NMR (DMSO-d_6, 298 K), δ: -78.3.

UV-VIS (CH_2Cl_2, r.t.), nm: 343 max (ε = 18840 $M^{-1}cm^{-1}$), 270 (ε = 5970 $M^{-1}cm^{-1}$).

PL (solid, $\lambda_{excitation}$ = 400 nm, r.t.), nm: 579 ($^5D_0 \rightarrow {}^7F_0$, 0.6%), 589, 592, 595 ($^5D_0 \rightarrow {}^7F_1$, 4.6%), 611, 614, 617 ($^5D_0 \rightarrow {}^7F_2$, 75.0%), 650, 654 ($^5D_0 \rightarrow {}^7F_3$, 3.9%), 690, 701 ($^5D_0 \rightarrow {}^7F_4$, 15.9%).

PLE (solid, $\lambda_{emission}$ = 614 nm, r.t.), nm: < 480 (388 max, ligands excitation), 464 ($^5D_2 \leftarrow {}^7F_0$).

τ (solid, $\lambda_{excitation}$ = 377 nm, $\lambda_{emission}$ = 613 nm), μs: 610. Q_{Eu}^{Eu}= 65%.

CIE coordinates: x = 0.665, y = 0.334. M.p. (°C) 78 (dec.)

Characterization of [Eu(dbm)$_3${O=P(MeNCH$_2$CH$_2$NMe)Ph}$_2$]

IR (KBr, cm^{-1}): 1596-1409 s (ν_{dbm}), 1185 sh, 1161 m ($\nu_{P=O}$).

NMR ^{1}H NMR (DMSO-d_6, 298 K), δ: 7.70-7.44 (m, 10H, P-Ph), 7.20 (s, 2H, β-dike-CH), 7.19 (s, 1H, β-dike-CH), 6.82 (t, 6H, J_{HH} = 7.4 Hz, β-dike-Ph), 6.67 (dd, 12H, J_{HH} = 6.3 Hz, J_{HH} = 7.4 Hz,

β-dike-Ph), 5.72 (d, 12H, J_{HH} = 6.3 Hz, β-dike-Ph), 3.30-3.23 (m, 4H, N-CH_2), 3.23-3.15 (m, 4H, N-CH_2), 2.36 (d, 12H, J_{PH} = 10.0 Hz, N-Me). $^{31}P\{^1H\}$ NMR (DMSO-*d*$_6$, 298 K), δ: 28.1 (FWHM = 30 Hz).

UV-VIS (CH_2Cl_2, r.t.), nm: 346 max (ε = 20360 $M^{-1}cm^{-1}$), 250 (ε = 9740 $M^{-1}cm^{-1}$).

PL (solid, $\lambda_{excitation}$ = 300 nm, r.t.), nm: 579 ($^5D_0 \rightarrow {}^7F_0$, 0.4%), 588, 591, 597 ($^5D_0 \rightarrow {}^7F_1$, 4.7%), 611, 613, 618, 623, 626 ($^5D_0 \rightarrow {}^7F_2$, 74.2%), 649, 651, 653, 656 ($^5D_0 \rightarrow {}^7F_3$, 5.0%), 690, 694, 699, 703, 706 ($^5D_0 \rightarrow {}^7F_4$, 15.7%).

PLE (solid, $\lambda_{emission}$ = 614 nm, r.t.), nm: < 480 (362 max, 318 max 403 max, ligands excitation), 464 ($^5D_2 \leftarrow {}^7F_0$). τ (solid, $\lambda_{excitation}$ = 377 nm, $\lambda_{emission}$ = 613 nm), μs: 482. Q_{Eu}^{Eu} = 51%.

CIE coordinates: x = 0.666, y = 0.334. M.p. (°C) 125 (dec.)

2.3.7 Reactions between the ligands L= O=P(NMe_2)$_2$Ph, O=P(NMe_2)$_2$1-Naph, O=P(NMe_2)$_2$2-Naph, O=P(NMe_2)$_2$Ind, O=P(MeNCH_2CH_2NMe)Ph and lanthanide nitrate fragments (Ln = Eu, Gd, Tb)

In a 100 ml flask, [Ln(NO_3)$_3$(H_2O)$_3$] (Ln = Eu, Gd, Tb; 1 mmol) were dissolved in 20 ml of THF. The desired ligand (2.1 mmol) was dissolved in 10 ml of THF and slowly added under stirring to the flask containing the lanthanide precursor. After 12 hours the solvent was evaporated under reduced pressure, the obtained solid re-dissolved in the minimum amount of CH_2Cl_2 and the solution was filtered on cotton. The product precipitated by addition of Et_2O and was then filtered and washed with fresh Et_2O.

Characterization: Ln = Eu, L = O=P(NMe_2)$_2$(1-Naph)

IR (KBr, cm^{-1}): 1481s ($\nu_{N=O}$), 1298s (ν^{as}_{ONO}), 1150-1129s ($\nu_{P=O}$), 1002 (ν_{PN}), 990s (ν_{PN}).

PL (solid, $\lambda_{excitation}$ = 375 nm, r.t.), nm: 580 ($^5D_0 \rightarrow {}^7F_0$, 0.7%), 592, 596 ($^5D_0 \rightarrow {}^7F_1$, 11.1%), 617, 619 ($^5D_0 \rightarrow {}^7F_2$, 74.8%), 653 ($^5D_0 \rightarrow {}^7F_3$, 3.1%), 691, 698, 702 ($^5D_0 \rightarrow {}^7F_4$, 10.3%).

CIE coordinates: x = 0.647, y = 0.338.

Characterization: Ln = Eu, L = O=P(NMe$_2$)$_2$(2-Naph)

IR (KBr, cm^{-1}): 1466s ($\nu_{N=O}$), 1293s (ν^{as}_{ONO}), 1124s ($\nu_{P=O}$), 987s (ν_{PN}).

PL (solid, $\lambda_{excitation}$ = 375 nm, r.t.), nm: 580 ($^5D_0 \rightarrow {}^7F_0$, 1.0%), 593 ($^5D_0 \rightarrow {}^7F_1$, 11.6%), 617 ($^5D_0 \rightarrow {}^7F_2$, 73.5%), 652 ($^5D_0 \rightarrow {}^7F_3$, 3.3%), 691, 697, 702 ($^5D_0 \rightarrow {}^7F_4$, 10.6%).

CIE coordinates: x = 0.657, y = 0.343.

Characterization: Ln = Eu, L = O=P(NMe$_2$)$_2$Ind

IR (KBr, cm^{-1}): 1473s ($\nu_{N=O}$), 1288s (ν^{as}_{ONO}), 1150-1123 s ($\nu_{P=O}$), 996s (ν_{PN}).

PL 581 ($^5D_0 \rightarrow {}^7F_0$, 1.4%), 593 ($^5D_0 \rightarrow {}^7F_1$, 10.2%), 617 ($^5D_0 \rightarrow {}^7F_2$, 75.2%), 653 ($^5D_0 \rightarrow {}^7F_3$, 2.9%), 690, 698 ($^5D_0 \rightarrow {}^7F_4$, 10.3%).

CIE coordinates: x = 0.640, y = 0.343.

Characterization: Ln = Eu, L = O=P(MeNCH$_2$CH$_2$NMe)Ph

IR (KBr, cm^{-1}): 1455s, 1438s ($\nu_{N=O}$), 1305s (ν^{as}_{ONO}), 1154-1119s ($\nu_{P=O}$), 989s (ν_{PN}).

PL (solid, $\lambda_{excitation}$ = 375 nm, r.t.), nm: 580 ($^5D_0 \rightarrow {}^7F_0$, 1.9%), 593 ($^5D_0 \rightarrow {}^7F_1$, 16.3%). 619 ($^5D_0 \rightarrow {}^7F_2$, 63.4%), 652 ($^5D_0 \rightarrow {}^7F_3$, 3.8%), 689, 695, 702 ($^5D_0 \rightarrow {}^7F_4$, 14.6%).

CIE coordinates: x = 0.634, y = 0.348.

Characterization: Ln = Gd, L = O=P(NMe$_2$)$_2$(1-Naph)

IR (KBr, cm^{-1}): 1477s ($\nu_{N=O}$), 1298s (ν^{as}_{ONO}), 1151-1130s ($\nu_{P=O}$), 1002 (ν_{PN}), 991s (ν_{PN}).

PL (solid, $\lambda_{excitation}$ = 375 nm, 193 K), nm: 445, 495 max, 543 max. PL (solid, $\lambda_{excitation}$ = 375 nm, r.t), nm: 445 sh, 495 max. Triplet state: < 19500 cm^{-1}.

Characterization: Ln = Gd, L = O=P(NMe$_2$)$_2$(2-Naph)

IR (KBr, cm^{-1}): 1461s ($\nu_{N=O}$), 1289s (ν^{as}_{ONO}), 1142-1124s ($\nu_{P=O}$), 984s (ν_{PN}).

PL (solid, $\lambda_{excitation}$ = 375 nm, 193 K), nm: 441, 493, 548 max. PL (solid, $\lambda_{excitation}$ = 375 nm, r.t), nm: 441, 493 max. Triplet state: < 19400 cm^{-1}.

Characterization: Ln = Gd, L = O=P(NMe$_2$)$_2$Ind

IR (KBr, cm^{-1}): 1477s ($\nu_{N=O}$), 1292s (ν^{as}_{ONO}), 1158-1143 s ($\nu_{P=O}$), 998s (ν_{PN}).

PL (solid, $\lambda_{excitation}$ = 375 nm, 193 K), nm: 498 sh, 514 max, 546 sh. PL (solid, $\lambda_{excitation}$ = 375 nm, r.t), nm: 498, 514 max, 546. Triplet state: 21800 cm^{-1}.

Characterization: Ln = Gd, L = O=P(MeNCH$_2$CH$_2$NMe)Ph

IR (KBr, cm^{-1}): 1456s, 1439s ($\nu_{N=O}$), 1307s (ν^{as}_{ONO}), 1154-1120s ($\nu_{P=O}$).

PL (solid, $\lambda_{excitation}$ = 375 nm, 193 K), nm: 507 max, 529 sh. FWHM = 4000 cm^{-1}. Triplet state: 21300 cm^{-1}.

Characterization: Ln = Tb, L = O=P(NMe$_2$)$_2$Ph

IR (KBr, cm^{-1}): 1448s ($\nu_{N=O}$), 1281s (ν^{as}_{ONO}), 1178s ($\nu_{P=O}$), 1138s ($\nu_{P=O}$), 980s (ν_{PN}).

PL (solid, $\lambda_{excitation}$ = 375 nm, r.t.), nm: 490 ($^5D_4 \rightarrow {}^7F_6$, 15.4%), 545 ($^5D_4 \rightarrow {}^7F_5$, 63.2%), 586 ($^5D_4 \rightarrow {}^7F_4$, 11.0%), 622 ($^5D_4 \rightarrow {}^7F_3$, 7.5%), 651 ($^5D_4 \rightarrow {}^7F_2$, 2.9%).

CIE coordinates: x = 0.343, y = 0.587.

Characterization: Ln = Tb, L = O=P(NMe$_2$)Ind

IR (KBr, cm^{-1}): 1469s ($\nu_{N=O}$), 1293s (ν^{as}_{ONO}), 1157-1136 s ($\nu_{P=O}$), 996s (ν_{PN}).

PL (solid, $\lambda_{excitation}$ = 375 nm, r.t.), nm: 491 ($^5D_4 \rightarrow {}^7F_6$, 15.9%), 545 ($^5D_4 \rightarrow {}^7F_5$, 65.1%), 586 ($^5D_4 \rightarrow {}^7F_4$, 10.5%), 622 ($^5D_4 \rightarrow {}^7F_3$, 6.4%), 649 ($^5D_4 \rightarrow {}^7F_2$, 2.1%).

CIE coordinates: x = 0.333, y = 0.595.

Characterization: Ln = Tb, L = O=P(MeNCH$_2$CH$_2$NMe)Ph

IR (KBr, cm^{-1}): 1455s ($\nu_{N=O}$), 1296s (ν^{as}_{ONO}), 1152-1131 s ($\nu_{P=O}$).

PL (solid, $\lambda_{excitation}$ = 375 nm, r.t.), nm: 490 ($^5D_4 \rightarrow {}^7F_6$), 544 ($^5D_4 \rightarrow {}^7F_5$), 587 ($^5D_4 \rightarrow {}^7F_4$), 622 ($^5D_4 \rightarrow {}^7F_3$), 652 ($^5D_4 \rightarrow {}^7F_2$), 400 – 700 (ligands luminescence).

CIE coordinates: x = 0.313, y = 0.558.

3. Results and discussion

3.1 Manganese complexes

The thesis work started with the preparation of Mn(II) compounds of general formula $[MnX_2L_2]$ by reacting MnX_2 salts (X = Cl, Br, I) with the proper phosphoramide or arylphosphonic diamide ligand $O=P(NMe_2)_2$(1-Naph), $O=P(NMe_2)_2$(2-Naph), $O=P(NMe_2)_2$Ind or $O=P(MeNCH_2CH_2NMe)Ph$. The reaction conditions were strictly comparable to those used in previous works to prepare species such as $[MnX_2\{O=P(NMe_3)_3\}_2]$ and $[MnX_2\{O=P(NMe_2)_2Ph\}_2]$, where X = Br and I. In particular, it was previously shown that the increase of ligand : precursor ratio from the stoichiometric 1 : 2 did not cause any variation in the final products.

The reactions with the new [O=P]-donor ligands afforded quite stable luminescent derivatives in all the cases where X = Cl or Br, while most of the preparations involving MnI_2 as reactant led to the isolation of unstable species with negligible luminescence, which were no further investigated. The following discussion is focused on the compounds that showed photoluminescence by excitation with Uv light.

The position of the emission band was a clear preliminary indication of the geometry of the complexes. Tetrahedral complexes of general formula $[MnX_2L_2]$, where L= $O=P(MeNCH_2CH_2NMe)Ph$ or $O=P(NMe_2)_2$Ind, showed emissions in the green region of the spectra. The coordination geometry was confirmed by single-crystal X-ray diffraction for $[MnCl_2\{O=P(NMe_2)_2(Ind)\}_2]$, $[MnBr_2\{O=P(NMe_2)_2(Ind)\}_2]$, $[MnCl_2\{O=P(MeNCH_2CH_2NMe)Ph\}_2]$ and $[MnBr_2\{O=P(MeNCH_2CH_2NMe)Ph\}_2]$.

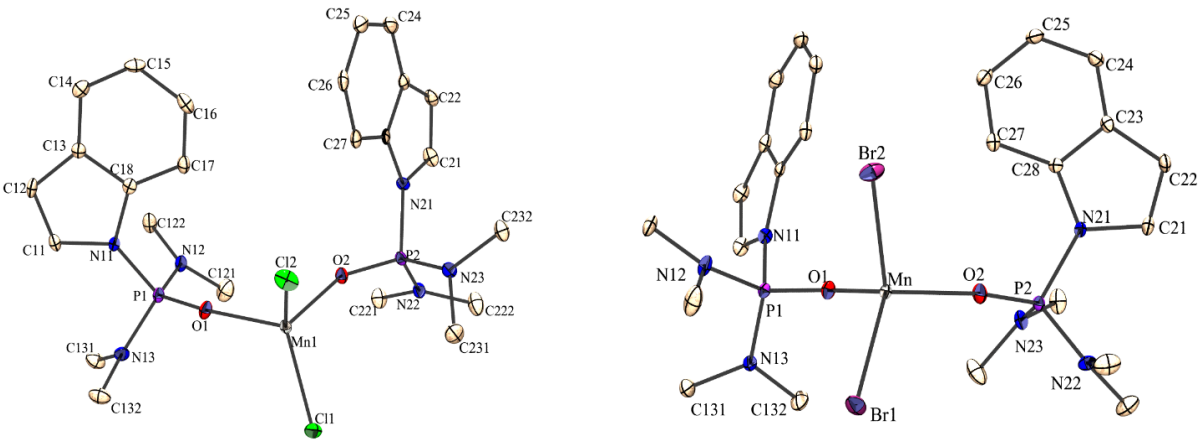

Figure 23. X-ray structure of $[MnCl_2\{O=P(NMe_2)_2(Ind)\}_2]$ and $[MBr_2\{O=P(NMe_2)_2(Ind)\}_2]$.

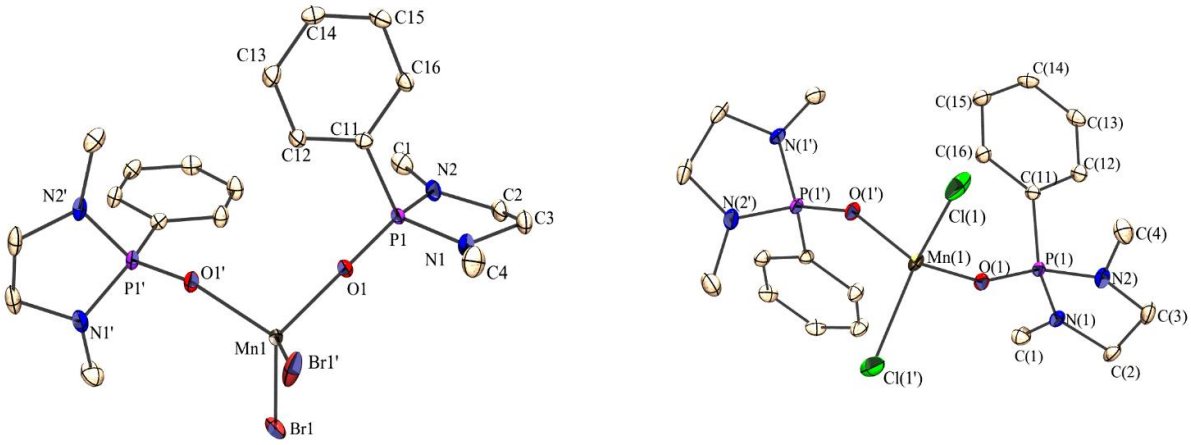

Figure 24. X-ray structure of [$MnCl_2${O=P(MeNCH$_2$CH$_2$NMe)Ph}$_2$] and [$MnBr_2${O=P(MeNCH$_2$CH$_2$NMe)Ph}$_2$].

All crystals are monoclinic. The space group of the complexes is C2/c when L= O=P(NPhCH$_2$CH$_2$NPh)Ph and P2$_1$/n when L= O=P(NMe$_2$)$_2$(Ind). It is worth noting that also complexes of general formula [MnX_2{O=P(NMe$_2$)$_2$Ph}$_2$] have tetrahedral geometry and show photoluminescence in the green region of the spectra. [99]

The absorptions of [MnX_2{O=P(NMe$_2$)$_2$Ph}$_2$] complexes start below 300 nm, and comparable absorption ranges were observed for the new derivatives of the ligands P=O(NMe$_2$)Ind and O=P(MeNCH$_2$CH$_2$NMe)Ph. The new compounds showed green emission centred between 535 and 519 nm when L = O=P(NMe$_2$)$_2$(Ind), while when L= O=P(MeNCH$_2$CH$_2$NMe)Ph the maximum of the emission band can be found between 508 and 512 nm. All the emissions are associated to the $^6A_1(^6S) \leftarrow {}^4T_1(^4G)$ transition of the metal centre.

Molecular formula	$\lambda_{max,\ em}$ (nm)	τ (μs)
[$MnCl_2${O=P(NMe$_2$)$_2$(Ind)}$_2$]	527	1248
[MBr_2{O=P(NMe$_2$)$_2$(Ind)}$_2$]	535	546
[MnI_2{O=P(NMe$_2$)$_2$(Ind)}$_2$]	519	---
[$MnCl_2${O=P(NMeCH$_2$CH$_2$NMe)Ph}$_2$]	508	916
[$MnBr_2${O=P(NMeCH$_2$CH$_2$NMe)Ph}$_2$]	509	683
[MnI_2{O=P(NMeCH$_2$CH$_2$NMe)Ph}$_2$]	512	137

Table 4. PL maximum and lifetime of green-emitting manganese complexes.

The FWHM of the emission bands for [MnX_2{O=P(MeNCH$_2$CH$_2$NMe)Ph}$_2$] is between 2500 and 2100 cm^{-1}, and the mono-exponential fitting of the decay curves indicates the presence of single-emitting species. Lifetime values strongly depend upon the different halides and decrease from 916 μs when X = Cl to 137 μs when X = I because of the increased spin-orbit coupling.

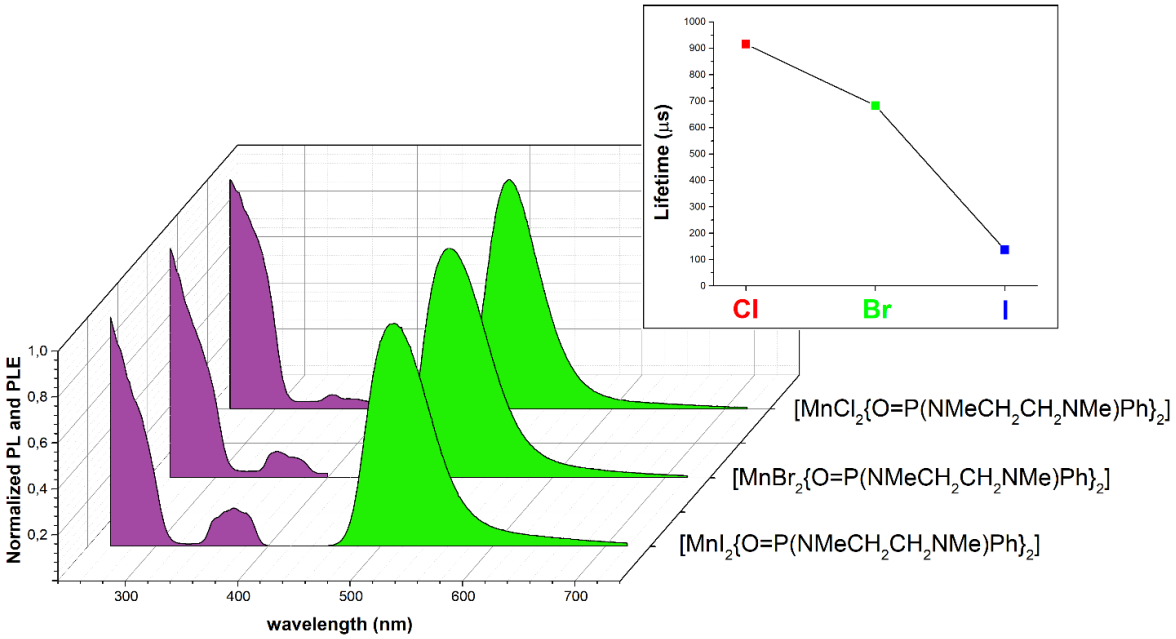

Table 25. Normalized PLE, PL spectra and lifetimes of green emitting manganese complexes where L= O=P(NMeCH₂CH₂NMe)Ph.

Manganese emissions are caused by excitation of the ligands for wavelengths below about 300 nm and also by the direct excitation of the metal centre, as can be seen by the PLE bands in the region 335-400 nm due to $^4P,^4D \leftarrow ^6S$ transitions. Colour purities for $[MnX_2\{O=P(MeNCH_2CH_2NMe)Ph\}_2]$ complexes are between 59% and 63%.

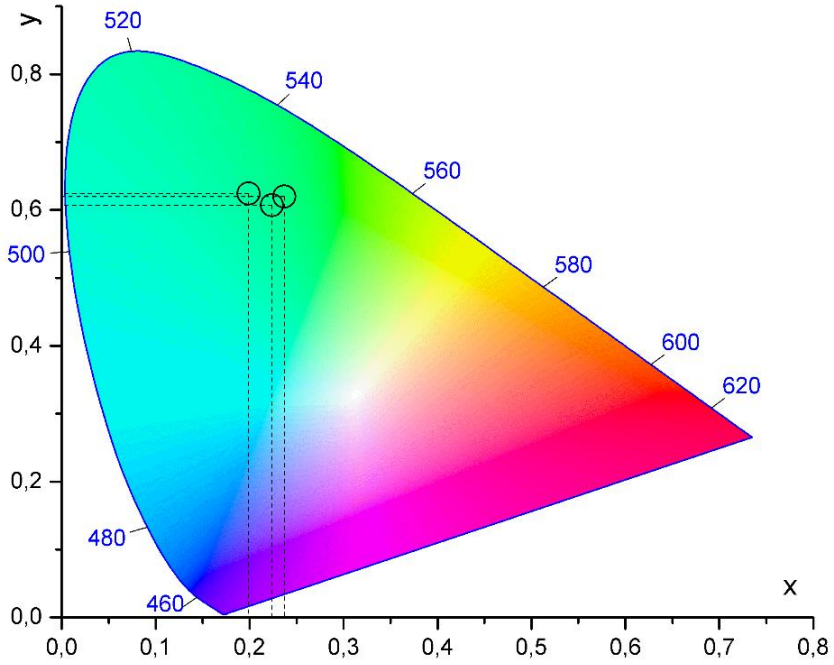

Figure 26. CIE diagram of $[MnX_2\{O=P(MeNCH_2CH_2NMe)Ph\}_2]$ complexes.

Despite the fact that Mn(II) chloro- and bromo-complexes with the indazolyl-based ligand showed photoluminescence roughly comparable with that of the 1,3-dimethyl-2-phenyl-1,3-diazaphospholidine-2-oxide derivatives, it is worth noting that the manganese iodo-complex of formula $[MnI_2\{O=P(NMe_2)_2Ind\}_2]$ showed a second broad emission band centred around 660 nm, corresponding to an emission in the red region of the spectrum. This band is probably due to the presence of a by-product with the same general formula $[MnX_2L_2]$, but experiencing different field strength. The red-emitting species probably corresponds to a dimerization or oligomerization product where Mn(II) can be penta- or hexa-coordinated. The formation of the by-product can be ascribed to the weak donor ability of iodide towards Mn(II) and to the reduced σ-donation of the [O=P]-donor ligand caused by the conjugation with the indolyl fragment. The lower electronic saturation of the coordination sphere can explain the tendency to increase the coordination number.

CIE 1931 colour spaces diagram for $[MnX_2\{O=P(NMe_2)_2Ind\}_2]$ complexes gives colour purity values of 74%, 73% and 79% for $[MnCl_2\{O=P(NMe_2)_2Ind\}_2]$, $[MnBr_2\{O=P(NMe_2)_2Ind\}_2]$ and $[MnI_2\{O=P(NMe_2)_2Ind\}_2]$ respectively.

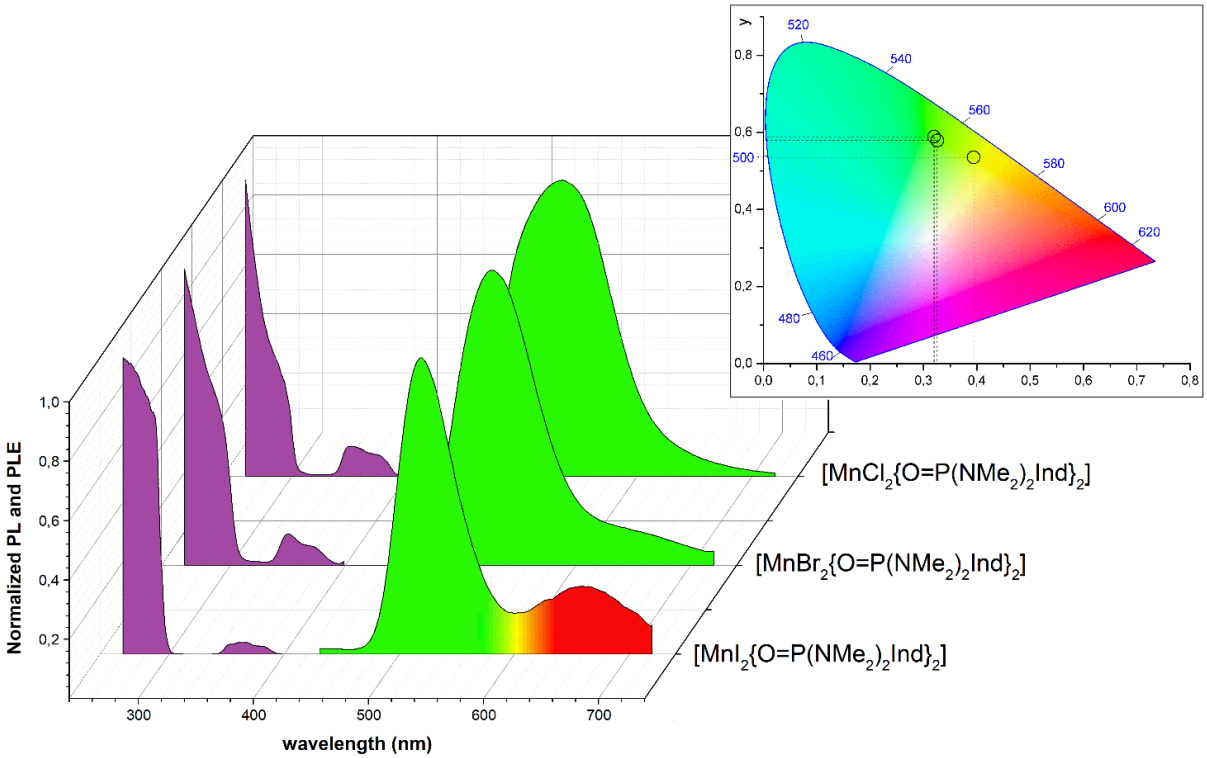

Figure 27. Normalized PLE and PL spectra of green emitting manganese complexes where L= $O=P(NMe_2)_2Ind$ and the corresponding CIE diagram.

The use of $O=P(NMe_2)_2$(1-Naph) or $O=P(NMe_2)_2$(2-Naph) as ligands afforded species characterized by emissions in the red region, suggesting an increment of the coordination number that can be related to bridging coordination mode of halide ions. Unfortunately, no crystal suitable for X-ray diffraction was obtained during the internship, so it is not possible in this moment to unambiguously determine the structure of the red-emitting manganese-based species.

$[MnX_2\{O=P(NMe_2)_2Ar\}_2]_n$ complexes where X=Cl, Br and Ar=1-Naph, 2-Naph showed red emission centred between 645 and 631 nm. The small differences among the luminescence bands suggest similar crystal field strength. The emissions are related to the $^6A_1$ (^6S)←$^4T_1$(^4G) transition of the metal centre, with FWHM around 2300 – 2600 cm^{-1}. Colour purity is around 96% for all complexes. Manganese emissions are mainly associated to absorptions below 380 nm in solid state, but also weaker excitation bands in the visible region between 400 nm and 500 nm can be seen, attributable to direct Mn(II) excitation.

The formal replacement of the phenyl fragment with 1- or 2-naphthyl caused an expected shift of the absorption bands at longer wavelengths. In the Uv-vis spectra of red-emitting complexes where Ar=2-Naph the absorption starts at 335 nm, reaches a maximum at 325 nm and it is then followed by a strong increment from 262 nm to lower wavelengths due to the absorptions associated to the aromatic fragment. The absorptions in complexes with Ar=1-Naph also start around 335 nm, with a broad absorbance band around 285 nm followed by a strong increment from 250 nm to lower wavelengths. The presence of different halides does not influence the absorption spectra. Absorptions due to Mn^{2+} transitions were not detected, but it is worth noting that d←d transitions are both spin and parity forbidden in octahedral environments and are parity forbidden for other coordination numbers.

Molecular formula	$\lambda_{max,\ em}$ (nm)	τ_1 (ms)	τ_2 (ms)
$[MnCl_2\{O=P(NMe_2)_2(1\text{-}Naph)\}_2]$	638	1.677	0.326
$[MnBr_2\{O=P(NMe_2)_2(1\text{-}Naph)\}_2]$	645	1.582	0.237
$[MnCl_2\{O=P(NMe_2)_2(2\text{-}Naph)\}_2]$	635	0.996	0.156
$[MnBr_2\{O=P(NMe_2)_2(2\text{-}Naph)\}_2]$	631	0.688	0.070

Table 5. PL maximum and lifetime of red-emitting manganese complexes.

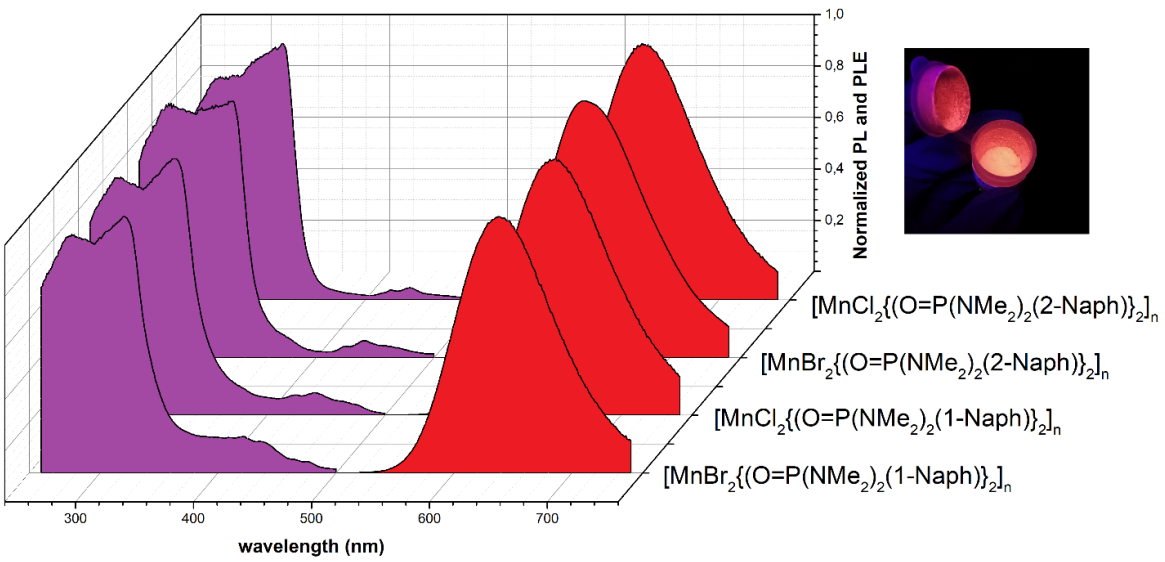

Figure 28. Normalized PLE and PL spectra of red emitting manganese complexes (λ_{ex}=300nm, λ_{em}=640nm).

The presence of more than one luminescent species is suggested by the double exponential fitting of the lifetimes. As reported in Figure 29, the logarithmic plot clearly shows the presence of two lifetime values τ_1 and τ_1. Bromide species always show shorter lifetime than the chloride analogues. As previously discussed, heavy atoms favours the intersystem crossing between singlet and triplet states of the ligands because of the stronger spin-orbit effect. [100]

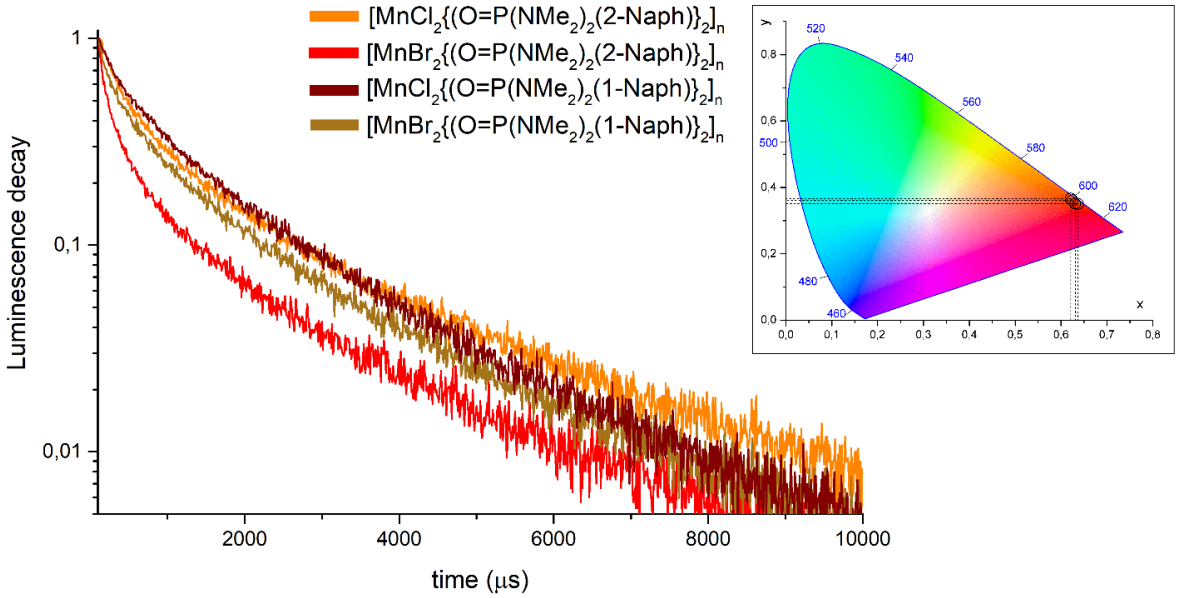

Figure 29. Log_{10} plot of luminescence decay of red-emitting manganese complexes.

The change of coordination geometry suggested by the shift in the red region of the emission bands was an unexpected result. The different coordination abilities of $O=P(NMe_2)_2Ph$, $O=P(NMe_2)_2$(1-Naph) and $O=P(NMe_2)_2$(1-Naph) might be due to both steric and electronic reasons, but the comparable behaviour of the two naphtyl-substituted ligands suggests that electronic factors are probably more important than steric ones. It is likely to suppose that the increased π conjugation favours the delocalization of the doublets of the ligands on the oxygen atoms, decreasing the σ-donation of the O-donor ligands towards Mn(II) and the repulsion in the first coordination sphere. Both these effects could explain the increment of coordination number, with formation of halide-bridged final products.

Magnetic susceptibilities confirmed that the proposed minimal formula $[MnX_2L_2]$ is the same for all the prepared species. It is worth remembering that the expected magnetic moment for a high-spin d^5 ion such as Mn(II) is 5.92 BM.

Molecular formula	χ_m,app (10^{-4} erg G^{-2} mol^{-1})	χ_m,para (10^{-4} erg G^{-2} mol^{-1})	μ_{calc} (BM)
$[MnCl_2\{O=P(NMe_2)_2(1\text{-Naph})\}_2]$	13.15	13.55	5.69
$[MnBr_2\{O=P(NMe_2)_2(1\text{-Naph})\}_2]$	14.18	14.61	5.91
$[MnCl_2\{O=P(NMe_2)_2(2\text{-Naph})\}_2]$	14.55	14.95	5.97
$[MnBr_2\{O=P(NMe_2)_2(2\text{-Naph})\}_2]$	14.45	14.88	5.96
$[MnCl_2\{O=P(NMe_2)_2(Ind)\}_2]$	16.54	16.93	6.36
$[MBr_2\{O=P(NMe_2)_2(Ind)\}_2]$	14.95	15.36	6.05
$[MnI_2\{O=P(NMe_2)_2(Ind)\}_2]$	14.79	15.22	6.03
$[MnCl_2\{O=P(NPhCH_2CH_2NPh)Ph\}_2]$	14.98	15.32	6.05
$[MnBr_2\{O=P(NPhCH_2CH_2NPh)Ph\}_2]$	14.12	14.48	5.88
$[MnI_2\{O=P(NPhCH_2CH_2NPh)Ph\}_2]$	14.71	15.09	6.00

Table 6. Magnetic susceptibilities of manganese complexes.

The coordination of the ligands to Mn(II) can be detected from the IR spectra, considering in particular the position of P=O stretching signal. This band can be found around 1160-1170 cm^{-1} in the complexes, while in the free ligands it falls between 1220 and 1190 cm^{-1}. The band shift to lower energy is due to the weakening of the P=O bond caused by coordination. According to the phosphoramide orientation around the metal, signals relative to both symmetric and anti-symmetric P=O stretchings of the two ligands might be found. However, because of bands superposition in that region of the spectra, it is difficult to clearly identify these two signals in the complexes. The remaining signals can be all attributed to other vibrations of the ligands and did not show relevant variations due to the coordination.

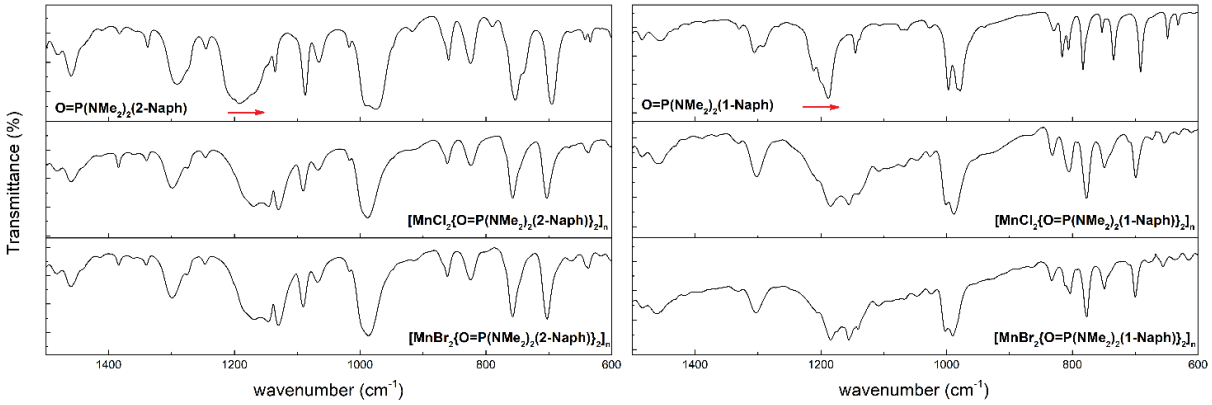

Figure 30. IR spectra of red-emitting manganese complexes and the $O=P(NMe_2)_2$(1-Naph) and $O=P(NMe_2)_2$(2-Naph) free ligands.

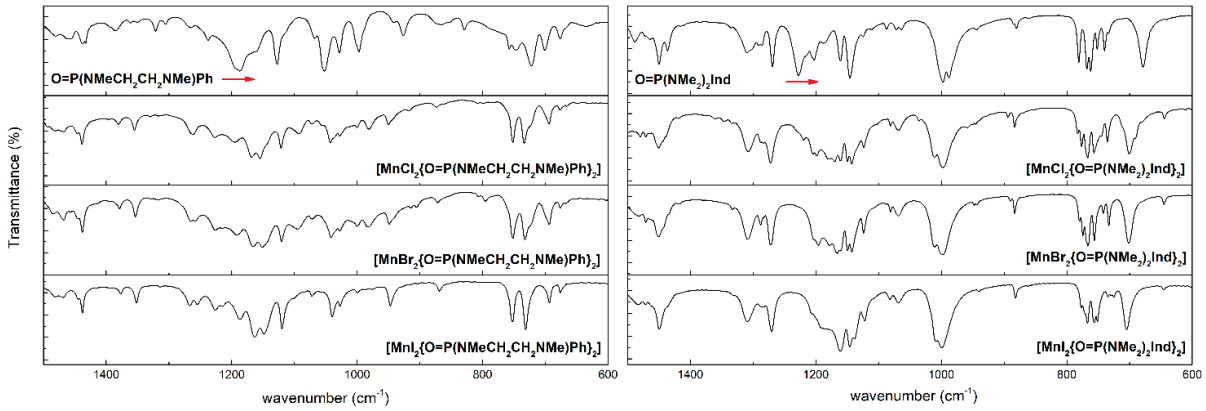

Figure 31. IR spectra of green-emitting manganese complexes and the $O=P(NMeCH_2CH_2NMe)Ph$ and $O=P(NMe_2)Ind$ free ligands.

The reduction of electron density on the [O=P] oxygen caused by conjugation with aromatic fragments was confirmed by the use of 1,3-diphenyl-2-phenyl-1,3-diazaphospholidine-2-oxide as potential ligand. Such a molecule was unable to coordinate the Mn(II) centre, this indicating a meaningful reduction of the Lewis base behaviour caused by the introduction of phenyl substituents on the nitrogen atoms.

Despite the relative stability of the new compounds, attempts of encapsulation in PMMA and PCL polymer matrices were unsuccessful and caused luminescence quenching, probably because of the displacement of the [O=P]-donor ligands by the polymer chains in the Mn(II) coordination sphere. Doped polymers were therefore no longer investigated.

3.2 Lanthanide complexes

The coordination properties of the newly prepared ligands toward Ln(III) centres were first tested by coordination to nitrate fragments [$Ln(NO_3)_3$]. The products of the syntheses rapidly decompose in presence of moisture, complicating the full characterization. [101] Nitrate complexes were prepared and stocked in glove-box under inert atmosphere. To record the IR spectra, the samples were prepared in glove-box using an air-tight sample holder with KBr windows, while for PL and PLE measurement sealed off cuvettes were used. The presence of coordinated nitrate groups κ^2-coordinated is confirmed by two stretching bands due to $\nu_{N=O}$ and ν^{as}_{ONO} vibrations centred around 1450 and 1290 cm^{-1}. Ligand bands relative to P-N and P=O vibrations are also clearly detectable, with the letter shifted to lower energy by a quantity between 40 and 60 cm^{-1} because of coordination. [102].

The emission spectra of europium nitrate complexes were recorded with near-Uv excitation at 375 nm, showing bands associated to $^5D_0 \rightarrow {}^7F_J$ transitions of the metal centre, with the most intense due to the hypersensitive $^5D_0 \rightarrow {}^7F_2$ centred at 617 nm for all complexes. The relative intensities seem not to be strongly affected by the different substituents in the ligands.

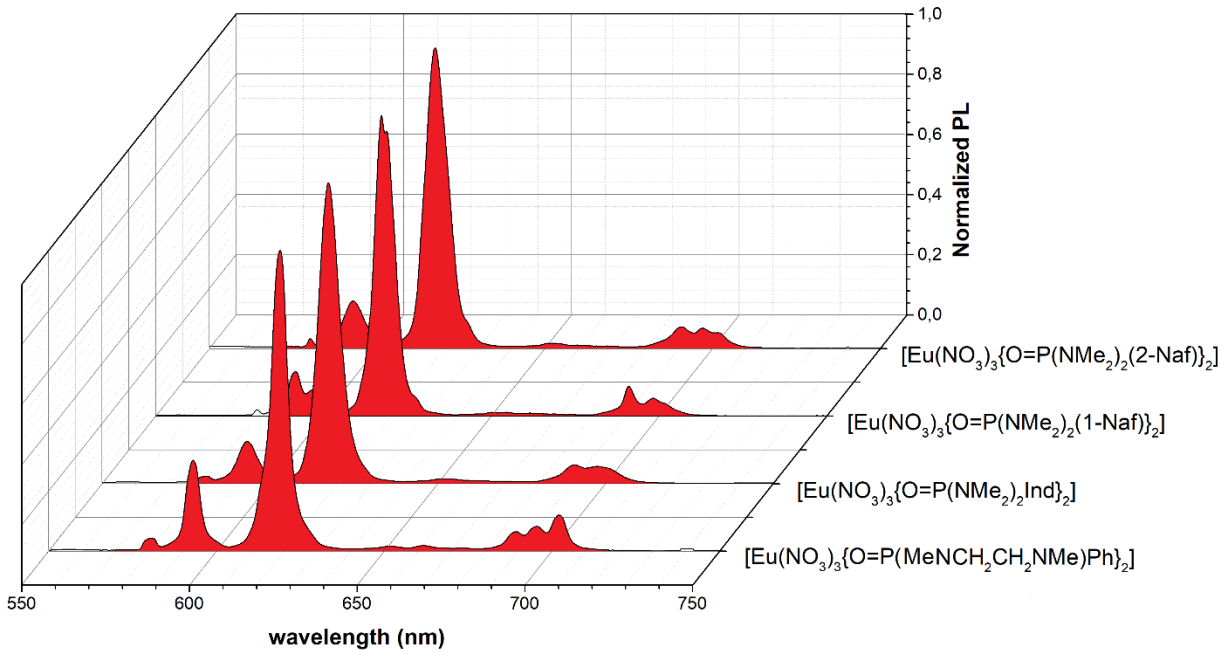

Figure 32. Normalized PL spectra of $[Eu(NO_3)_3L_2]$ complexes (λ_{ex}=375nm).

The triplet states of the ligands were calculated on the basis of the PL spectra of the analogous Gd(III) complexes. No metal-centred photoluminescence can be observed for Gd(III)

complexes because of the high energy of its $^6P_{7/2}$ resonant level, therefore only fluorescence and phosphorescence bands can be detected. Phosphorescence band is often covered by fluorescence and vibrational relaxation from triplet to ground state is more efficient at room temperature because of better wavefunctions superposition. To evaluate the triplet state, the PL spectra at room and low temperature needs to be compared. In fact, at low temperature vibrational relaxation from triplet state is less effective, and the phosphorescence band increases its intensity. The energy of the triplet state is then assumed to coincide with the first inflexion point of that band. The as calculated triplet energy levels of coordinated $O=P(NMe_2)_2$(1-Naph) and $O=P(NMe_2)_2$(2-Naph) are ≈ 19.500 cm^{-1} and ≈ 19400 cm^{-1} respectively, while the value is greater than 21200 cm^{-1} for the other ligands. The lower triplet state energy level for 1-Naph and 2-Naph substituted ligands is probably due to the increased π conjugation. In all the cases the triplet state is above the $^5D_0$ resonant level of Eu(III), 17.250 cm^{-1}, in agreement with the previously discussed luminescence results.

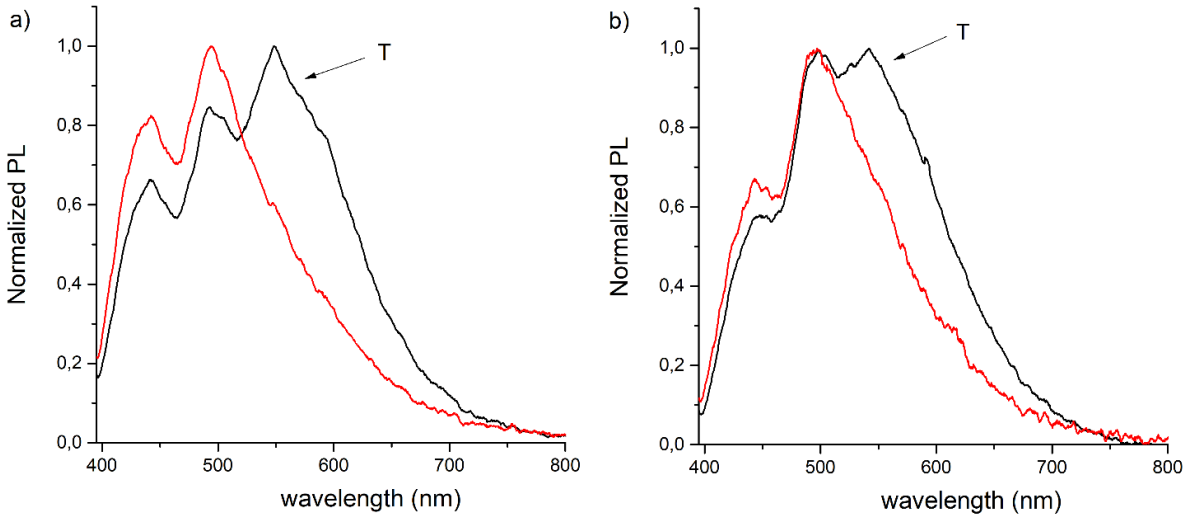

Figure 33. Normalized PL spectra of a) [$Gd(NO_3)_3${$O=P(NMe_2)_2$(2-Naph)}] and b) [$Gd(NO_3)_3${$O=P(NMe_2)_2$(1-Naph)}] recorded at 298,5 K (red line) and 218,5 K (black line) ($\lambda_{excitation}$=375nm).

The Tb(III) $^5D_4$ resonant level falls at 20.430 cm^{-1}, therefore the $O=P(NMe_2)_2$(1-Naph) and $O=P(NMe_2)_2$(2-Naph) should be unable to sensitize the luminescence of this lanthanide ion. This fact was experimentally confirmed, because derivatives of Tb(III) nitrate with naphyl-based ligands did not show any appreciable luminescence.

Ligand	Triplet state energy, cm^{-1}
$O=P(NMe_2)_2$(1-Naph)	≈ 19.500
$O=P(NMe_2)_2$(2-Naph)	≈ 19.400
$O=P(NMe_2)_2Ph$	21.600
$O=P(NMe_2)_2Ind$	21.800
$O=P(MeNCH_2CH_2NMe)Ph$	21.300

Table 7. Triplet state energy of the ligands.

All the Tb(III) complexes with L= $O=P(NMe_2)_2Ph$, $O=P(NMe_2)_2Ind$ and $O=P(MeNCH_2CH_2NMe)Ph$ where instead able to undergo the typical Tb(III) luminescence, despite the fact that the energy difference between triplet and $^5D_4$ levels is lower than the suggested value for an efficient energy transfer. [103] Photoluminescence spectra with excitation at 375 nm show $^5D_4 \rightarrow {}^7F_J$ transitions of the metal ion, the most intense centred at around 545 nm and associated to $^5D_4 \rightarrow {}^7F_5$ transition. Again, different ligands seem not to affect the relative intensities of the emission bands.

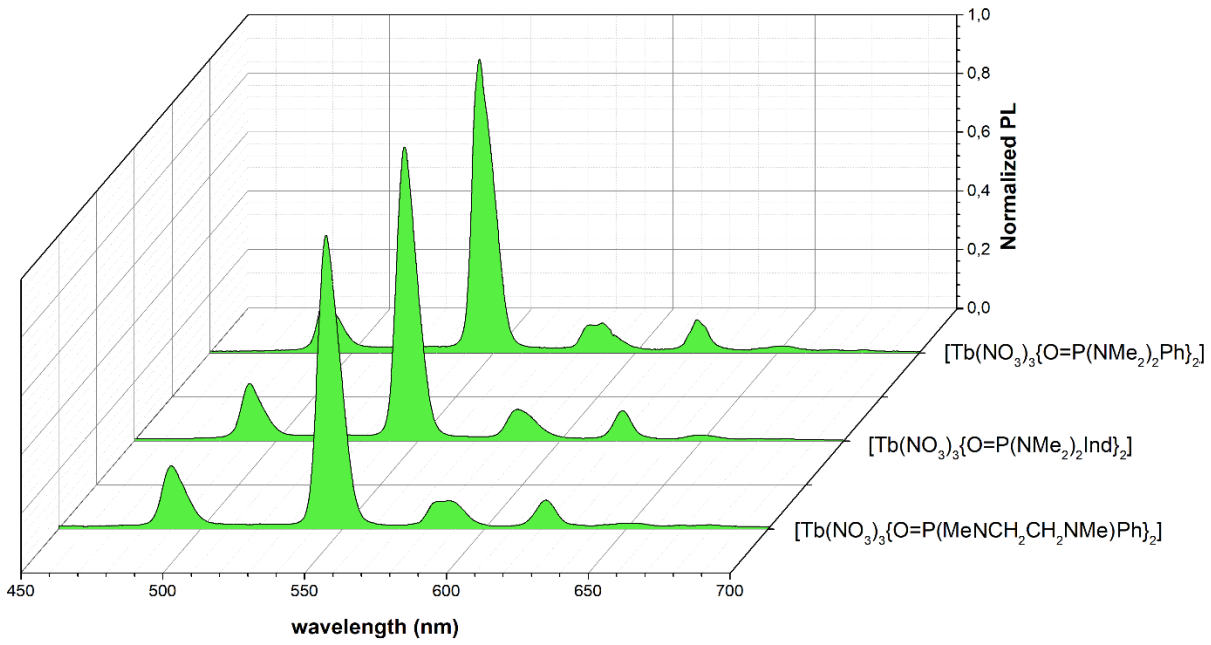

Figure 34. PL complexes of $[Tb(NO_3)_3L_2]$ complexes (λ_{ex}=375nm).

The efficiency of acting as antenna ligands for europium emission was then studied by preparing β-diketonate complexes of formulae $[Eu(\beta\text{-dike})_3L]$ and $[Eu(\beta\text{-dike})_3L_2]$, where β-dike is dibenzoylmethanate (dbm) or tenoyltrifluoroacetonate (tta). The complexes were synthesized by addition of the proper ligand to a solution containing the *in situ* formed $[Eu(\beta\text{-dike})_3]$ precursors. The coordination of the phosphoramide ligands to the metal saturates the

coordination sphere, giving heptacoordinate species when $O=P(NMe_2)_2$(1-Naph), $O=P(NMe_2)_2$(2-Naph), $O=P(NMe_2)_2Ph$, $O=P(NMe_2)_2$Ind were used as ligands. Since the x-ray structure of the heptacoordinate compound $[Eu(dbm)_3(hmpa)]$, with monocapped trigonal prismatic geometry, was reported by Panin et al., the use of even more sterically demanding phosphoramides, such as those reported above, were supposed to lead to the coordination of a single ligand. [94] The coordination of more than one phosphoramide ligand to Eu(III) was also tested, in order to prepare eight-coordinated complexes of general formula $[Eu(\beta\text{-dike})_3L_2]$. For this purpose, the less sterically demanding $O=P(MeNCH_2CH_2NMe)Ph$ ligand was considered and used in 2:1 molar ratio with respect to the metal centre. Magnetic susceptibilities of complexes with general formulae $[Eu(\beta\text{-dike})_3L]$ and $[Eu(\beta\text{-dike})_3L_2]$ confirmed the proposed formulae, associated to hepta- and octa-coordinated geometries. The expected value for an Eu(III) complexes is 3.3 BM.

All the isolates lanthanide β-diketonate complexes have good air stability and did not show any decrease in the luminescence intensity over a period of 6 months. Decomposition temperatures range from 65°C to 95°C. The ligand 1,3-diphenyl-2-phenyl-1,3-diazaphospholidine-2-oxide $[O=P(NPhCH_2CH_2NPh)Ph]$ did not show any coordination ability to any lanthanide centre, in agreement with the results previously described for Mn(II).

Molecular formula	$\chi_{m,app}$ (10^{-4} erg G^{-2} mol^{-1})	$\chi_{m,para}$ (10^{-4} erg G^{-2} mol^{-1})	μ_{calc} (BM)
$[Eu(tta)_3\{P=O(NMe_2)_2Ph\}]$	3.55	4.02	3.10
$[Eu(dbm)_3\{O=P(NMe_2)_2(1\text{-Naph})\}]$	3.95	4.54	3.29
$[Eu(tta)_3\{O=P(NMe_2)_2(1\text{-Naph})\}]$	3.99	4.48	3.27
$[Eu(dbm)_3\{O=P(NMe_2)2\text{-Naph})\}]$	4.21	4.78	3.38
$[Eu(tta)_3\{O=P(NMe_2)_2(2\text{-Naph})\}]$	4.22	4.79	3.34
$[Eu(dbm)_3\{O=P(NMe_2)_2(Ind)\}]$	4.03	4.61	3.32
$[Eu(tta)_3\{O=P(NMe_2)_2(Ind)\}]$	3.77	4.25	3.19
$[Eu(dbm)_3\{O=P(MeNCH_2CH_2NMe)Ph\}_2]$	3.58	4.18	3.16
$[Eu(tta)_3\{O=P(MeNCH_2CH_2NMe)Ph\}_2]$	3.21	3.91	3.06

Table 8. Magnetic susceptibilities of lanthanide complexes.

The coordination of the ligands was confirmed by the presence of the typical stretching bands ν^{as}_{NPN}, $\nu_{P\text{-}N}$, $\nu_{P\text{-}O}$ in the IR spectra of the complexes. The P=O stretching band is always shifted to lower wavenumbers by a quantity between 80 and 25 cm^{-1} because of coordination. In $[Eu(\beta\text{-dike})_3L]$ complexes a single P=O stretching band is present, while for $[Eu(\beta\text{-dike})_3L_2]$ two stretching bands due to both the symmetric and asymmetric P=O vibrations of the ligands are

found. Bands involving C-C and C=O vibrations of β-diketonate are also clearly observable in the IR spectra.

NMR spectra of the as obtained complexes helped in the identification and the quantification of the ligands. All $^{31}P\{^{1}H\}$ NMR spectra show a singlet signal, broad if compared to the that of the corresponding free ligand, indicating the interaction of the [O=P] fragments with Eu(III). ^{19}F NMR spectra of the tta derivatives show a singlet at around -78.3 ppm, confirming the presence of the $-CF_3$ group. For these complexes ^{1}H NMR spectra show three singlet signals of the aromatic protons of thiophene fragments at 7.44, 6.51 and 6.35 ppm. In the case of dibenzoylmethanate complexes, integration data and multiplicity helped for the identification of para, meta and ortho aromatic protons of dbm, which fall at 6.82 (t), 6,67 (t, dd), 5.73 (d) ppm respectively. The β-dike CH resonances can be found at about 7.2 and 3.8 ppm for the dbm and tta complexes respectively.

All the signal for the aromatic substituents of the [O=P]-donor ligands are shifted with respect to the free ligand because of paramagnetic effects, and their complete identification is complicated by signals superpositions. These signals fall in the high frequency region of the ^{1}H NMR spectra and are poorly resolved when the steric bulk makes difficult the free rotation of the substituents, as occurs in $[Eu(dbm)_3\{O=P(NMe_2)_2Ind\}]$, $[Eu(dbm)_3\{O=P(NMe_2)_2(1\text{-}Naph)\}]$ and $[Eu(tta)_3\{O=P(NMe_2)_2(1\text{-}Naph)\}]$. The N-Me resonance is instead clearly observable, with a doublet between 2.63 and 2.56 ppm and J_{PH}= 9-10 Hz. ^{1}H NMR integration data are in agreement with the presence of only one neutral ligand in the complexes $[Eu(\beta\text{-}dike)_3L]$ where L= $O=P(NMe_2)_2(1\text{-}Naph)$, $O=P(NMe_2)_2(2\text{-}Naph)$, $O=P(NMe_2)_2Ph$ and $O=P(NMe_2)_2Ind$. The ^{1}H, $^{31}P\{^{1}H\}$ and ^{19}F NMR spectra of $[Eu(tta)_3\{O=P(NMe_2)_2Ind\}]$ are reported as examples in Figure 35.

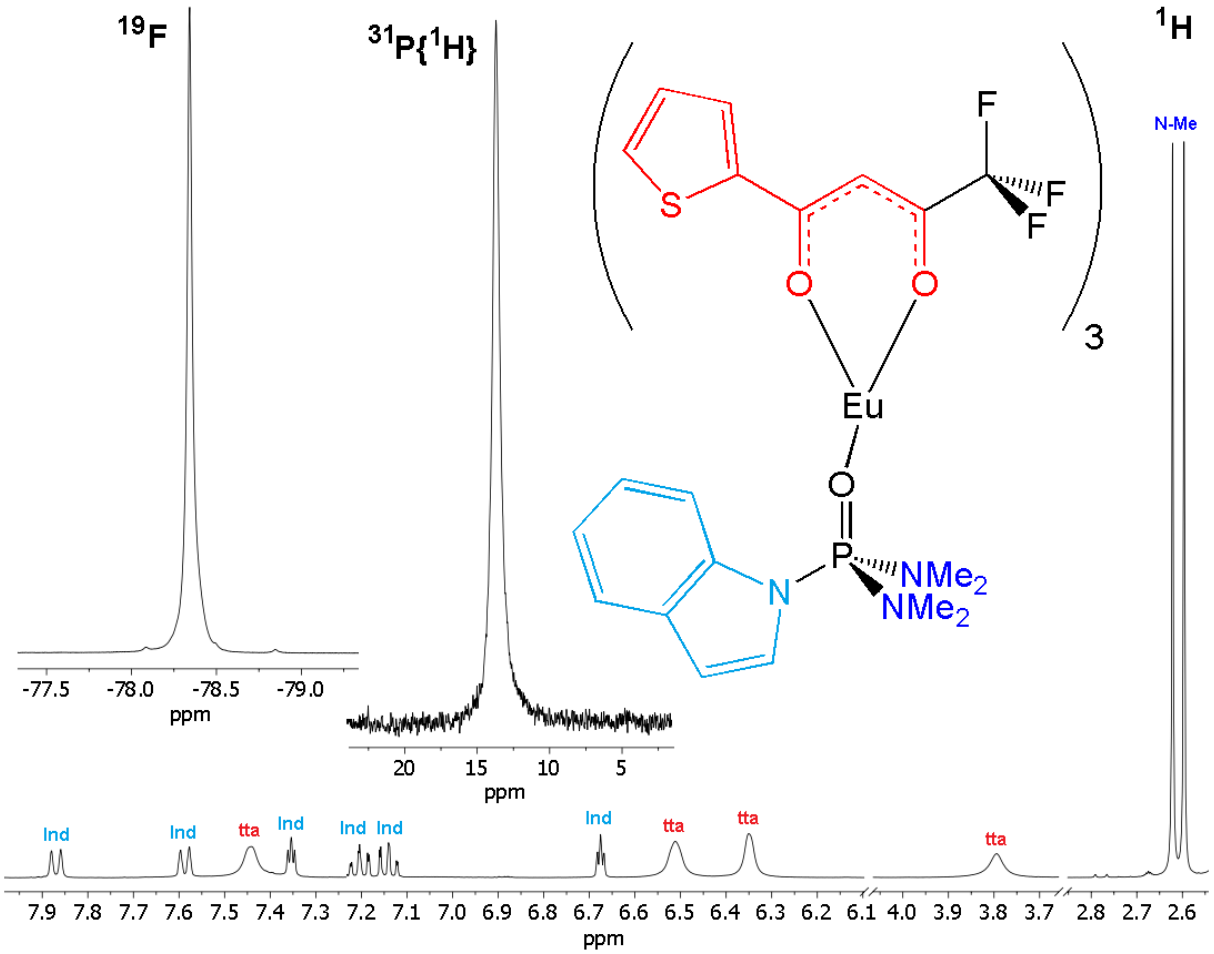

Figure 35. NMR spectra of [Eu(tta)$_3${O=P(NMe$_2$)$_2$Ind}].

NMR spectra of complexes with general formulae [Eu(β-dike)$_3$L$_2$] helped in the identification and quantification of the ligands. The ^{1}H and ^{19}F NMR spectra showed the above described resonances for the β-diketonate ligands. The 1,3-diazaphospholidine-2-oxide ligand can be detected in the ^{1}H NMR spectrum by the N-Me resonance around 2.36 ppm, with $^3J_{PH}$ coupling constant of 10 Hz. Two second-order multiplets are also present in the range 3.30 – 3.15 ppm, attributable to the [N-CH$_2$-CH$_2$-N] fragment of the five-membered cycle. The presence of two groups of signals is associated to the lack of equivalence of the protons in *E* and *Z* position with respect to the *P*-bonded phenyl ring. The aromatic substituent is associated to a series of signals in the high frequency region of the ^{1}H NMR spectra. Integration data support the formation of eight-coordinated complexes with three β-diketonate and two [O=P]-donor ligands. Only one singlet is present in the ^{31}P{^{1}H} NMR spectra, broadened with respect to the free ligand, suggesting that the 1,3-diazaphospholidine-2-oxide ligand interacts with the Eu(III) centre in DMSO-d_6 solution. The FWHM values are 30 and 170 Hz respectively for the dbm

and tta derivatives, while the FWHM value for the free ligand is 3 Hz. The higher broadening in $[Eu(tta)_3L_2]$ with respect to $[Eu(dbm)_3L_2]$ agrees with the lower steric bulk of tta, that probably allows a stronger coordination of L. The ^{1}H, $^{31}P\{^{1}H\}$ and ^{19}F NMR spectra of $[Eu(tta)_3\{O=P(NMeCH_2CH_2NMe)Ph\}_2]$ are reported as examples in Figure 36.

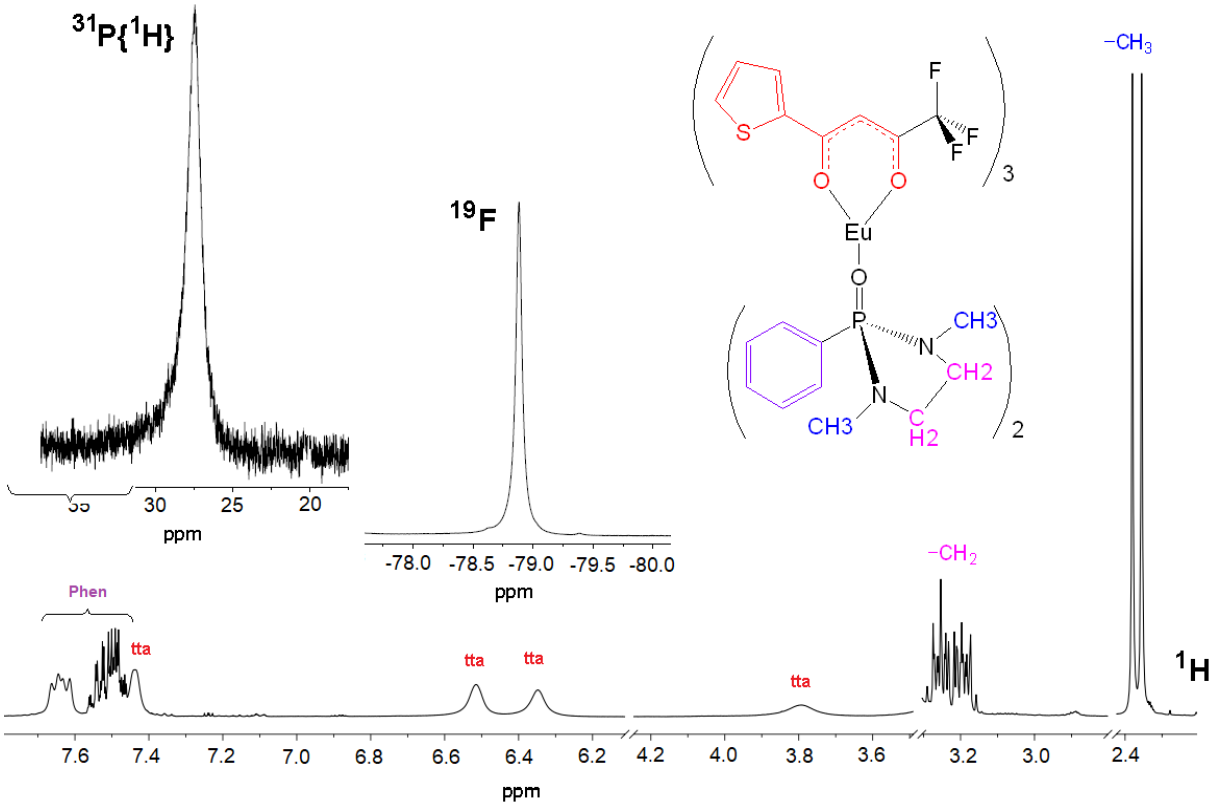

Figure 36. NMR spectra of $[Eu(tta)_3\{O=P(NMeCH_2CH_2NMe)Ph\}_2]$.

The computational geometry optimizations first involve a semi-empirical method, followed by more refined DFT calculations. The DFT-optimized geometries of the $[Eu(\beta\text{-dike})_3L_2]$ complexes, depicted in Figure 37, support the formation of eight-coordinated compounds, being the two 1,3-diazaphospholidine-2-oxide ligands coordinated to Eu(III) with comparable bond lengths. As deduced from the ^{31}P NMR data, the Eu-O(L) distances are slightly shorter (2.322 - 2.354 Å) in the tta derivative with respect to the dbm complex (2.395 - 2.420 Å) as a consequence of the lower steric bulk. The bond lengths related to the coordination of dbm and tta are in line with data reported for several other Eu(III) β-diketonate complexes [64]. The first coordination spheres of both the complexes are asymmetric. The analysis carried out with the SHAPE software (Table 9) indicates that the geometries more similar to the $[EuO_8]$

fragment of $[Eu(dbm)_3L_2]$ are the square antiprism and the triangular dodecahedron, while in the case of $[Eu(tta)_3L_2]$ the first coordination sphere resembles the bi-augmented trigonal prism.

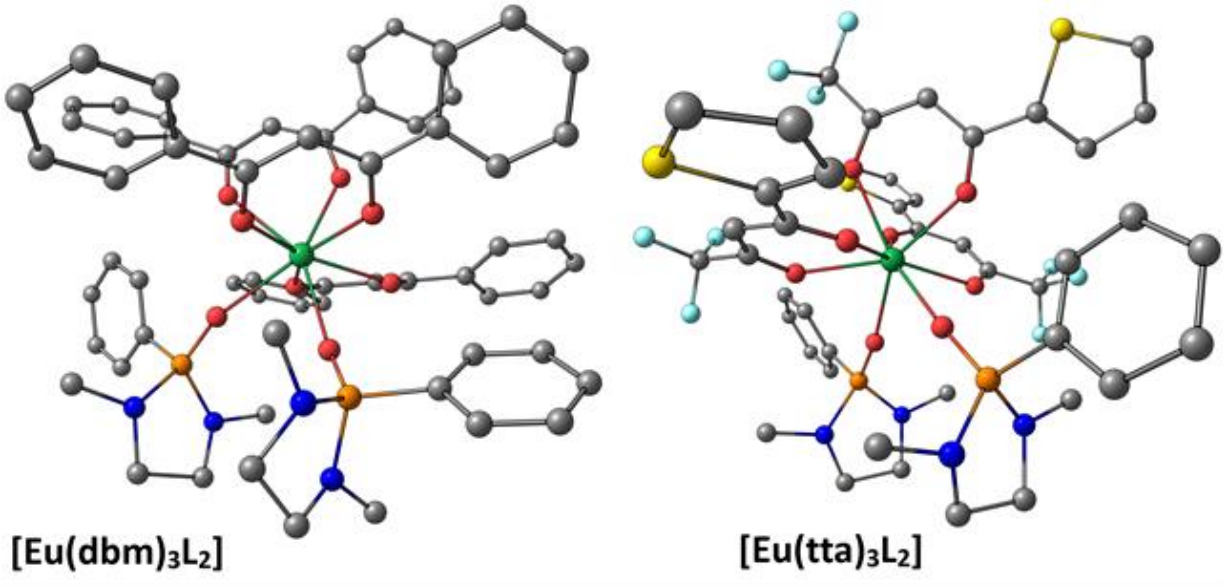

Figure 37. DFT-optimized structures of the $[Eu(\beta\text{-dike})_3L_2]$ complexes. Hydrogen atoms are omitted for clarity. Colour map: Eu, green; C, grey; O, red; N, blue; F, light blue; P, orange; S, yellow. Selected computed bond lengths for $[Eu(dbm)_3L_2]$, Å: Eu-O(dbm) 2.333, 2.377, 2.353, 2.373, 2.359, 2.364; Eu-O(L) 2.395, 2.420. Selected computed bond lengths for $[Eu(tta)_3L_2]$, Å: Eu-O(tta) 2.342, 2.369, 2.355, 2.376, 2.324, 2.450; Eu-O(L) 2.322, 2.354

	OP	*HPY*	*HBPY*	*CU*	*SAPR*	*TDD*	*J26*	*J14*	*J50*	*BTPR*	*J84*	*TT*
$[Eu(dbm)_3L_2]$	31.02	23.59	15.83	9.401	0.944	0.978	15.15	29.27	2.161	1.542	3.675	10.24
$[Eu(tta)_3L_2]$	31.66	23.28	15.89	10.53	1.346	1.434	14.23	29.16	1.574	1.071	3.677	11.18

Table 9. Output of the SHAPE software for the $[Eu(\beta\text{-dike})_3L_2]$ complexes. OP D_{8h} octagon; HPY C_{7v} heptagonal pyramid; HBPY D_{6h} hexagonal bipyramid; CU O_h cube; SAPR D_{4d} square antiprism; TDD D_{2d} triangular dodecahedron; J26 D_{2d} Johnson gyrobifastigium; J14 D_{3h} Johnson elongated triangular bipyramid; J50 C_{2v} biaugmented trigonal prism; BTPR C_{2v} biaugmented trigonal prism; J84 D_{2d} Snub disphenoid; TT T_d triakis tetrahedron.

Europium complexes with dbm and tta as ligands show absorption starting at 430 and 395 nm respectively, with maximum at around 347 nm in both cases. The presence of different phosphoramides seems not to influence the position and the intensity of the main absorption band.

Photoluminescence spectra of β-diketonate complexes did not show any relevant variation on varying the excitation wavelength. The excitation of the coordinated ligands with wavelengths below 500 nm causes the emissions from the Eu(III) centre. Direct excitation of the metal centre is also observable in the PLE spectra and corresponds to the $^5D_2 \leftarrow {}^7F_0$ transition centred

at 464 nm [104]. The PL spectra display only the typical $^5D_0 \rightarrow {}^7F_J$ bands with J =0 – 4. Emissions due to $^5D_0 \rightarrow {}^7F_5$ and $^5D_0 \rightarrow {}^7F_6$ are centred between 740-760 and 790-840 nm respectively, but are extremely weak and difficult to distinguish from the background in all the cases. The most intense emission is due to the hypersensitive $^5D_0 \rightarrow {}^7F_2$ transition, centred between 611 and 615 nm.

The $^5D_0 \rightarrow {}^7F_2/{}^5D_0 \rightarrow {}^7F_1$ intensity ratio ranges from 13 to 19 and the $^5D_0 \rightarrow {}^7F_1$ transition is separated into three peaks because of the Stark effect, suggesting a low symmetry environment of the first coordination sphere and a strong effect of the crystal field. The occurrence of only one $^5D_0 \rightarrow {}^7F_0$ transition supports the presence of only one Eu(III) emitting centre, even if such information is not conclusive [104]. The emissions of all the compounds fall in the reddish orange region of the CIE 1931 chromaticity diagram [105].

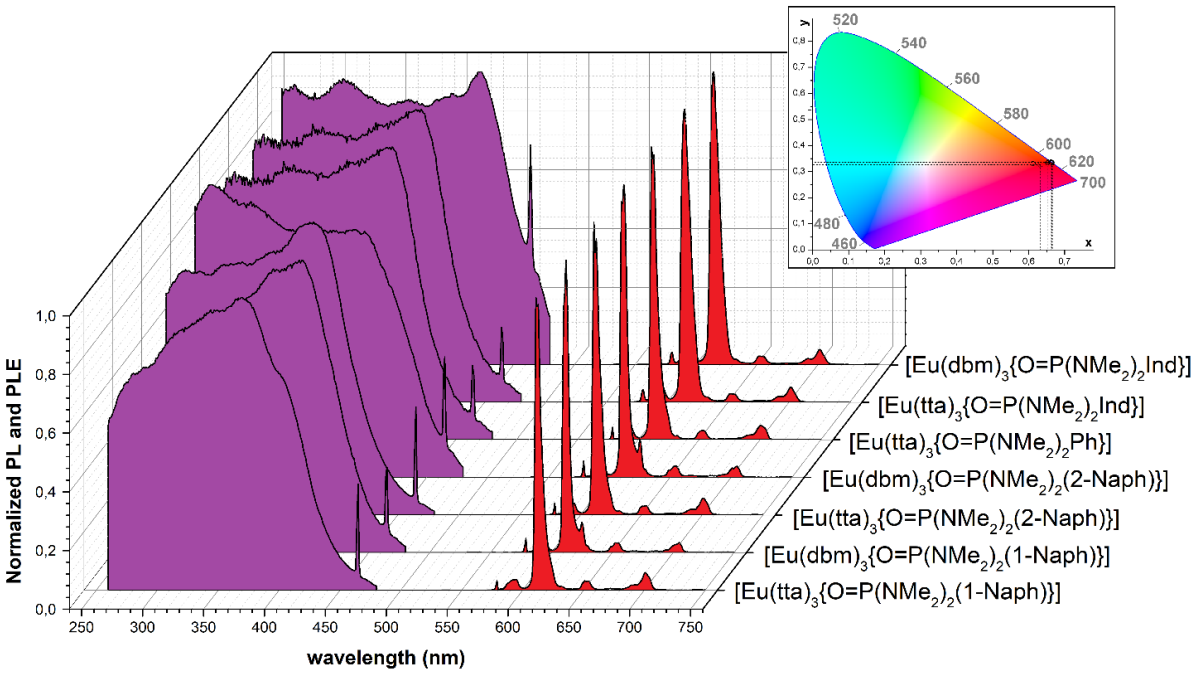

Figure 38. Normalized PLE and PL spectra of [Eu(β-dike)$_3$L] complexes and the corresponding CIE diagram.

The lifetimes (τ) were determined from the mono-exponential interpolation of the luminescence decay curves, with $\lambda_{excitation}$ = 377-380 nm and $\lambda_{emission}$ = 612-613 nm. As observable, the complexes containing the [NMe_2] fragments can be divided in two groups depending upon the choice of the β-diketonate. In the case of dbm as ancillary ligand the lifetime values are comprised between 215 and 274 μs, while longer lifetimes were measured for the corresponding tta complexes, in the range 346 – 380 μs. The intrinsic quantum yield

Q_{Eu}^{Eu} was estimated from the lifetime values and the $^5D_0 \rightarrow {}^7F_J/{}^5D_0 \rightarrow {}^7F_1$ intensity ratio, where $I(^5D_0 \rightarrow {}^7F_J)$ is the total integrated intensity.

$$Q_{Eu}^{Eu} = 14.65 \cdot n^3 \cdot \frac{I\left({}^5D_0 \rightarrow {}^7F_J\right)}{I({}^5D_0 \rightarrow {}^7F_1)} \cdot \tau(s)$$

In the equation *n* is the refraction index of the sample, which is conventionally equal to 1.5 for solid state samples. [73]

Molecular formula	λ_{max} ($^5D_0 \rightarrow {}^7F_2$)	τ(μs)	Q_i^{Eu} (%)
[Eu(dbm)$_3${P=O(NMe$_2$)$_2$Ph}]	614	274	18
[Eu(tta)$_3${P=O(NMe$_2$)$_2$Ph}]	614	380	30
[Eu(dbm)$_3${O=P(NMe$_2$)$_2$(1-Naph)}]	613	215	24
[Eu(tta)$_3${O=P(NMe$_2$)$_2$(1-Naph)}]	614	346	34
[Eu(dbm)$_3${O=P(NMe$_2$)2-Naph)}]	613	240	27
[Eu(tta)$_3${O=P(NMe$_2$)$_2$(2-Naph)}]	614	360	36
[Eu(dbm)$_3${O=P(NMe$_2$)$_2$(Ind)}]	614	274	29
[Eu(tta)$_3${O=P(NMe$_2$)$_2$(Ind)}]	614	376	33

Table 10. PL maximum, lifetimes and quantum yields of [Eu(β-dike)$_3$L] complexes.

In order to completely evaluate the effect of different aryl substituents in the phosphoramide ligands [O=P(NMe$_2$)$_2$Ar], the already reported data for [Eu(dbm)$_3${O=P(NMe$_2$)$_2$Ph}] are also shown in Table 10. Compared to the β-diketonate complexes where the phenyl-substituted ligand is present, all the new derivates showed slight decreased lifetime value. However, the substitution of the phenyl fragment with new aryl structures led to a slight improvement of the intrinsic quantum yields because of an increase of the $^5D_0 \rightarrow {}^7F_J/{}^5D_0 \rightarrow {}^7F_1$ intensity ratio. The calculated values are between 18% and 36% and highlight that a great amount of the energy accumulated in the Eu(III) resonance level is not converted in radiative emission. The replacement of the phenyl ring with the bulkier naphthyl and indolyl substituents probably increases the steric crowding and reduces the possibility of some vibrational modes in the coordination spheres.

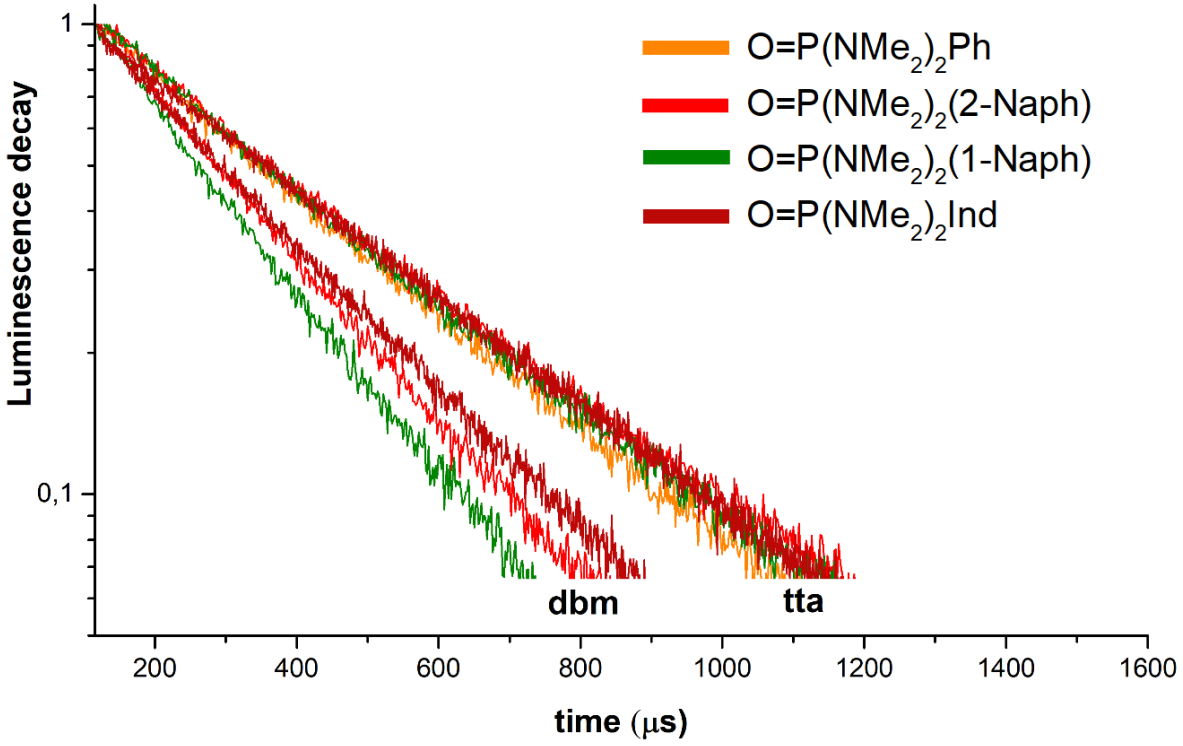

Figure 39. Lifetime of [Eu(β-dike)$_3$L] complexes.

Absorption and photoluminescence data of the [Eu(β-dike)$_3${O=P(MeNCH$_2$CH$_2$NMe)Ph}$_2$] complexes are shown in Figures 40 and 41. In dichloromethane solutions both compounds are characterized by strong absorptions in the near-UV range, starting at 425 nm and with maxima at around 350 nm. Solid-state photoluminescence measurements showed that the excitation of the coordinated ligands with wavelengths below about 500 nm causes the emission from the Eu(III) centre. PLE spectra are comparable to those of [Eu(β-dike)$_3$L] species where L= O=P(NMe$_2$)Ph. The direct excitation of Eu(III) is also present in the PLE spectra, corresponding to the $^5D_2 \leftarrow {}^7F_0$ transition centered at 464 nm [104]. As for the [Eu(β-dike)$_3$L] derivatives, the PL spectra display only the typical $^5D_0 \rightarrow {}^7F_J$ bands, the most intense occurring for J = 2. The $^5D_0 \rightarrow {}^7F_2/{}^5D_0 \rightarrow {}^7F_1$ intensity ratio ranges from 15.8 (β-dike = dbm) to 19.2 (β-dike = tta) and the $^5D_0 \rightarrow {}^7F_1$ transition is again separated in three peaks because of the Stark effect. These data suggest low symmetry of the first coordination sphere, being 2 the maximum possible rotational symmetry order, in line with the results of DFT calculations. The occurrence of only one $^5D_0 \rightarrow {}^7F_0$ transition supports the presence of only one Eu(III) emitting centre. [104].

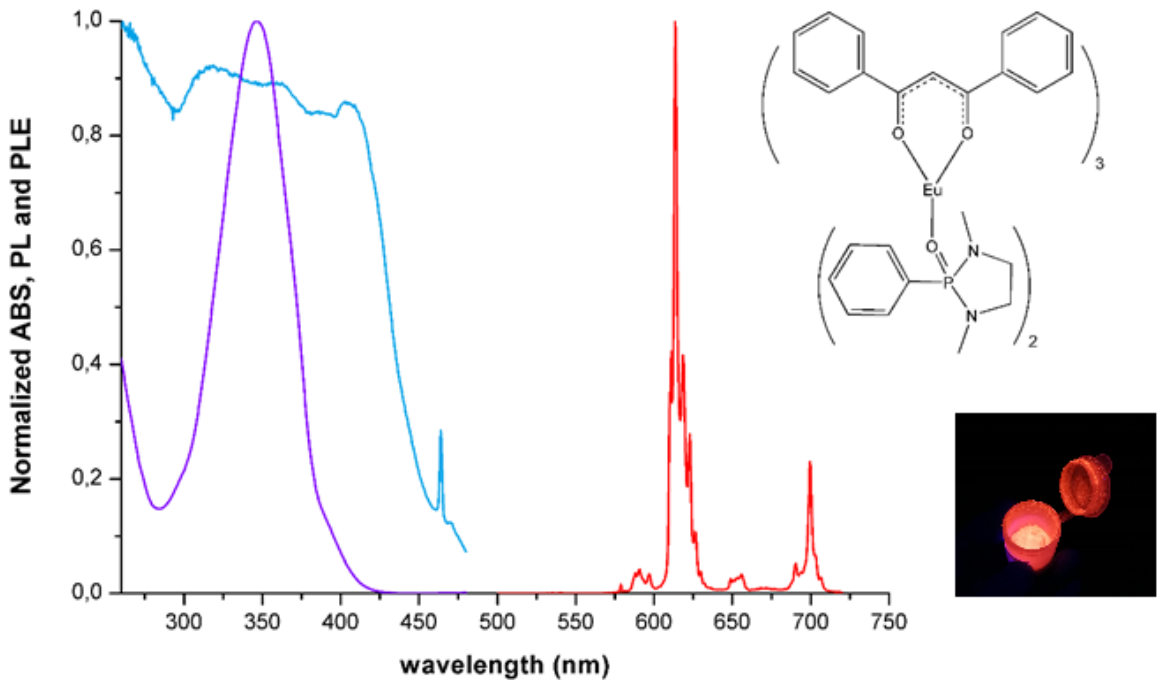

Figure 40. Normalized absorption (CH_2Cl_2 solution, violet line), emission (solid, red line) and excitation (solid, light blue line) spectra of the $[Eu(dbm)_3\{O=P(MeNCH_2CH_2NMe)Ph\}_2]$ complexes.

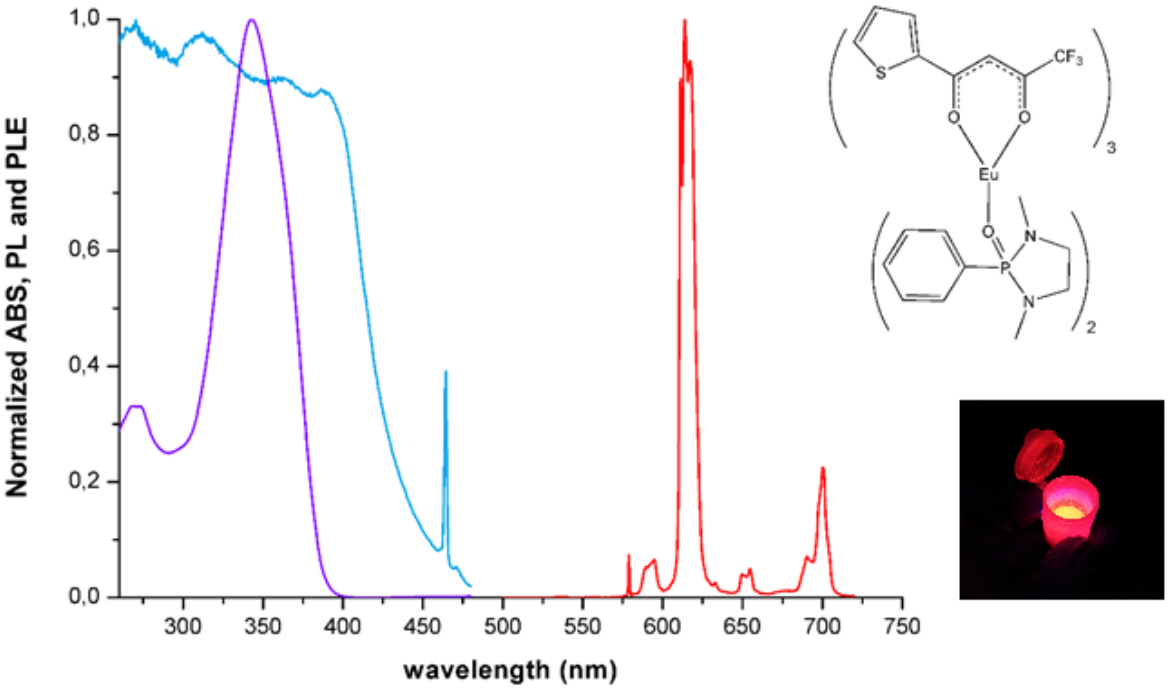

Figure 41. Normalized absorption (CH_2Cl_2 solution, violet line), emission (solid, red line) and excitation (solid, light blue line) spectra of the $[Eu(tta)_3\{O=P(MeNCH_2CH_2NMe)Ph\}_2]$ complexes.

The emissions of all the compounds fall in the reddish orange region of the CIE 1931 chromaticity diagram with unitary colour purity [105], as shown in Figure 42. The main

differences between of [Eu(β-dike)$_3$L] and of [Eu(β-dike)$_3$L$_2$] species are lifetimes and consequently quantum yields.

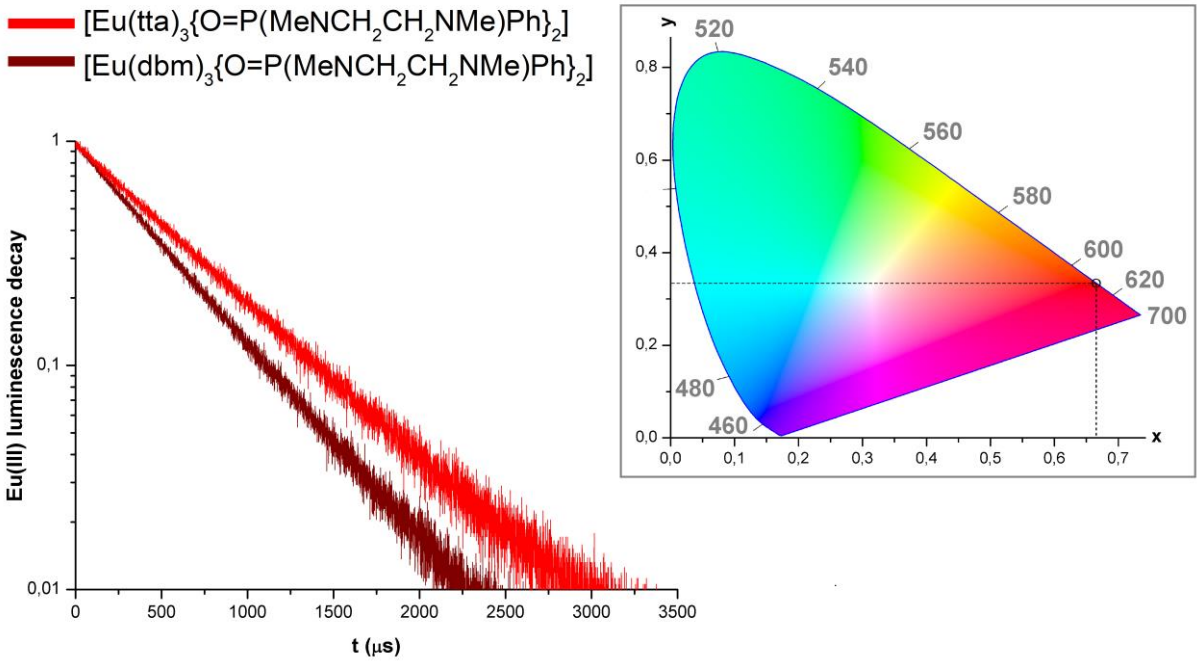

Figure 42. Lifetimes and CIE diagram of [Eu(dbm)$_3${O=P(MeNCH$_2$CH$_2$NMe)Ph}$_2$] and [Eu(tta)$_3${O=P(MeNCH$_2$CH$_2$NMe)Ph}$_2$].

The lifetimes (τ) were determined from the mono-exponential interpolation of the luminescence decay curves, with $\lambda_{excitation}$ = 377 nm and $\lambda_{emission}$ = 612 nm. Lifetime values are 482 μs and 610 μs respectively in the case of dbm and tta derivatives and are both meaningfully longer than [Eu(β-dike)$_3$L] species. The lifetime of the tta derivative is comparable to that reported for [Eu(tta)$_3$(ptso)$_2$] (ptso = p-tolyl sulfoxide), 598 μs. [106] Calculated values for the intrinsic quantum yields are 51% for [Eu(dbm)$_3${O=P(MeNCH$_2$CH$_2$NMe)Ph}$_2$] and 65% for [Eu(tta)$_3${O=P(MeNCH$_2$CH$_2$NMe)Ph}$_2$].
The improvement of the quantum yields perhaps arises from the presence of higher rigidity in the ligand's skeleton, coming from the presence of the bridging group between the -NMe fragments and the formation of a stable five-membered cycle. The increased coordination number is another factor that probably reduces the probability of non-radiative decay because of the increment of steric crowding.

The stability of the obtained β-diketonate complexes in doped plastic materials was tested. The encapsulation in PMMA polymer matrix leads to the obtainments of solid plastic samples with strong luminescence associated to the typical $^5D_0 \rightarrow {}^7F_J$ transitions. However, PL spectra

display some differences on the relative intensities and on the Stark levels with respect to the pure compounds, indicating alterations of the first coordination sphere of the complexes. Moreover, also lifetime and PLE measurements showed relevant variations. The polymer chains are therefore supposed to interact with the complexes, perhaps causing the displacement of the [O=P]-donor ligands or however leading to changes in the coordination geometry and number.

4. CONCLUSIONS

Manganese(II) complexes $[MnX_2\{O=P(NMe_2)_2(Ind)\}_2]$ and $[MnX_2\{O=P(MeNCH_2CH_2NMe)Ph\}_2]$ where X= Cl, Br showed emissions in the green region of the spectra and their tetrahedral geometry was confirmed by single-crystal X-ray diffraction. On the other hand, the use of $O=P(NMe_2)_2$(1-Naph) or $O=P(NMe_2)_2$(2-Naph) as ligands afforded species showing emissions in the red region, probably associated to an increment of the coordination number. The use of arylphophonic diamides with more extended π conjugation shifted the absorption bands towards longer wavelengths, but it is likely to suppose that it also reduced the σ-donation from the oxygen atoms, this explaining the tendency to the expansion of the coordination sphere. The role of σ-donation of the coordination number and therefore on the luminescence was confirmed by the introduction of iodide as halide. In fact, tetrahedral iodo-complexes were isolated in pure form only with [O=P] donor moieties characterized by poor delocalization.

The electronic delocalization in the ligands here considered is of paramount importance also in lanthanide chemistry for different reasons. The presence of π-extended fragments varies the triplet state level of the ligand, avoiding an efficient energy transfer to Tb(III). All the ligands were instead able to sensitize Eu(III) luminescence. Differently from manganese complexes, the coordination geometry is determined by steric factors and plays a role on quantum yields, since eight-coordinated derivatives are more efficient than analogous seven-coordinated complexes.

To summarize, small variations on the arylphosphonic diamide ligands have deep influences on the luminescence features of Mn(II) and Ln(III) complexes, because both electronic and steric changes can alter the coordination geometries of the final products. Moreover, the possible sensitization of different lanthanide ions is related to the choice of the aromatic fragment.

5. BIBLIOGRAPHY

[1] (a) M. Montalti, A. Credi, L. Prodi, M. T. Gandolfi, Handbook of Photochemistry, 5 (2006) 377. (b) F. Puntoriero, Photochemistry, 39 (2011) 65. (c) V. Balzani, S. Campagna, Topics in Current Chemistry, 280-281 (2007). (d) D. M. Roundhill, Photochemistry and Photophysics of Metal Complexes (1994).

[2] (a) L. Pereira, Organic Light-Emitting Diodes (2012) 209. (b) H. Xu, R. Chen, Q. Sun, W. Lai, Q. Su, W. Huang, X. Lu, Chem. Soc. Rev. 43 (2014) 3259. (c) V. W.-W. Yam, K. M.-C. Wong, Chem. Commun. 47 (2011) 11579.

[3] (a) M. S. Wrighton, D. L. Morse, J. Am. Chem. Soc. 96 (1974) 998. (b) K. S. Schanze, D. B. MacQueen, T. A. Perkins, L. A. Cabana, Coord. Chem. Rev. 122 (1993) 63. (c) R. J. Shaver, D. P. Rillema, Inorg. Chem. 31 (1992) 4101. (d) L. A. Sacksteder, A. P. Zipp, E. A. Brown, J. Streich, J. N. Demas, B. A. DeGraff, Inorg. Chem. 29 (1990) 4335.

[4] M. D. Ward, Dalton Trans. 39 (2010) 8851.

[5] (a) W. Holzer, A. Penzkofer, T. Tsuboi, Chem. Phys. 308 (2005) 93. (b) M. A. Baldo, S. Lamansky, P. E.Burrows, M. E. Thompson, S. R. Forrest, Appl. Phys. Lett. 75 (1999) 4. (c) K. Y. Zhang, S. Liu, Q. Zhao, F. Li, W. Huang, Luminescent and Photoactive Transition Metal Complexes as Biomolecular Probes and Cellular Reagents, (2015) 131-180. (d) J. A. G. Williams, Chem. Soc. Rev. 38 (2009) 1783.

[6] (a) J. A. G. Williams, S. Develay, D. L. Rochester, L. Murphy, Coord. Chem. Rev. 252 (2008) 2596. (b) J.Kalinowski, V. Fattori, M. Cocchi, J. A. G. Williams, Coord. Chem. Rev. 255 (2011) 2401. (c) K. M.-C. Wong, V. W.-W. Yam, Coord. Chem. Rev. 251 (2007) 2477. (d) C. Bronner, O. S. Wenger, Dalton Trans. 40 (2011) 12409. (e) E. R. T. Tieknik, J.-G. Kang, Coord. Chem. Rev. 253 (2009) 1627. (f) C.-M. Che, S.-W. Lai, Gold Chemistry. Applications and Future Directions in the Life Sciences, (2009) 249-281.

[7] K. Tsuge, Y. Chishina, H. Hashiguchi, Y. Sasaki, M. Kato, S. Ishizaka, N. Kitamura, Coord. Chem. Rev. 306 (2016) 636.

[8] Y. Liu, S.-C. Yiu, C.-L. Ho, W.-Y. Wong, Coord. Chem. Rev. 375 (2018) 514.

[9] K. F. Renk, Basics of Laser Physics: For Students of Science and Engineering (2012) 291-308.

[10] (a) A. D. Kirk, Chem. Rev. 99 (1999) 1607. (b) L. S. Forster, Chem. Rev. 90 (1990) 331. (c) L. A. Büldt, O. S. Wenger, Chem. Sci. 8 (2017) 7359.

[11] www.rsc.org/periodic-table/element/25/manganese

[12] M. Gaft, R. Reisfeld, G. Panczer, Modern Luminescence Spectroscopy of Minerals and Materials, (2005) 168.

[13] D. Chen, Y. Zhou and J. Zhong, RSC Adv. 89 (2016) 86285-86296.

[14] J. E. Murphy, F. Garcia-Santamaria, A. A. Setlur, S. Sista, The Society for Information Display, 46 (2015) 927.

[15] M. Gaft, R. Reisfeld, G. Panczer, G. Boulon, S. Shoval, B. Champagnon, Optical Materials, 8 (1997) 149.

[16] S. Kück, S. Hartung, S. Hurling, K. Petermann, and G. Huber, Phys. Rev. 57 (1998) 2203.

[17] M. Gaft, R. Reisfeld, G. Panczer, Modern Luminescence Spectroscopy of Minerals and Materials, (2015) 45.

[18] (a) K. Nikolič, F. Lignou, H. Payen de la Garanderie, J. Lumin. 8 (1973) 137. (b) B. P. Chandra, B. Rao Kaza, J. Lumin. 27 (1982) 101. (c) J. I. Zink, G. E. Hardy, G. Gliemann, Inorg. Chem. 19 (1980) 488. (d) S. Balsamy, P. Natarajan, R. Vedalakshmi, S. Muralidharan, Inorg. Chem. 53 (2014) 6054. (e) S. Pitula, A.-V. Mudring, Chem. Eur. J. 16 (2010) 3355. (f) F. A. Cotton, L. M. Daniels, P. Huang, Inorg. Chem. 40 (2001) 3576.

[19] (a) D. M. L. Goodgame, F. A. Cotton, J. Chem. Soc. (1961) 3735. (b) F. A. Cotton, D. M. L. Goodgame, M. Goodgame, J. Am. Chem. Soc. 84 (1962) 167.

[20] S. Balsamy, P. Natarajan, R. Vedalakshmi, S. Muralidharan, Inorg. Chem. 53 (2014) 6054.

[21] M. Wrighton, D. Ginley, Chem. Phys. 4 (1974) 295.

[22] C. Jiang, N. Zhong, C. Luo, H. Lin, Y. Zhang, H. Peng, C.-G. Duan, Chem. Commun. 53 (2017) 5954-5957.

[23] X. -W. Cai, Y. -Y. Zhao, H. Li, C. -P. Huang, Z. Zhou, Journal of Molecular Structure, 1161 (2018) 262.

[24] J. Chen, Q. Zhang, F.-K. Zheng, Z.-F. Liu,S.-H. Wang, A.-Q. Wu, G.-C. Guo, Dalton Trans. 44 (2015) 3289.

[25] M. Bortoluzzi, J, Castro, F. Enrichi, A. Vomiero, M. Busato, W. Huang, Inorganic Chemistry Communications, 92 (2018) 145.

[26] (a) A. Hosseiny, C. A. McAuliffe, K. Minten, M. J. Parrott, R. Pritchard and J. Tames, Inorganica Chimica Acta, 39 (1980) 221. (b) H. Zhao, R. Clérac, J.-S. Sun, X. Ouyang, J. M. Clemente-Juan, C. J. GoHmez-Garcìa, E. Coronado, K. R. Dunbar, Journal of Solid State Chemistry 159 (2001) 281. (d) S. Gorter, A.D. Van Ingen Schenau, G. C. Verschoor, Acta Cryst. 30 (1974) 1867.

[27] B. C. Unni Nair, J. E. Sheats, R. Ponteciello, D. Van Engen, V. Petrouleas, G. C. Dismukes, Inorg. Chem. 28 (1989) 1582.

[28] (a) J. Orive, J. Mesa, R. Balda, J. Fernández, J. R. Fernández, T. Rojo, M. I. Arriortua, Inorg. Chem. 50 (2011) 12463. (b) Z. Deng, L. Tong, M. Flores, S. Lin, J.-X. Cheng, H. Yan, Y. Liu, J. Am. Chem. Soc. 133 (2011) 5389. (c) O. Chen, D. E. Shelby, Y. Yang, J. Zhuang, T. Wang, C. Niu, N. Omenetto, Y.C. Cao, Angew. Chem. 122 (2010) 10330. (d) J. Lin, L. Wang, Q. Zhang, F. Bu, T. Wu, X. Buc, P. Feng, J. Mater. Chem. 4 (2016) 1645. (e) P. Li, M. Peng, L. Wondraczek, Y. Zhao, B. Viana, J. Mater. Chem. 3 (2015) 3406.

[29] (a) Y. Zhang, W.-Q. Liao, D.-W. Fu, H.-Y. Ye, C.-M. Liu, Z.-N. Chen, R.-G. Xiong, Adv. Mater. 27 (2015) 3942. (b) Y. Zhang, W.-Q. Liao, D.-W. Fu, H.-Y. Ye, Z.-N. Chen, R.-G. Xiong, J. Am. Chem. Soc. 137 (2015) 4928. (c) H.-Y. Ye, Q. Zhou, X. Niu, W.-Q. Liao, D.-W. Fu, Y. Zhang, Y.-M. You, J. Wang, Z.-N. Chen, R.-G. Xiong, J. Am. Chem. Soc. 137 (2015) 13148. (d) Y.-M. You, W.-Q. Liao, D. Zhao, H.-Y. Ye, Y. Zhang, Q. Zhou, X. Niu, J. Wang, P.-F. Li, D.-W. Fu, Z. Wang, S. Gao, K. Yang, J.-M. Liu, J. Li, Y. Yan, R.-G. Xiong, Science 357 (2017) 306.

[30] Y. Mei, H. Yu, Z. Wei, G. Mei, H. Cai, Polyhedron 127 (2017) 458.

[31] D. Hausmann, A. Kuzmanoski, C. Feldmann, Dalton Trans. 45 (2016) 6541.

[32] A.S. Berezin, K.A. Vinogradova, V.A. Nadolinny, T.S. Sukhikh, V.P. Krivopalov, E.B. Nikolaenkova, Dalton Trans., 47 (2018) 1657.

[33] A. V. Artem'ev, A. S.Berezin, V. K. Brel, V.P. Morglyuk, D.G. Samsonenko, Polyhedron 148 (2018) 184.

[34] M. Bortoluzzi, J. Castro, E. Trave, D. Dallan, S. Favaretto, Inorg. Chem. Commun. 90 (2018) 105.

[35] Y. Wu, X. Zhang, L.-J. Xu, M. Yang, Z.-N. Chen, Inorg. Chem. 57 (2018) 9175.

[36] S. Cotton, Lanthanide and Actinide Chemistry, (2006).

[37] P. Falconnet, J. Alloys and Compounds, 192 (1993) 114.

[38] L. Armelao, G. Bottaro, S. Quici, C. Scalera, M. Cavazzini, G. Accorsi, Coord. Chem. Rev. 254 (2010) 487.

[39] J.-C. G. Bünzli and S. V. Eliseeva, Lanthanide Luminescence, 7 (2010) 1.

[40] (a) A. de Bettencourt-Dias, Luminescence of Lanthanide Ions in Coordination Compounds and Nanomaterials (2014) 1. (b) K. Binnemans, Coord. Chem. Rev. 295 (2015) 1.

[41] M. Hatanaka, S. Yabushita, Chem. Phys. Lett. 504 (2011) 113.

[42] S. Comby, J.-C. G. Bünzli, Handbook on the Physics and Chemistry of Rare Earths, 37 (2007) 217.

[43] J. D. Roberts, M. C. Caserio, Basic Principles of Organic Chemistry, (1977).

[44] C. Yang, L. Fu, Angew. Chem, 43 (2004) 5009.

[45] S.I. Weissman, J. Chem. Phys. 10 (1942) 214.

[46] (a) T. Forster, Ann. Phys. 2 (1948) 55. (b) D.L. Dexter, J. Chem. Phys. 21 (1953) 836.

[47] M. D. Seltzer, S. Fallis, R. A. Hollins, N. Prokopuk, R. N. Bui, J. of Fluorescence, 15 (2005) 597.

[48] K. Binnemans, Chem. Rev. 109 (2009).

[49] K. Binnemans, Handbook on the Physics and Chemistry of Rare Earths, 35 (2005).

[50] (a) I. B. Liss, W. G. Bos, J. Inorg. Nucl. Chem., 39 (1977) 443. (b) J. M. Koehler, W.G. Bos, Inorg. Nucl. Chem. Lett. 3 (1967) 545.

[51] N. Filipescu, W. F. Sager, F. A. Serafin, J. Phys. Chem. 68 (1964) 3324.

[52] (a) G. A. Crosby, R. E. Whan, R. M. Alire, J. Chem. Soc. 34 (1961) 743. (b) G. A. Crosby, R. E. Whan, J. J. Freeman, J. Am. Chem. Soc. 66 (1962) 2493.

[53] L. R. Crisler, US Patent, 3, 919 (1975) 214.

[54] N. A. Stump, G.K. Schweitzer, Spettrosc. Lett. 25 (1992) 1421.

[55] M. George, C. Golden, Inorg. Chem. 45 (2006) 1739.

[56] (a) A. Gassner, C. Duhot, Inorg. Chem. 47 (2008) 17. (b) A. D'Aleo, A. Picot, Inorg. Chem. 47 (2008) 10269.

[57] (a) D. Guillaumont, H. Bazin, Chem. Phys. Chem. 8 (2007) 480. (b) R. Rodriguez-C., F. Avecilla, Inorg. Chem, 41 (2002) 21. (c) D. Guillaumont, H. Bazin, J. M. Benech, M. Boyer, G. Mathis, Chem. Phys. Chem. 8 (2007) 480.

[58] S. Trofimenko, Scorpionate: The Coordination Chemistry of polypyrazolilborate Ligands, (1999).

[59] K. W. Bagnall, A. C. Tempest, J. Takatas, A. P. Masino, Inorg. Nucl. Chem. Lett. 12 (1976) 555.

[60] (a) M. Bortoluzzi, G. Paolucci, S. Polizzi, L. Bellotto, F. Enrichi, S. Ciorba, B. S. Richards, Inorg. Chem. Commun. 14 (2011) 1762. (b) N. Marques, A. Sella, Chem. Rev. 102, 6 (2002) 2157. (c) A. C. Hillier, S. Liu, J. Inorg. Chem. 39 (2000) 2635. (d) G. M. Davies, R. J.Aarons, G. R. Motson, Dalton Trans. 8 (2004) 1136.

[61] L. R. Matthews, E. T. Knobbe, Chem. Mater. 5 (1993) 1697.

[62] (a) B. Yan, H. J. Zhang, S. B. Wang, J. Z. Ni, Mater. Chem. Phys. 51 (1997) 92. (b) W. Strek, L. Sokolnicki, J. Legendziewicz, K. Maruszewski, R. Reisfeld, T. Pavich, Opt. Mater. 13 (1999) 41.

[63] C. Sanchez, F. Ribot, New J. Chem. 18 (1994) 1007.

[64] D. Sendor, U. Kynast, Adv. Mater. 14 (2002) 1570.

[65] (a) J. Boyaval, F. Hapiot, C. Li, N. Isaert, M. Warenghem, P. Carette, Mol. Cryst. Liq. Cryst. 330 (1999) 1387. (b) J. Boyaval, C. Li, F. Hapiot, M. Warenghem, N. Isaert, Y. Guyot, G. Boulon, P. Carette, Mol. Cryst. Liq. Cryst., 359 (2001) 337. (c) K. Binnemans, D. Moors, J. Mater. Chem. 12 (2002) 3374.

[66] (a) J.-C. G. Bünzli, C. Piguet, Chem. Soc. Rev. 34 (2005) 1048. (b) J.-C. G. Bünzli, S. V. Eliseeva, Chem. Sci. 4 (2013) 1939. (c) J.-C. G. Bünzli, Journal of Luminescence, 170 (2016) 866.

[67] V. W. W. Yam, K. K. W. Lo, Coord. Chem. Rev. 184 (1999) 157.

[68] A. Beeby, S. W. Botchway, I. M.Clarkson, J. Photochem. Photobiol. 57 (2000) 83.

[69] (a) G. M. Davies, S. J. A. Pope, H.4 Adams, Inorg. Chem. 4 (2005) 4656. (b) S. Faulkner, S. J. A. Pope, Appl. Spectros. Rev. 40 (2005) 1. (c) S. Faulkner, S.J.A. Pope, J. Am. Chem. Soc. 125 (2003) 10526. (d) G. A. Hebbink, S. I. Klink, L. Grave, P. G. B. O. Alink, F. Van Veggel, Chem. Phys. Chem. 3 (2002) 1014. (e) R .S. Dickins, S. Aime, A. S. Batsanov, A. Beeby, J. Am. Chem. Soc. 124 (2002) 12697.

[70] (a) K. Kuriki, Y. Koike, Y. Okamoto, Chem. Rev. 102 (2002) 2347. (b) J. Kido, Y. Okamoto, Chem. Rev. 102 (2002) 2357.

[71] (a) D. J. Edmonds, D. Johnston, D. J. Procter, Chem. Rev. 104 (2004) 3371. (b) G. A. Molander, J. A. C. Romero, Chem. Rev. 102 (2002) 2161.

[72] A. Beeby, S. W. Botchway, I. M. Clarkson, J. Photochem. Photobiol. 57 (2000) 83.

[73] J.-C. G. Bünzli, Chem. Rev. 110 (2010) 2729.

[74] P. Caravan, Chem. Soc. Rev. 35 (2006) 512.

[75] C. S. Bonnet, F. Buron, F. Caillé, C. M. Shade, B. Drahoš, L. Pellegatti, J. Zhang, S. Villette, L. Helm, C. Pichon, F. Suzenet, S. Petoud, E. Tóth, Chemistry, 18 (2012) 1419.

[76] T. Yamada, S. Shinoda, H. Tsukube, Chem. Commun. 11 (2002) 1218.

[77] (a) T. Gunnlaugsson, D. A. Mac Donail, Chem. Commun. (2000) 93. (b) D. Parker, J. A. G. Williams, Chem. Commun. (1998) 245. (c) D. Parker, K.Senanaayake, J. A. G. Williams, Chem. Commun. (1997) 1777.

[78] Y. Oshishi, T. Kanamori, T. Kitagawa, Opt. Lett. 16 (1991) 1747.

[79] (a) T. Trupkea, A. Shalava, B. S. Richards, P. Wu, Solar Energy Materials & Solar Cells, 90 (2006) 1189. (b) E. Klampaftis, D. Ross, K. R. McIntosh, B. S. Richards, Solar Energy Materials & Solar Cells, 93 (2009) 1182.

[80] (a) A. de Bettencourt-Dias, Dalton Trans. (2007) 2229. (b) O. M. Khreis, R. J. Curry, M. Somerton, W. P. Gillin, J. Appl.Phys. 88 (2000) 777. (c) P. He, H. H. Wang, S. G. Liu, W. Hu, J. X. Shi, G. Wang, M. L. Gong, J. Electrochem. Soc. 156 (2009) 46.

[81] (a) Y. Abe, G. Wada, Bull. Chem. Soc. Jpn. 53 (1980) 3547. (b) Y. Abe, G. Wada, Bull. Chem. Soc. Jpn. 54 (1981) 3334.

[82] M. Bortoluzzi, J, Castro, F. Enrichi, A. Vomiero, M. Busato, W. Huang, Inorg. Chem. Commun. 92 (2018) 145.

[83] (a) Z.-M. Jin, B. Tu, Y.-Q. Li, M.-C. Li, Acta Cryst. (2005), E61, m2510. (b) M. Bortoluzzi, J. Castro, Journal of Coordination Chemistry, (2019) DOI: 10.1080/00958972.2018.1560430.

[84] (a) J. T. Donoghue, D. A. Peters, J. Inorg. Nucl. Chem. 31 (1969) 467. (b) N. B. Mikheev, A. N. Kamenskaya, N. A. Konovalova, T. A. Zhilina, Russ. J. Inorg. Chem. 22 (1977) 955.

[85] J. T. Donoghue, D. A. Peters, J. Inorg. Nucl. Chem. 31 (1969) 467.

[86] (a) D. K. Koppikar, P. V. Sivapullaiah, L. Ramakrishnan, S. Soundararajan, Novel Aspects, 34 (2007) 135 (b) C. Airoldi , Y. Gushikem, C. R. Puschel, J. of Coord. Chem. 6 (1976) 1.

[87] C. Premlatha, S. Soundararajan, Chem. Sci. 88 (1979) 291.

[88] (a) A. G. Silva, G. Vicentini, J. Zukerman-Schpector, E. E. Castellano, J. Alloy. Compd. 225 (1995) 354.

[89] S. Petricek, A. demsar, L. Golic, J. Kosmrlj, Polyhedron, 19 (2000) 199.

[90] F. A. Silva Jr., H. A. Nascimento, D. K. S. Pereira, J. Braz. Chem. Soc. 24 (2013) 601.

[91] B. V. Bukvetskii, A. G. Mirochnik, P. A. Zhikhareva, Luminescence 32 (2016) 341.

[92] X. Huang, Y. Xu, K. Fan, S. Bao, M. Kurmoo, L. Zheng, Angew. Chem. 57 (2018) 8577.

[93] Y. Makioka, T. Hayashi, M. Tanaka, L.B. Hao, Novel phosphonamides, process for producing the same, and use thereof, WO 2003/074538.

[94] E. S. Panin, S. B. Ivanov, V. Y. Kavun, I. N. Botova, Koordinatsionnaya Khimiya 18 (1992) 663.

[95] G. A. Bain, J. F. Berry, J. Chem. Ed. 85 (2008) 532.

[96] R. Keat, R.A. Shaw, J. Chem. Soc., (1965) 4802.

[97] B. G. Van den Bos, C. J. Schoot, M. J. Koopmann, J. Meltzer, Recl. Trav. Chim. (1961).

[98] H. Ulrich, B. Tucker, A. A. R. Sayigh, J. Org. Chem. 32 (1967) 1360.

[99] M. Bortoluzzi, J. Castro, F. Enrichi, A. Vomiero, M. Busato, W. Huang, Inorg. Chem. Commun. 92 (2018) 145.

[100] M. Wrighton, D. Ginley, Chem. Phys. 4 (1974) 295.

[101] S. Wang, Q. Lou, X. Zhou, Z. Zeng, Polyhedron, (1993).

[102] S. P. Sinha, T. T. Pallanen, T. A. Pakkanen, L. Niinistö, Polyhedron, 1 (1982) 355.

[103] M. Latva, H. Takalo, V. Mukkala, C. Matachescu, J. C. Rodriguez-Ubis, J. Kankare, J. Lumin. 75 (1997) 149.

[104] K. Binnemans, Coord. Chem. Rev. 295 (2015) 1.

[105] E. F. Schubert, Light-Emitting Diodes, (2006) 292.

[106] F.R. Gonçalves, F.R. Silva, J. F. S. Menezes, G. B. Rocha, S. Alves, H. F. Brito, R. L. Longo, O. L. Malta, J. Alloy. Comp. 303-304 (2000) 364.